NORTHWESTERN UNIVERSITY

Surface-Specific Explorations at the Nano-Bio Interface

A DISSERTATION

SUBMITTED TO THE GRADUATE SCHOOL
IN PARTIAL FULFILMENT OF THE REQUIREMENTS

for the degree

DOCTOR OF PHILOSOPHY

Field of Chemistry

By

Merve Doğangün

EVANSTON, ILLINOIS

June 2018

Abstract

Surface Specific Explorations at the Nano-Bio Interface

Merve Doğangün

The increasing production and use of nanoscale transition metal oxide materials in the next generation of consumer electronics and electric vehicle batteries, specifically lithium intercalation compounds, may lead to environmental release and exposure, with poorly understood biological outcomes. As the toxicity mechanism of nanomaterials may vary fundamentally from their bulk material counterparts due to specific nanoparticle properties, the environmental consequences of these materials need to be kept in mind as new materials are developed. When nanomaterials encounter unicellular and multicellular organism in the environment, the surface of the nanoparticles and the surface of the cell membrane are the first points of contact. Therefore, understanding the molecular level interactions at the nano-bio interface can provide insight into the mechanisms of nanotoxicity. However, it is difficult to elucidate specific molecular level information regarding the interactions between nanomaterials and cell membranes, given the inherently complex nature of the surface chemistries. To identify the roles that (1) nanomaterial surface charge and chemical composition and (2) membrane charge and constituents play in these interactions, this thesis uses idealized model membranes and transition metal oxide nanomaterials that are well characterized and allow control of chemical composition.

This thesis focuses on mitigating non-contact interactions between nanomaterials and model membranes and point towards a path for enabling the design of new energy storage materials with reduced environmental impacts. Using vibrational sum frequency generation (SFG) spectroscopy to probe idealized model membrane-nanomaterial interactions, this thesis investigates the structural alterations in model membranes at the nano-bio interface in situ, in real

time, with surface-specificity, and under environmentally relevant aqueous conditions. Along with complementary surface-specific techniques, this thesis highlights how electrostatics and nanomaterial transformations impact the interactions between the nanoscale transition metal oxides and supported lipid bilayers, identifying environmental behaviors that may be used in the future to predict the impact of nanomaterials based on their physical and chemical properties. Finally, this thesis demonstrates an approach to probe the C–H stretches of lipid alkyl tails in supported lipid bilayers detected along with the O–H stretching continuum of the hydrogen bonding network system to capture changes in the interfacial water structure. The ability to probe hydrogen bond networks over supported lipid bilayers along with the C–H stretches of alkyl tails holds the promise of opening paths for understanding specific and non-specific interactions at the nano-bio interface.

Professor Franz M. Geiger

Research Advisor

Acknowledgements

First and foremost, I would like to thank my advisor Prof. Franz Geiger for his enthusiasm about science, his constant source of guidance over the years and the opportunity to work in the Geiger group starting as a summer undergraduate trainee followed by my role as graduate student. He has always encouraged me to come up with new ideas and think outside the box, which I know will be very helpful in my future career. I would also like to thank my past and current committee members Prof. George Schatz, Prof. Nathan Gianneschi, Prof. Teri Odom and Prof. Chad Mirkin for inspiring science discussions.

This work wouldn't have been possible if it hadn't been for the fantastic collaborators in the Center for Sustainable Nanotechnology (CSN). I would like to thank all the PIs for their time and ideas they provided for us to grow as innovative researchers. Special thanks to Prof. Robert Hamers, Prof. Joel Pedersen and Prof. Qiang Cui for the insightful research meetings, fostering discussion and their generous support. I am glad to work with an excellent team of scientists and I would like to extend my thanks to all the students and postdocs in the center for creating a friendly and fun atmosphere. Extra thanks to Dr. Hang, Dr. Melby, Dr. Mensch, Dr. Vartanian, Dongyue Liang and Ben Frank for providing materials, helping out with numerous experiments and their timely responses to emails making it possible to meet tight deadlines. Dr. Schwartz and Dr. Krause, thank you for always making time for students, being patient and supportive beyond research including communication, professional development and setting up career aspirations.

I am lucky to have worked with the best group I can imagine. I would like to thank to Steph, Jen, Dave, Ehow, Sarah, Mona, Juli, Laura, Mary Alice, Hilary, Alicia, Danielle, Paul, Mavis, Ariana, Johnny, Naomi, Dawning, Tianzhe, HanByul, and Jo. Thank you for your endless

help with lasers, editing manuscripts and chapters, and making grad school bearable with all the fun times. Many thanks to the staff in the Chemistry Department Office and the Business Office as well as to Jake Thornberry for making sure we were on track during graduate school.

I owe a debt of gratitude to my undergraduate advisor, Prof. Okan Esenturk. Without his motivation, encouragement and support, I wouldn't have made it this far. I would like to extend my sincere thanks to my high school chemistry teacher Mustafa Ustunisik, for his energy, patience and for showing how fun chemistry is.

I would like to thank to my friends and family for their continuous support throughout the years and for making my journey a great experience. Tugce and Mehmet, Fernanda, Nil, Emirhan, David, Dhika, Newell, Marco, AMG, Tuncay, and many other friends have helped me feel home being an ocean away from home. My dear friends from high school and college, scattered around the world now, Ecehan, Defne, Ecem, Ozen, Deniz, Seda, Enis, Umay, Sezin, Aylin, and Hande, I always have a special place for you in my heart.

Mom and Dad, thank you for always being by my side and inspiring me to pursue my dreams. I don't think I can explain my gratitude with words. Special acknowledgements to my brother, his wife Pelin and my niece Ipek for their emotional support and countless Skype calls over the years. Dear Karaarslan family, thank you for the great memories we have shared. Grandma, I wish I had a way to thank you for reminding me that there is a fascinating world outside the lab. Grandpa, I really appreciate the efforts to use a laptop, just to be able to talk to me. Ben, thank you for the friendship, laughter and joy you bring into my life. Especially the past three months, I have been on an emotional rollercoaster, thank you for always being there.

To my parents and my brother

TABLE OF CONTENTS

LIST OF FIGURES

LIST OF TABLES

CHAPTER 1

Importance of Nano-Bio Interfaces

Portions of this chapter are reproduced in part
with permission from the American Chemical Society:

Doğangün, M.; Hang, M. N.; Troiano, J. M.; McGeachy, A. C.; Melby, E. S.; Pedersen, J. A.; Hamers, R. J.; Geiger, F. M. *ACS Nano.* **2015**, *9* (9), 8755-8765.

1.1. Introduction: Nanomaterials in the Environment

Nanomaterials, defined as having at least one dimension of 100 nm or less, are ubiquitous. Nature is an enormous laboratory that produces nanomaterials, and natural phenomena taking place on the nano-scale have existed throughout the history.[1] Examples of naturally produced nanomaterials include ash from volcanic activity,[2] salt particles from ocean spray,[3] fullerenes from combustion,[4] and iron-based nanomaterials from icebergs,[5] which overall sum to over 100 teragrams of nanomaterials per year.[6]

Engineered nanomaterials differ from natural nanomaterials as they are intentionally developed for a functional purpose.[7] They can be produced from a variety of materials,[8] with different sizes,[9] shapes,[10] surface charges,[11] and surface functionalities, allowing for chemical tailoring of the unique physicochemical properties that arise on the nano-scale.[12] Recent advances in nanomaterial synthesis and manufacturing have led to the exploitation of nanomaterials and their characteristic physicochemical properties in a variety of applications with the potential to benefit society in numerous ways. Indeed, they are increasingly being used for commercial purposes including electronics,[13-14] energy storage,[15] cosmetics,[16] and agriculture.[17-19] For the purpose of this thesis, we will only discuss engineered nanomaterials, so we will refer to engineered nanomaterials as simply nanomaterials.

Significant nanotechnology research is underway to meet the global demand for batteries in portable electronics and electric vehicles. Due to their low molecular weight and favorable electrochemical properties, transition metal oxide (TMO) nanomaterials have received particular attention as promising candidates for cathode materials in energy storage systems. The layered structure of these nanomaterials allows Li^+ ions to travel between the cathode and anode for several thousand charge and discharge cycles with little memory effect. This capability, coupled with the

high energy density offered by Li-ion intercalation compounds, makes these nanomaterials suitable candidates to meet the rigorous demands of present-day and next-generation devices and vehicles.

Correspondingly, Li-ion intercalation batteries have been dominant in the market with their high-performance characteristics. These batteries rely heavily on the use of nanomaterials and nanometer thick coatings.[20] As the global battery-making capacity is set to double by 2021, waves of disposed batteries will arrive in the near future. Assessments indicate that the electric car stock will be between 9 million to 20 million by 2020,[21] generating lithium ion battery wastes about 120–190 thousand tons globally.[22-23]

While these TMO nanomaterials are being produced and used in increasing abundance, there is rising concern regarding the consequences of introducing large amounts of these materials into the environment. With higher abundance comes an increased chance of nanomaterials entering the environment and coming into contact with unicellular and multicellular organisms. As the toxicity mechanism of nanomaterials may vary fundamentally from their bulk material counterparts due to specific nanoparticle properties, the environmental consequences of these materials need to be elucidated directly and kept in mind as new materials are developed. In particular, given these unknown biological consequences,[24] developing a fundamental understanding of molecular interactions occurring at this interface, commonly referred to as the nano-bio interface (where nanotechnology meets biology), is the main focus of this thesis.

1.2. Importance of Surface Chemistry

Surfaces and interfaces define the boundary between a material and its surrounding environment. At the molecular level, surface atoms have a different chemical environment (i.e. fewer nearest neighbors) from those in bulk.[25-26] This difference in chemical environments leads

to dissimilar chemical behavior; thus, surface chemistry plays an important role in understanding the chemical processes that occur in complex environments with a wide variety of practical applications, such as energy conversion,[27] heterogeneous catalysis,[28] and nanotechnology[29] and environmental protection.[30]

When nanomaterials encounter cells, the surface of the nanoparticles and the surface of the cellular membrane are the first points of contact. Therefore, understanding the molecular level interactions at the nano-bio interface can provide crucial insight into the mechanisms of nanotoxicity.[29, 31] The consequences of these dynamic interactions determine nanomaterial uptake, bioavailability, and mechanisms for bio-physicochemical reactions. Although the physicochemical properties of some biomolecules and materials may be well studied in the bulk, it is necessary to address processes occurring at the nano-bio interface, and thus, surface-specific techniques are needed to ultimately gain a complete picture of how both biomolecules and materials behave in the cellular environment. While the chemical composition, surface functionalization, and shape of nanomaterials are important characteristics,[29, 32-33] parameters of the suspending media, including the ionic strength, pH, and temperature, will determine the effective surface charge,[34] dissolution characteristics,[35] and aggregation.[36] Considering these variations in nanomaterials coupled with the range in properties of cell membranes — such as type of constituent phospholipids, proteins, surface charge, lipid density, and fluidity influencing the interactions — characterizing the nano-bio interface has proven to be challenging.[25, 29] Yet, understanding these interactions at the molecular level remains necessary for developing and enabling the sustainable use of emerging nanotechnologies.

1.3. Common Methods for Studying the Nano-Bio Interface

It is difficult to elucidate specific molecular level information regarding the interactions between nanomaterials and cell membranes, given the inherently complex nature of the surface chemistries.[29] To identify the roles that (1) nanomaterial surface charge and chemical composition and (2) membrane charge and constituents play in these interactions, this thesis uses idealized model membranes and metal oxide nanomaterials that are well characterized and allow control of chemical composition.

We focus on supported lipid bilayers (SLBs), motivated by recent explorations of the uptake and accumulation of various engineered nanomaterials, typically composed of metal oxide cores, by prokaryotic and eukaryotic cells, as well as their interactions with model cell membranes.[37-40] SLBs offer many advantages as idealized model membranes due to the ease of formation, stability on a solid support, applicability of a large range of compositions, and the degree of translational and rotational freedom of lipid molecules.[41-43] Consequently, SLBs have been used to mimic biological membranes to study applications in drug delivery,[44] biosensor development,[45-46] and toxicity assays,[47] as well as to study binding interactions[48-49] and basic membrane processes.[41, 50-51]

Nanoparticle-phospholipid bilayer interactions have been investigated through a host of analytical techniques, including electrochemical impedance spectroscopy (EIS),[52-53] attenuated total reflectance Fourier transform infrared (ATR-FTIR) spectroscopy,[54] x-ray photoelectron spectroscopy (XPS),[55-56] electron microscopy,[56-57] atomic force microscopy (AFM),[58] quartz crystal microbalance with dissipation monitoring (QCM-D),[59-61] and scanning probes.[57, 62] However, these methods lack inherent surface sensitivity, are not chemically specific, or require ultra-high vacuum (UHV) conditions.

Fluorescence microscopy, known for its versatility and specificity, has shown remarkable growth in the biological sciences and has been widely applied to study various biomolecules and their binding characteristics.[63-64] Although very useful, fluorescence microscopy relies on organic fluorophores, fluorescent proteins and fluorescent biomolecules. Such labels introduce complexity and only allow for probing the fluorescently labeled structures, and not their unlabeled biological counterparts.

Label-free optical sensing is a strong alternative to study nano-bio interactions without tags or labels. Surface plasmon resonance (SPR), a versatile technique for nanomaterial-based biosensing, has been used to probe biomolecules such as DNA and proteins with real time detection.[65-67] However, some challenges in SPR applications are its limitation to metal surfaces, low sensitivity to low molecular weight compounds, and lack of specificity.

1.4. Investigating the Nano-Bio Interface using Sum Frequency Generation

Vibrational sum frequency generation (SFG) spectroscopy is a powerful label-free method to provide structural and orientational information on molecules at surfaces and interfaces *in situ* in real time.[68-71] The theoretical basis for vibrational SFG spectroscopy will be detailed in Chapter 2. SFG spectroscopy has proven useful to study various oscillators directly at liquid/air and solid/liquid interfaces with surface specificity,[69, 72-73] including many important biologically-relevant interactions on surfaces and at buried interfaces. In particular, SFG spectroscopy has been used to probe phase transitions of lipid bilayers,[74-75] kinetics of lipid transbilayer movement,[76-78] bilayer asymmetry,[79] protein adsorption,[80-82] and DNA interactions,[83-84] as well as to characterize the structure of nanoparticle surfaces.[85-86] Many research groups have focused on monolayer surfaces,[68, 87-88] lipid bilayers with one or both leaflets deuterated,[89] or used D_2O as a solvent.[90]

Throughout this thesis, we extend the use of vibrational SFG spectroscopy to investigate SLB structure and orientation at aqueous/solid interfaces without using deuterated lipids or solvents. This method allows us to determine molecular level information at the nano-bio interface with surface specificity. This technique is particularly powerful when applied in conjunction with complementary methods for investigating nanomaterial–membrane interactions. This multi-technique approach is detailed in the following section.

1.5. The Center for Sustainable Nanotechnology

This thesis work is integral to the NSF funded Center for Chemical Innovation on Sustainable Nanotechnology (CSN), whose goal is to develop guidelines that will allow for predicting the biological responses induced by engineered nanomaterials in order to develop safe and sustainable nanotechnologies. The CSN is composed of scientists from thirteen U.S. institutions with diverse expertise.

Due to the complexity of the problem, the CSN uses a feedback loop mechanism where the studies on model systems, organisms, and computational methodologies inform one another to develop a fundamental understanding on nanomaterial toxicity and associated redesign strategies. In this way, nanomaterial interactions with whole organisms can determine the hazardous categories of nanomaterials, while experimental probes of simplified model systems and computational methods can provide a deeper understanding of the underlying chemical interaction mechanisms. Comparably, simple model systems can be used to identify the effect of each constituent and inform the consequences to the overall biological system. Equally important, the knowledge obtained from the computational studies can be integrated into experimental research, providing guidance to future experiments. This work, aimed at understanding interactions between

model cell membranes and nanomaterials, serves as a bridge between the computational approaches and whole organism studies.

The SFG work presented here is supported by other techniques including second harmonic generation (SHG) spectroscopy, scanning electron microscopy (SEM), QCM-D, time of flight secondary ion mass spectrometry (ToF-SIMS), XPS, fluorescence microscopy, and atomistic calculations to obtain mechanistic insights into nanomaterial interactions with biological interfaces.

1.6. Scope and Organization of this Thesis

The present work aims to understand the fundamental chemical interactions that occur at the nano-bio interface in order to facilitate the design of environmentally sustainable nanotechnologies. This thesis highlights key cases in which investigations of surface chemistry at the molecular level with a collaborative approach can lead to important information about nanomaterial transformations and identification of environmental behaviors that may be used in the future to predict the impact of nanomaterials based on their intrinsic properties.

The main focus of this work is to use vibrational SFG spectroscopy to probe the structural and orientational alterations in model membranes at the nano-bio interface *in situ*, in real time, with surface-specificity, and under environmentally relevant aqueous conditions. Complementary experiments that support the interpretation of the SFG results and provide additional insight into the nano-bio interactions will also be discussed. This thesis has been organized as follows:

Chapter 2 outlines the theoretical framework of SFG vibrational spectroscopy, the experimental setups and protocols used, and the methods used to form and characterize SLBs.

Chapter 3 focuses on structural changes in supported lipid bilayers upon interactions with metal oxide nanomaterials of lithium intercalation compounds. The research presented in this

chapter explores the origins of nanomaterial-induced membrane asymmetry by employing vibrational SFG spectroscopy in the C–H stretching region.

Chapter 4 investigates how electrostatics and ion dissolution impact the interaction between nanomaterials of lithium intercalation compounds and supported lipid bilayers. This work demonstrates a possible avenue for redesign strategies that mitigate noncontact interactions between nanomaterials and biological interfaces, facilitating the design of new energy storage materials with reduced environmental impacts.

Chapter 5 reports vibrational SFG spectra in which the C–H stretches of lipid alkyl tails in fully hydrogenated single- and dual-component supported lipid bilayers are detected along with the O–H stretching continuum from water molecules located above the bilayer. The ability to probe hydrogen bond networks over SLBs, presented in this chapter, holds the promise of opening paths for understanding specific and non-specific interactions at the nano-bio interface.

Chapter 6 reports lipopolysaccharide-incorporated supported lipid bilayers, in an attempt to move towards more biologically relevant SLBs and concludes the thesis.

CHAPTER 2

Sum Frequency Generation Spectroscopy to Investigate the Nano-Bio Interface

Portions of this chapter are reproduced in part
with permission from the American Chemical Society:

Doğangün, M.; Hang, M. N.; Troiano, J. M.; McGeachy, A. C.; Melby, E. S.; Pedersen, J. A.; Hamers, R. J.; Geiger, F. M. *ACS Nano* **2015**, *9* (9), 8755-8765.

Doğangün, M.;[#] Ohno, P. E.;[#] Liang, D.;[#] McGeachy, A. C.; Be, A. G.; Dalchand, N.; Li, T.; Cui, Q.; Geiger, F.M. *J. Phys. Chem. B* **2018**, *122* (18), 4870–4879.

2.1. Brief Overview of Vibrational Sum Frequency Generation Spectroscopy

Vibrational SFG spectroscopy is a nonlinear optical technique wherein the response of the system to the incident electric field is not linearly dependent on the field strength. Vibrational SFG, utilized in this thesis, is created by the temporal and spatial overlap of a tunable infrared beam and a fixed visible beam in systems that lack an inversion center, such as at interfaces.[1-3] As a result, light at a frequency equal to the sum of the two incident frequencies is generated.[4-6] Figure 2.1 shows the energy level description of sum frequency generation. The intensity of the sum frequency light is resonantly enhanced when the frequency of the tuneable infrared beam coincides with a vibrational mode of the molecules at the interface.[4, 7] This resonant enhancement provides spectral information on characteristic vibrational transitions.

Vibrational SFG spectroscopy allows for the characterization of molecules at interfaces and surfaces with high selectivity and sensitivity in a non-destructive manner.[8-10] By probing the characteristic vibrational modes, molecular structure and orientation can be deduced. This method can produce *in situ,* real time measurements of solid/vapor,[11-13] solid/liquid,[6-7, 10, 14] liquid/vapor,[14-16] and liquid/liquid interfaces.[1, 8, 14, 17] SFG spectroscopy has been used to probe the vibrational structures of biomolecules in the O–H stretching region (3800–3000 cm^{-1}),[18-23] N–H stretching region (3500–3100 cm^{-1}),[23-25] C–H stretching region (3100–2700 cm^{-1}),[8, 19, 21, 23, 26-27] O–D stretching region (2800–2200 cm^{-1}),[28-29] C–D stretching region (2250–2000 cm^{-1}),[30-31] C=O stretching region (1950–1500 cm^{-1}),[24, 32-34] PO_2^- stretching region (1200–1000 cm^{-1}),[35-36] and SO_3 symmetric stretching region (1150–950 cm^{-1}).[37] Throughout this thesis, we demonstrate how vibrational SFG spectroscopy in the C–H stretching region (Chapters 3-6) and O–H stretching region (Chapter 5) is utilized to gain molecular level insight into the nano-bio interface.

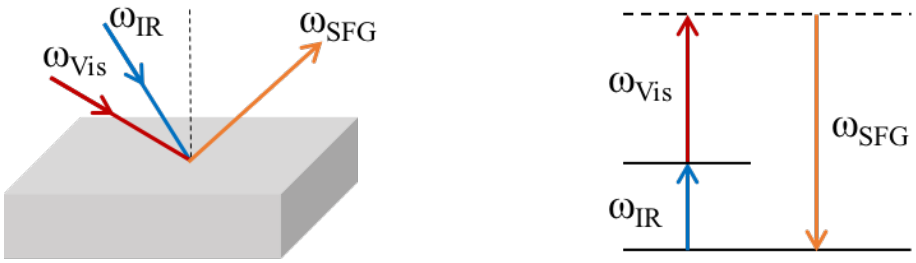

Figure 2.1. (A) Schematic of visible and IR beams producing an observable SFG signal. (B) Energy level diagram for vibrational SFG spectroscopy.

2.2. Sum Frequency Generation Spectroscopy Theory

Sum frequency generation (SFG) is defined by the second-order polarization response of a material due to the interaction of two high intensity electric fields, often generated by high energy pulsed laser beams.[4, 38] The theory of SFG has been explained in detail elsewhere and it is briefly outlined here.[1, 3, 6, 38-39]

Nonlinear optical responses are commonly described by the induced polarization as a function of the applied electric field strength:

$$P(t) = \varepsilon_o \left(\chi^{(1)} E(t) + \chi^{(2)} E(t) E(t) + \chi^{(3)} E(t) E(t) E(t) \right) \quad (2.2.1)$$

where $\chi^{(1)}$, $\chi^{(2)}$ and $\chi^{(3)}$ are the linear, second and third order nonlinear susceptibilities, $P(t)$ is the polarization, and $E(t)$ is the electric field strength. SFG originates from the second order polarization.

The electric field $E(t)$ at an interface is expressed in terms of the two input laser beams with incident electric fields E_1 and E_2, and frequencies ω_1 and ω_2:

$$E(t) = E_1 cos(\omega_1 t) + E_2 cos(\omega_2 t) \quad (2.2.2)$$

Combining equations 2.2.1 and 2.2.2, the second order polarization can be expressed as:

$$P^{(2)}(t) = \varepsilon_o \chi^{(2)} \left(E_1 cos(\omega_1 t) + E_2 cos(\omega_2 t) \right)^2 \quad (2.2.3)$$

where $\chi^{(2)}$ is the second-order nonlinear susceptibility tensor describing the relationship between electric field and second order polarizability.[34] Equation 2.2.3 is expanded to

$$P^{(2)}(t) = \varepsilon_o \chi^2 \left[(E_1^2 + E_1^2) + \left(E_1^2 cos(2\omega_1 t) + E_2^2 cos(2\omega_2 t) \right) + E_1 E_2 cos\left((\omega_1 - \omega_2) t \right) + E_1 E_2 cos\left((\omega_1 + \omega_2) t \right) \right] \quad (2.2.4)$$

in which each term represents a different second-order nonlinear optical interaction. The first term in Equation 2.2.4 corresponds to optical rectification, the second term to second harmonic generation at each of the input frequencies, and the third term to difference frequency generation. The fourth term in Equation 2.2.4 corresponds to SFG, indicating the frequency of the SFG oscillates at $\omega_1 + \omega_2$, or ω_{SFG}. Thus, overlapping two incident beams in time and in space at the interface generates signal at the sum of the two incident frequencies:

$$\omega_{\mathrm{SFG}} = \omega_{\mathrm{Vis}} + \omega_{\mathrm{IR}} \tag{2.2.5}$$

and the nonlinear polarization of the SFG can be described as:

$$P^{(2)}_{\mathrm{SFG}} = \varepsilon_o \chi^{(2)} E_{\mathrm{Vis}} E_{\mathrm{IR}} \tag{2.2.6}$$

The intensity of the sum frequency signal, I_{SFG}, is proportional to the square modulus of the SFG component of second order polarization, which is proportional to the product of the effective second-order nonlinear susceptibility tensor, $\chi^{(2)}_{\mathrm{eff}}$ and intensities of the incoming beams:

$$I_{\mathrm{SFG}} \propto \left| P^{(2)}_{\mathrm{SFG}} \right| \propto \left| \chi^{(2)}_{\mathrm{eff}} \right|^2 I_{\mathrm{Vis}} I_{\mathrm{IR}} \tag{2.2.7}$$

where the susceptibility tensor depends on the orientational average of the transition dipole moments in the sample.[3-4]

The second order nonlinear susceptibility term has a resonant component, $\chi^{(2)}_{\mathrm{R}}$ and a non-resonant component $\chi^{(2)}_{\mathrm{NR}}$, which are associated by phase, φ:

$$\chi^{(2)} = \chi^{(2)}_{\mathrm{R}} + \chi^{(2)}_{\mathrm{NR}} e^{i\varphi} \tag{2.2.8}$$

The non-resonant term depends on the instantaneous polarizability of the surface molecules; while the resonant contribution depends on the number of SFG-active oscillators (N_{surf}) at a particular

resonance frequency multiplied by their molecular hyperpolarizability tensors $\langle\beta\rangle$, averaged over all molecular orientations:

$$\chi_{\mathrm{R}}^{(2)} = \frac{\mathrm{N_{surf}}}{\varepsilon_0}\langle\beta\rangle \propto \frac{\mathrm{A}_K \mathrm{M}_{IJ}}{\omega_{\mathrm{Vis}} - \omega_{\mathrm{IR}} - \mathrm{i}\Gamma_{\mathrm{Vis}}} \tag{2.2.9}$$

where A_K is the IR transition moment, M_{IJ} is the Raman transition probability, and Γ_{Vis} is the natural linewidth of the transition. Equation 2.2.9 clearly shows that SFG provides sensitivity to molecular structures when the incident IR beam is resonant with a vibrational mode that is both Raman- and IR-active. Due to the mutual exclusion principle, which states that a vibrational mode may be either IR-active or Raman-active in a centrosymmetric media, vibrational SFG spectroscopy is sensitive to surfaces and interfaces where inversion symmetry is inherently broken.[40] Within this thesis, we will focus on studies at aqueous/solid interfaces in the C–H stretching frequency region (2800–3200 cm^{-1}) in Chapters 3, 4 and 6, and the C–H and O–H stretching frequency regions (2800–3800 cm^{-1}) in Chapter 5.

2.3 SFG Experimental Setup

2.3.1 C–H Stretching Region

Following our previously published approaches,[41-44] the SFG experiments presented in Chapters 3, 4 and 6 were conducted using a regeneratively amplified Ti:Sapphire system (Spectra Physics, Spitfire) producing 800 nm pulses with an energy of 2.5 mJ/pulse, 1 kHz repetition rate, and 120 femtosecond pulse duration. Half of the beam was pumped into an optical parametric amplifier (OPA-800CF, difference frequency mixing, Spectra Physics) to produce an infrared (IR) beam in the C−H stretching frequency region (~3.4 μm, 140 cm^{-1} FWHM). The OPA output beam was directed through an IR filter (Newport Corporation, 2702-0271) and was focused onto the sample using a BaF_2 IR focusing lens (ISP optics, BF-PX- 200). The remaining 50% of the 800

nm beam was used as an upconverter beam, which was directed through two variable density filters (ThorLabs, NDC-50C-4), a home built delay stage with two gold mirrors, a narrow band pass filter (CVI, Melles Griot, F1.1-800.0-UNBLK-1.00), a half waveplate (Karl Lambrecht Corp., MWPAA2-12-700-1000), and was focused onto the sample using a plano-convex focusing lens. The IR and visible beams were overlapped in time and in space at the sample at 60° and 45° angles from the surface normal, respectively. The generated SFG beam was recollimated using an achromatic lens, and sent through a polarizer (ThorLabs, Glan polarizer, GL15), a half waveplate (Karl Lambrecht Corp., MWPAA2-12-400-700), a short pass filter (Edmund Optics, 45646), a long pass filter (Edmund Optics, 600 nm, 66054), a plano-convex focusing lens, and a notch filter (Kaiser Optical Systems, Inc., holographic notch-plus filter, HNPF-800.0-1.0). The SFG signal was detected with a charged coupled device (CCD) camera (Roper Scientific, 1340 × 100 pixels) connected to a 0.5 m spectrograph (Spectra Pro 500i Acton Research).

All SFG spectra were collected in the internal reflection geometry and the *ssp* polarization combination (*s*-polarized SFG, *s*-polarized 800 nm light, *p*-polarized IR light). Each SFG spectrum was recorded at the fused silica/SLB/H_2O interface with an integration time of 4 minutes and an average of five acquisitions. Following the pioneering approach by Esenturk and Walker,[15-16] each spectrum was taken at multiple IR center frequencies, in order to cover the frequency range of interest (3200-2700 cm^{-1}). All spectra were then background subtracted, calibrated to polystyrene peaks at 2850 and 3060 cm^{-1},[16, 45] and normalized to the non-resonant sum frequency signal of a gold substrate to account for the distribution of the IR intensity.[15, 46] All spectra were taken in triplicate.

2.3.2 Extension to the O–H Stretching Region

The SFG experiments described in Chapter 5 utilized a Ti:Sapphire laser system (Spectra Physics Solstice) producing 795 nm pulses with an energy of 3 mJ/pulse, 1 kHz repetition rate, and 120 femtosecond pulse duration. The optical set up is shown in Figure 2.2. The 795 nm beam was directed through a 90/10 beam splitter (CVI, BS1-800-90-1012-45P) and 90% of the beam was used to pump a TOPAS tunable optical parametric amplifier (TOPAS-C, Light Conversion) with a difference frequency generation (DFG) stage to generate a broadband tunable IR beam. The TOPAS output was directed through a longpass IR filter to eliminate the signal and idler beams, and the IR beam was focused onto the sample using a BaF_2 IR focusing lens with 200 mm focal length (ISP Optics, BF-PX-25-200). The remaining 10% of the 795 nm beam was used as a visible upconverter beam, which was directed through a variable density filter (ThorLabs, NDC-50C-4), and a home-built delay stage with two 3 mm thick gold mirrors (CVI, PW1-1025C) to achieve temporal overlap with the IR beam at the sample. The visible beam was then sent through a narrow band-pass filter (Andover Corp. 795 nm, 1.0 nm bandwidth), to obtain a spectral resolution of ca. 10 cm^{-1}, and an achromatic half-waveplate (Karl Lambrecht Corp., MWPAA2-12-700-1000) for polarization rotation. The visible beam was focused on the sample stage using an achromatic lens with 75 mm focal length (Edmund Optics, 32-325). The incident IR beam and the 795 nm beam were directed towards the optical substrate mounted on an xyz-sample stage at 60° and 45° from the surface normal, respectively. Due to refraction, the beams were incident at the substrate/water interface at approximately 38° and 30° for the IR and visible, respectively. At the sample, the incident visible pulse energy is kept at 3.0 μJ and the IR pulses are typically 8-15 μJ in the O–H and 15-25 μJ in the C–H stretching region. The output SFG beam was recollimated using an achromatic lens with 150 mm focal length (Edmund Optics, 32-494), and sent through a polarizer

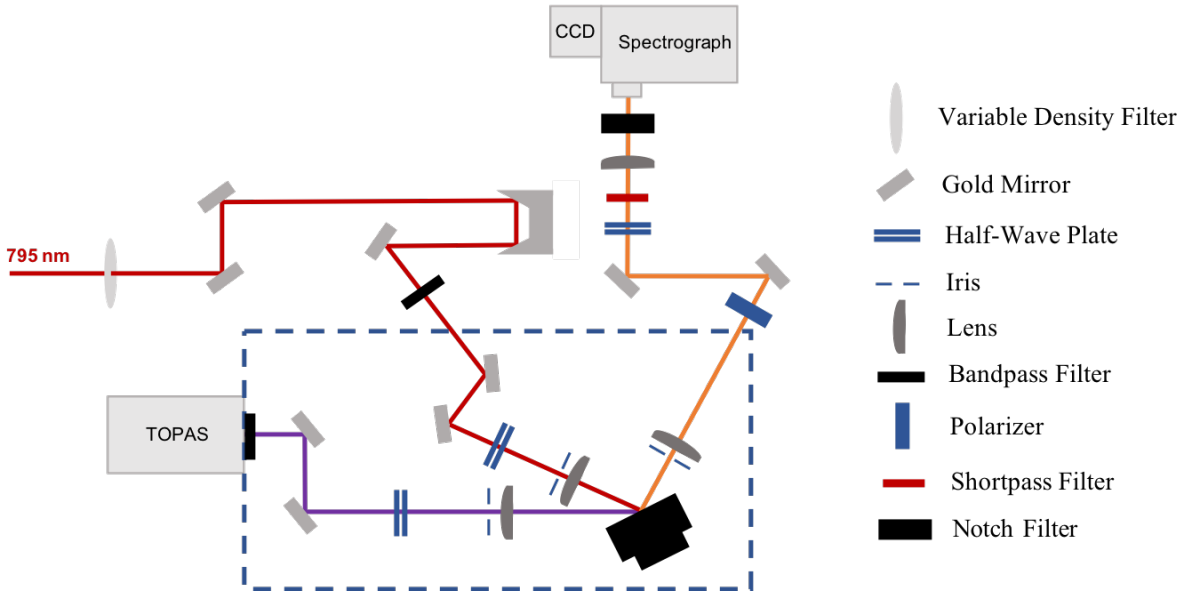

Figure 2.2. A schematic layout of the broadband laser setup utilized to study vibrational transitions in the C–H and O–H stretching regions.

(ThorLabs, Glan polarizer, GL15) and a half-wave plate (Karl Lambrecht Corp., MWPAA2-12-400-700) to control the SFG polarization for optimizing signal collection at the detector. The SFG beam was directed through a 700 nm shortpass filter (Edmund Optics, 47-291), a plano-convex focusing lens, and a notch filter (Kaiser Optical Systems, Inc., holographic notch-plus filter, 61193622) to remove excess 795 nm light and other light resulting from other nonlinear optical processes. A 0.5 m spectrograph (Acton SP-2558 Imaging Spectrograph and Monochromator) coupled to a liquid nitrogen cooled charged coupled device (CCD) camera (Roper Scientific, 1340 × 100 pixels) was used to detect the SFG signal. To direct beams, gold mirrors (Edmund Optics, 45606) were used in the incident IR and visible beam paths and silver mirrors (Edmund Optics, 49194) were used in the output beam paths. The set-up was enclosed with a Plexiglas box and was purged with dry house N_2 to avoid water absorption bands that appear in this stretching region.

Similar to the procedure described in the previous section, all the SFG experiments reported here were carried out in the internal reflection geometry, using the *ssp* polarization combination to probe the components of the vibrational transition dipole moments that are oriented along the surface normal,[15, 47] and in triplicate. SFG spectra were recorded at the SLB/aqueous interface with an integration time of 1 to 4 min with an average of 3 acquisitions. Spectra were recorded sequentially using an automated Python script to adjust the IR center wavelengths (2600-3600 nm) and spectrograph center wavelength (615-655 nm) to cover the frequency range of interest (2800-3800 cm^{-1}). Each SFG spectrum was recorded using nine different center IR wavelengths to cover the frequency range of interest, background-corrected to account for the optical scattering of the 795 nm upconverter beam and calibrated to the 2850 cm^{-1} and 3060 cm^{-1} (NIST 1921b) peaks of a 70 μm thick standard polystyrene film (International Crystal Laboratories).[15-16]

Each spectrum was normalized to the incident IR energy profile by recording a non-resonant spectrum from a gold film on CaF_2, following the procedure detailed by Liljeblad and Tyrode.[19] A gold spectrum is recorded (Figure 2.3a) for each IR center wavelength used in recording the sample spectrum (Figure 2.3b). The individual gold spectra are then smoothed with a Gaussian filter and truncated at a cutoff value of 5% of their maxima (Figure 2.3c). The individual sample spectra are truncated at the same positions as their gold counterparts (Figure 2.3d). This truncation prevents adding into the final spectrum noise generated at the detector from spectral regions where there was little to no incident IR energy present. After truncation, the individual gold (Figure 2.3e) and sample (Figure 2.3f) spectra are summed into the total, composite spectra. The final normalization occurs when the summed and truncated sample spectrum is divided by the normalized, summed and truncated gold spectrum.

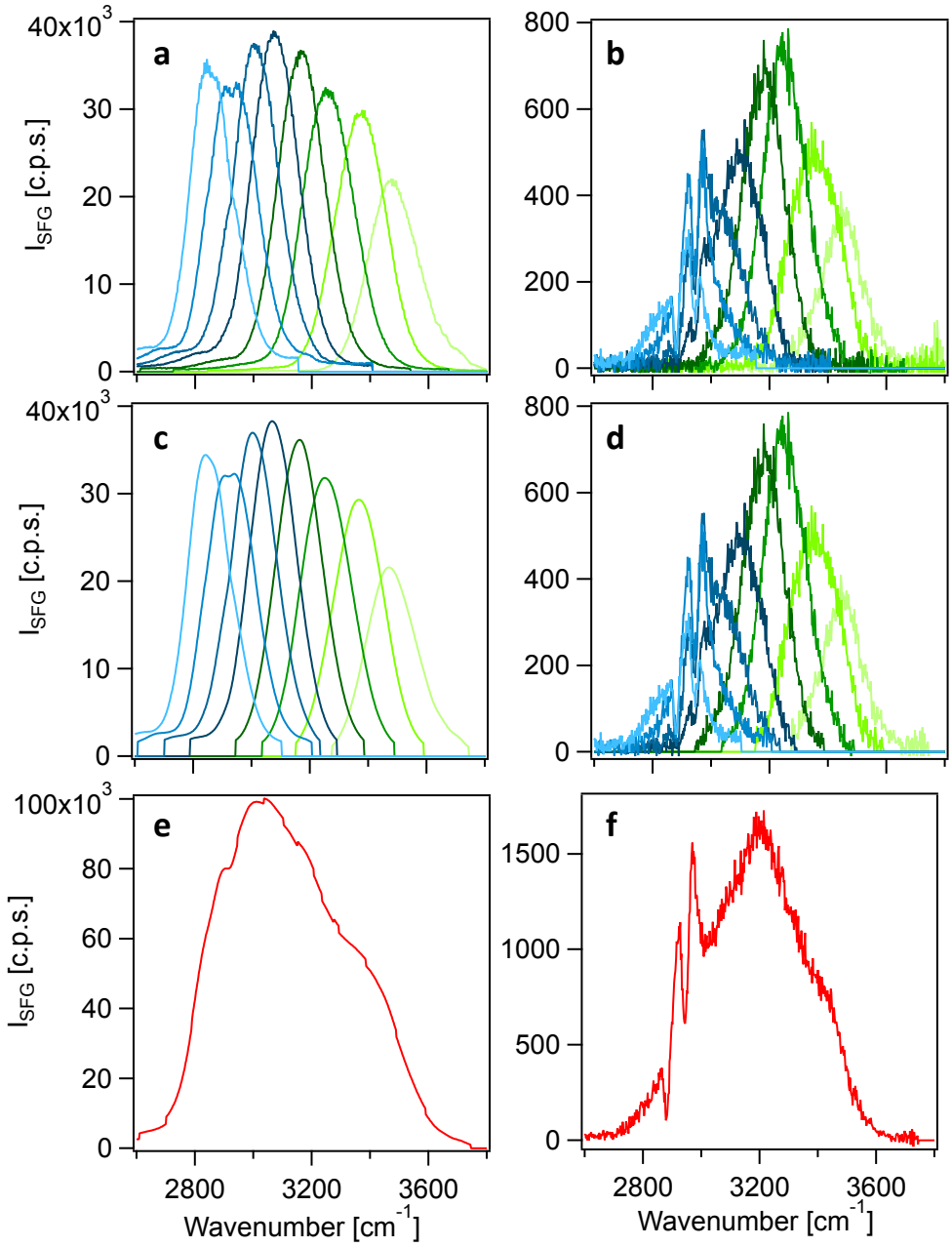

Figure 2.3. Gold normalization example (a) Individual non-resonant gold spectra (b) individual sample spectra (c) gold spectra smoothed and truncated at 5% of their maximum value (d) sample spectra truncated at positions determined by gold counterparts (e) summed gold spectrum (f) summed sample spectrum. Note the removal of baseline noise between (b) and (d) prior to the final summation.

2.4. Sample Preparation

2.4.1. Optical Windows

For the experiments described in Chapters 3, 4 and 6, IR-grade fused SiO_2 windows (ISP Optics, #QI-W-25-3) were used as solid substrates. The fused silica windows were cleaned in Nochromix solution (Godax Laboratories) overnight, rinsed with Millipore water (18 Ω·cm resistivity; Millipore), and dried with N_2. For the experiments reported in Chapter 5, CaF_2 windows (ISP Optics, #CF-W-25-3) were used as solid substrates due to optical adsorption from the fused SiO_2 substrate in the O-H stretching region. The CaF_2 window was soaked in a dilute aqueous solution of Alconox for 30 min, rinsed with Millipore water, sonicated in methanol (Fisher Scientific, HPLC-Grade) for 30 min, rinsed with Millipore water, and dried under a stream of N_2. Both fused SiO_2 and CaF_2 windows were plasma cleaned (Harrick Plasma Cleaner, PDC-32G, 18W) for 10 min immediately before use.

2.4.2. Flow Cell

All SFG spectra were collected using a home-built Teflon flow-cell with a volume of approximately 3 mL. The Teflon cell was sealed off with a Viton O-ring (Chemglass) and an optical window (ISP Optics, 1" diameter) was clamped onto the sample stage. For experiments described in Chapter 5, instead of the sample stage clamps, an aluminum face plate attached to Teflon cell was used to hold the optical window securely in place. A diagram of the flow cell is shown in Figure 2.4. The sample solutions were flowed through the reservoir across the interface with a variable flow rate controller at 1.5 mL/min. The CaF_2 window was sonicated in methanol (Fisher Scientific, HPLC-Grade) for 30 min, rinsed with Millipore water (18.2 Ω·cm resistivity; Millipore), and dried under a stream of N_2. The flow cell and PTFE tubing were sonicated in

methanol for 15 min, rinsed with Millipore water and dried with N_2. The flow cell and O-ring were plasma cleaned (Harrick Plasma Cleaner, PDC-32G, 18W) for 10 min immediately before use.

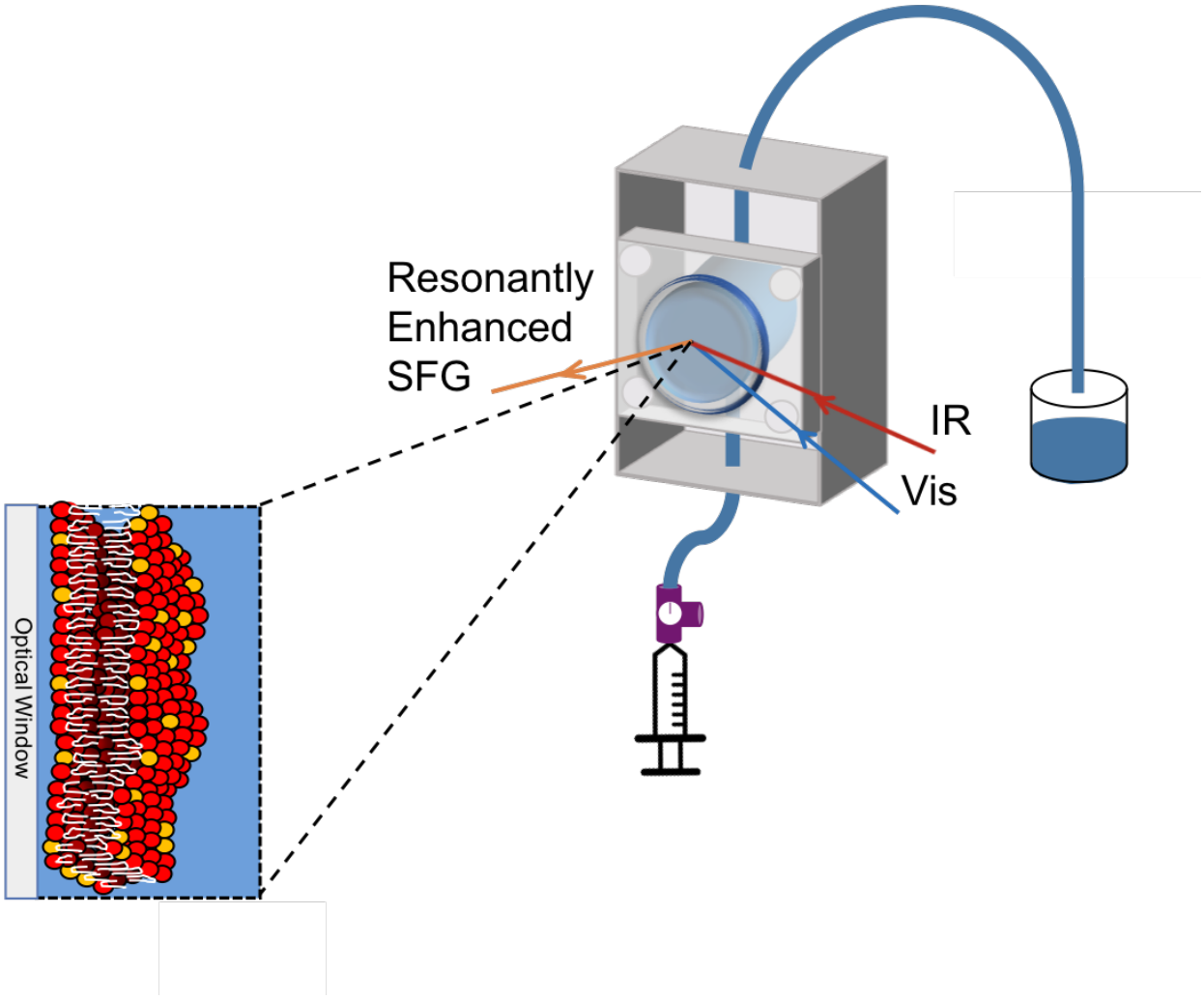

Figure 2.4. Schematic of the custom-built Teflon flow cell and experimental setup used for measurements at *aqueous*/solid interfaces.

2.4.3. Bilayer Formation

DMPC, DMPG, and DMPS were purchased from Avanti Polar Lipids and used without further purification. Pure DMPC lipids, and lipid mixtures containing 9:1 DMPC/DMPG, 9:1 DMPC/DMPS and 8:2 DMPC/DMPG (by mole) were dried under a stream of N_2 and rehydrated in 4 mL of a 0.01 M Tris buffer solution at pH 7.4, with 0.1 M NaCl and 0.005 M $CaCl_2 \cdot 2H_2O$. The lipids (0.5 mg/mL) were extruded using a mini-extruder kit (Avanti Polar Lipids) and a 0.05 μM polycarbonate membrane filter to form small unilamellar vesicles.[48] The extruded lipids were injected into the flow cell and lipid bilayers were formed on optical windows via the vesicle fusion method, which has been previously described.[49-50] Unless otherwise noted in the following chapters, all bilayers were formed in 0.01 M Tris buffer, 0.1 M NaCl, in the presence of 0.005 M $CaCl_2$ at pH 7.40 ± 0.03 and rinsed with 30 mL buffer of the same composition but lacking $CaCl_2$ to ensure removal of excess vesicles at the interface. The temperature (22 ± 2 °C) and the pH were held constant throughout the experiment.

2.5. Summary

Chapter 2 described the theoretical framework of SFG vibrational spectroscopy. The experimental setups and protocols used, as well as the methods used to form the SLBs are also detailed in this chapter. Additional experiments employing dynamic light scattering (DLS), time-of-flight secondary ion mass spectrometry (ToF-SIMS), second harmonic generation (SHG), scanning electron microscopy with energy dispersive X-ray analysis (SEM/EDX) and quartz crystal microbalance with dissipation monitoring (QCM-D) are included in the following chapters where applicable. Next, Chapter 3 will describe the use of SFG to probe the molecular order and orientation of SLBs upon exposure to nanomaterials of Li-intercalation compounds.

CHAPTER 3

Alteration of Membrane Compositional Asymmetry by $LiCoO_2$ Nanosheets

Portions of this chapter are reproduced in part
with permission from the American Chemical Society:

Doğangün, M.; Hang, M. N.; Troiano, J. M.; McGeachy, A. C.; Melby, E. S.; Pedersen, J. A.; Hamers, R. J.; Geiger, F. M. *ACS Nano* **2015**, *9* (9), 8755-8765.

3.1. Introduction

As discussed in Chapter 1, $LiCoO_2$ is among the most commonly used commercial cathode material in portable electronics.[1-3] Nano- and micro-formulated $LiCoO_2$, in particular, features high capacity and cyclability,[4-5] while a related material, lithium nickel manganese cobalt oxide (NMC), offers improved rate performance at a reduced cost.[6-8] $LiCoO_2$ and NMC nanoformulations are projected to be widely used in consumer electronics, all-electric/hybrid vehicle batteries, and in grid energy storage applications.[9-12] The redox potentials of these materials overlap with those of several biologically important redox pairs, suggesting that exposure to them may perturb cellular function.[13-14] Therefore, it is important to develop a molecular level understanding of how these nanomaterials interact with biological interfaces, including lipid membranes.[15-17] Chapter 3 makes a first step in this direction by using a molecular approach to probe the interaction of $LiCoO_2$ and NMC nanosheets with supported phospholipid bilayers. We find that some cobalt oxide nanoformulations cause alterations to the compositional asymmetry in our idealized model membranes that persist even upon rinsing, and that some of the nanosheets irreversibly interact with the membranes under the conditions of our experiments. This finding is important as alterations in the compositional asymmetry of membranes are known to signal multiple negative consequences for cellular processes, as discussed recently.[18-21]

Chapter 3 aims to address the molecular basis of the interactions of lithiated and delithiated $LiCoO_2$ nanosheets, as well as those composed of NMC, with single and binary component supported phospholipid bilayers under environmentally relevant pH and ionic strength conditions. This chapter presents results from SFG spectroscopy experiments that probe changes in the structure and chemical composition of supported lipid bilayers held at constant temperature, ionic strength, and pH. This study provide evidence that compositional asymmetry is induced between

the two leaflets of binary phospholipid mixtures near the gel-to-liquid crystalline phase transition temperature (T_m), upon addition of positively charged lithiated and near neutral delithiated $LiCoO_2$ nanosheets under isothermal conditions. 1,2-Dimyristoyl-*sn*-glycero-3-phosphocholine (DMPC) was selected as a model lipid since zwitterionic phosphocholine-derived lipids are among the most common phospholipids found in eukaryotic membranes.[22] 1,2-Dimyristoyl-*sn*-glycero-3-phospho-(1-*rac*-glycerol) (DMPG) was chosen because its T_m is comparable with that of DMPC and because the negatively charged headgroup allows investigations into the importance of electrostatics in the interaction. 1,2-Ditetradecanoyl-*sn*-glycero-3-phospho-L-serine (DMPS) was selected as a second anionic phospholipid because phosphatidylserine is among the most abundant anionic headgroups in eukaryotic cell membranes.[23] All lipids were purchased from Avanti Lipids and the molecular structures are shown in Figure 3.1.

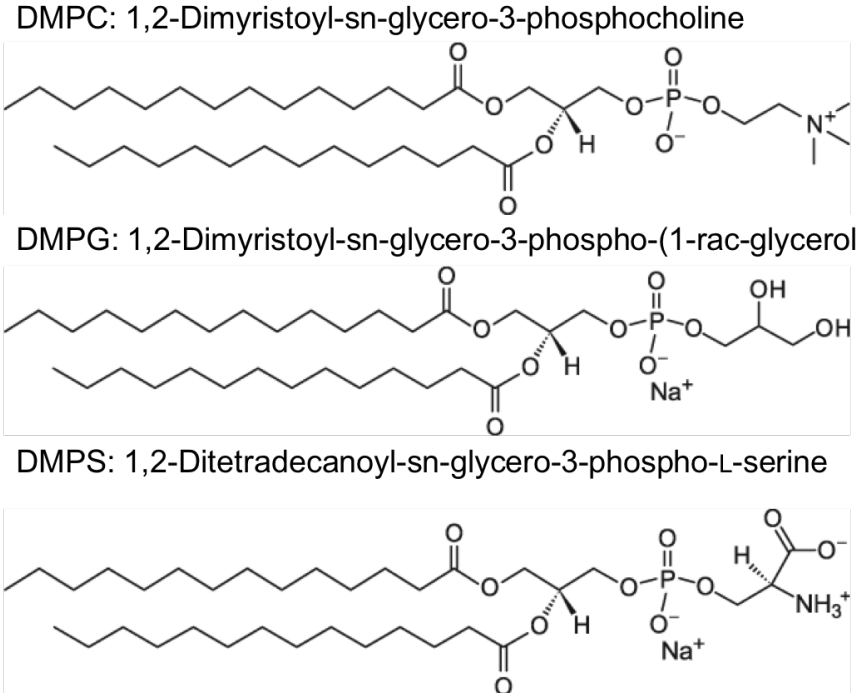

Figure 3.1. Molecular structure of the lipids used in this chapter.

3.2. Experimental Details

3.2.1. SFG Approach

The details of our SFG approach to study the nano−bio interface have been presented in Chapter 2 and in previously published work.[24-30] In the study reported here, the frequency of the incident femtosecond IR light is tuned to resonance with the C–H stretches of the system (2700−3200 cm^{-1}), as Liu and Conboy have previously shown that the terminal CH_3 groups of the lipid alkyl chains can be used as an intrinsic probe of the symmetry of the bilayer.[31] Here, we probe the SFG intensity due to the alkyl CH_3 symmetric stretch (ν_s) to evaluate the change in the bilayer asymmetry upon interaction with $LiCoO_2$, delithiated $LiCoO_2$, and NMC nanosheets.

3.2.2. Supported Lipid Bilayer (SLB) Preparation

Lipid bilayers from small unilamellar vesicles of pure DMPC and lipid mixtures containing 9:1 DMPC/DMPG, 9:1 DMPC/DMPS and 8:2 DMPC/DMPG (by mole) were formed on IR-grade fused silica windows (ISP Optics) *via* the vesicle fusion method, which has been previously described.[32-33] Experiments were carried out at room temperature (22 ± 1 ºC). All bilayers were formed in 0.01 M Tris buffer, 0.1 M NaCl, in the presence of 0.005 M $CaCl_2$ at pH 7.40 ± 0.03, and rinsed with buffer of the same composition but lacking $CaCl_2$. The temperature and the pH were held constant throughout the experiment. Buffer solutions were filtered through a 0.2 μm PVDF membrane (Acrodisc, LC 25 mm) before each experiment. Throughout this chapter, we use the word “bilayer” interchangeably with “supported lipid bilayer” or “SLB”.

3.2.3. Nanomaterial Synthesis and Characterization

$LiCoO_2$ nanosheets were synthesized by Dr. Mimi Hang in the Hamers group by adapting a molten-salt method previously reported.[34] Varying the degree of lithiation in $LiCoO_2$ while

maintaining comparable size, shape, and crystal structure is synthetically difficult. To achieve this, we used an electrochemical delithiation method, which is explained in previously published work.[35] Figure 3.2 shows the scanning electron microscopy (SEM) and transmission electron microscopy (TEM) images, indicating comparable size, shape, and crystal structure. The purified particles were further characterized by Dr. Mimi Hang in the Hamers group by X-ray photoelectron spectroscopy (XPS) and Raman spectroscopy. The characterization data are provided in previously published work.[35] NMC material was synthesized and characterized extensively as described elsewhere.[36]

The nanosheet suspensions ($LiCoO_2$, delithiated $LiCoO_2$, and NMC) were freshly prepared before each experiment by sonicating in a solution of 0.01 M and 0.1 M NaCl at pH 7.4 for 8 min, vortexed for 30 s, and introduced into the sample cell within 15 minutes of suspension. Unless indicated otherwise, nanosheet solutions at 5 mg/L concentration were used in the interaction experiments due to well-formed suspensions that were stable over the time period studied. An Ocean Optics Chem2000 UV-vis spectrophotometer was used for absorbance measurements. UV-vis measurements indicate only minor differences in the electronic properties of the nanosheets maintained in the buffer solution over the time period studied.[35]

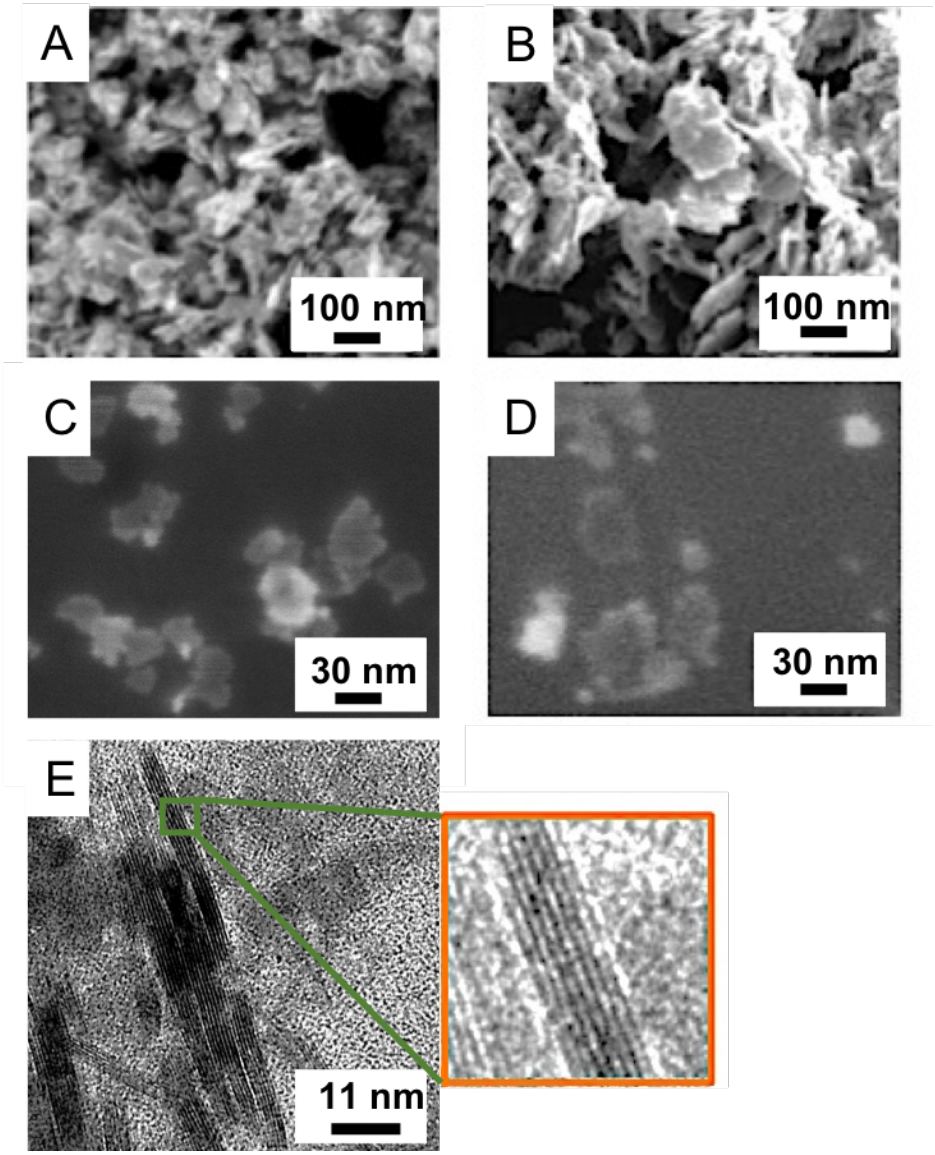

Figure 3.2. Scanning electron microscopy shows that the (A,C) sheet-like structure of $LiCoO_2$ is retained, (B,D) after electrochemical delithiation. (A,B) Clumps of the nanosheets (C,D) Individually resolved nanosheets. Synthesized $LiCoO_2$ is irregularly shaped and are approximately 30-50 nm in diameter. Transmission electron microscopy image (E) shows that the $LiCoO_2$ nanoparticles are of 7-8 atomic layers thick.

3.2.3.1. ζ-Potential measurements

ζ-Potential measurements were obtained using Malvern Zetasizer Nano ZS. Diffusion coefficients, hydrodynamic diameters, and apparent ζ-potentials, shown in Table 3.1, are the averages of three measurements, each consisting of 15 runs. For ζ-potential measurements, nanosheet suspensions (1 mL) were transferred into a clear, disposable folded capillary cell (Malvern Instruments, part no. DTS1060). Under the conditions of our experiments lithiated and delithiated $LiCoO_2$ nanosheets possessed ζ potentials of +12.9 ± 0.6 and +0.5 ± 1.2 mV, respectively (Table 3.1). We note that the $LiCoO_2$ and the delithiated $LiCoO_2$ nanosheets suspended in ultrapure water exhibit ζ-potentials of −21.7 ± 1.2 and −19.2 ± 0.9 mV, respectively, whereas Table 3.1 shows the ζ-potentials for nanosheets suspended in the buffer solution at pH 7.4. This difference is assumed to be due to the surface-active nature of the Tris cation, which has been previously recorded to be present at silica and bilayer surfaces.[33] The NMC material is associated with a ζ-potential of −19.5 ± 1.4 mV under the conditions of our experiments.

Table 3.1. Diffusion coefficients, Estimated Z-average hydrodynamic diameters ($d_{h,z}$),[a] and Apparent ζ-potentials for Fresh Suspensions (5 mg/L) of Lithiated and Delithiated $LiCoO_2$ Nanosheets and NMC Nanosheets in 0.01 M Tris buffer and 0.1 M NaCl at pH 7.4.

	diffusion coefficient (μm²/s)	**$d_{h,Z}$ [a] (nm)**	**apparent ζ-potential (mV)**
$LiCoO_2$ nanosheets	0.65 ± 0.08	760 ± 79	+12.9 ± 0.6
delithiated nanosheets	0.38 ± 0.02	1320 ± 55	+0.5 ± 1.2
NMC nanosheets	0.96 ± 0.23	536 ± 155	−19.5 ± 1.4

[a] Estimate assumes spherical particles.

3.2.4. Time-of-Flight Secondary Ion Mass Spectrometry (ToF-SIMS)

A Phi Trift III ToF-SIMS was used for trace detection, specifically to identify lithium. The high-energy pulsed metal ions were used to bombard the sample surface which causes the emission of secondary elemental ions from the surface. The detailed description of instrumentation can be found elsewhere.[37] A 15 keV liquid metal (Ga^+) ion gun (LMIG) with a spot size of 100 μm was used to desorb ions from the uppermost layers of a sample within an ultrahigh vacuum environment. Silica substrates were cleaned with methanol, rinsed with ultrapure water, and plasma cleaned for 5 min prior to bilayer exposure. The experiments were carried in a similar flow cell setup having 1 mL total volume and rinsed with 7 mL of buffer after the bilayer formation and nanosheet interaction. Substrates were then left to air-dry for approximately an hour before the measurements.

3.2.5. Second Harmonic Generation Spectroscopy (SHG) and Quartz Crystal Microbalance with Dissipation Monitoring (QCM-D) Measurements

Following the approaches described in our earlier work,[33] fellow graduate students Dr. Julianne Troiano and Alicia McGeachy employed SHG and Dr. Eric Melby from the Pedersen group performed QCM-D measurements to monitor the interfacial electronic and mass response of the bilayers in the presence and absence of nanosheets, respectively. There was no observed signal change upon the addition of the $LiCoO_2$ nanosheets.

3.2.6. Scanning Electron Microscopy

A Leo Supra55 VP scanning electron microscope was used to characterize $LiCoO_2$ nanosheet morphology. Specifically, these images were obtained using 1 kV incident electron energy with a standard in-lens detector located above the final Gemini lens in the column of the

SEM instrument. Scanning electron microscopy coupled with a Thermo Scientific UltraDry energy-dispersive X-ray spectroscopy (EDS) detector was used to characterize $LiCoO_2$ interaction with supported lipid bilayers from small unilamellar vesicles of pure DMPC and lipid mixtures containing 9:1 DMPC/DMPG formed on ultraflat SiO_2 wafers (200 nm ± 5 % thermal oxide). The supported lipid bilayer exposed to $LiCoO_2$ was prepared using the same method as previously described in the sample preparation. Ultraflat SiO_2 wafers (200 nm ± 5 % Thermal Oxide) were cleaned with ethanol, rinsed with ultrapure water and plasma cleaned for 5 min prior to bilayer exposure. An atomic force microscopy fluid cell (Bruker MTFML-V2) was used to prepare the substrates, and the cell was rinsed with 6 mL of buffer after the bilayer formation and nanosheet interaction. Substrates were then left to air-dry before the measurements. SEM images coupled with EDS were taken using 14 kV incident electron energy with the standard in-lens detector.

3.3. Results and Discussion

3.3.1. Nanosheet Attachment

SHG and QCM-D measurements showed no attachment of lithiated $LiCoO_2$ nanosheet to the supported lipid bilayers. While the SHG limit of detection for the particles under investigation here is not known, the QCM-D limit of detection is on the order of 1 ng/cm^2. We therefore proceeded to probe for the Li^+ ions of the $LiCoO_2$ nanosheets by using time-of-flight secondary ion mass spectrometry (ToF-SIMS). ToF-SIMS has been previously applied in structural analysis of lipid monolayers and bilayers.[38-39] Figure 3.3 shows the ToF-SIMS spectra of 9:1 DMPC/DMPG bilayers before and after interaction with 5 mg/L of $LiCoO_2$ and NMC nanosheet solution over the spectral region of interest (m/z 0-200). Following $LiCoO_2$ and NMC exposure and rinse, the spectrum shows the presence of a mass peak at m/z = 7 corresponding to the atomic mass of lithium.

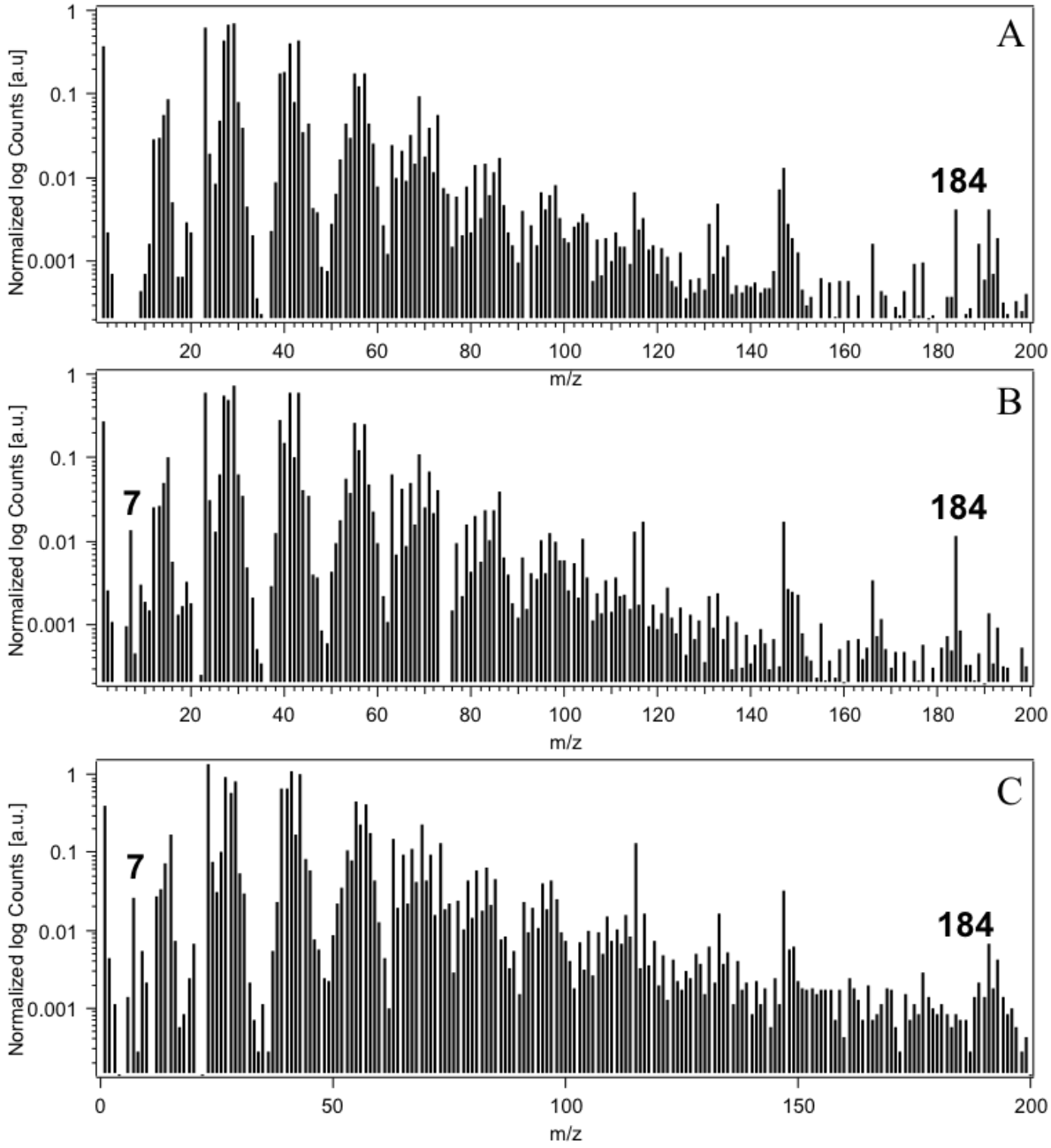

Figure 3.3. Normalized ToF-SIMS spectra of bilayers formed from 9:1 mixture of DMPC/DMPG lipids in 0.01 M Tris buffer, 0.1 M NaCl at 23 ºC, and pH 7.4 (m/z 0-200 range) (A) before the addition of nanosheets (B) upon exposure to 5 mg/L $LiCoO_2$ nanosheets and rinse with 0.01 M Tris buffer solution in the presence of 0.1 M NaCl at 23 ºC, and pH 7.4 (C) upon exposure to 5 mg/L NMC nanosheets and rinse with 0.01 M Tris buffer solution in the presence of 0.1 M NaCl at 23 ºC, and pH 7.4. Each spectrum is the average of three spectra taken on three different spots for a given sample, repeated for three different samples, for a total of nine spectra averaged for (A) and nine spectra averaged for (B) and three spectra averaged for (C). m/z = 184 corresponds to the phosphocholine headgroup and is marked as an indication to the presence of the bilayer.

To determine if the lithium peak was due to the attachment of Li^+ released from the nanosheets or the nanosheets themselves, ToF-SIMS spectra over the spectral region of interest (*m*/*z* 0-50) were acquired prior to the nanosheet exposure (Fig. 3.4A) and upon exposure of bilayer formed from 9:1 mixture of DMPC/DMPG lipids to 1.0 mg/L LiCl (Fig. 3.4B). Figure 3.4A shows no mass peak at *m*/*z* = 7, which indicates that no lithium was present at the bilayer surface prior to particle exposure. Control experiments carried out with 1.0 mg/L LiCl solution reveals no lithium present at the bilayer surface.

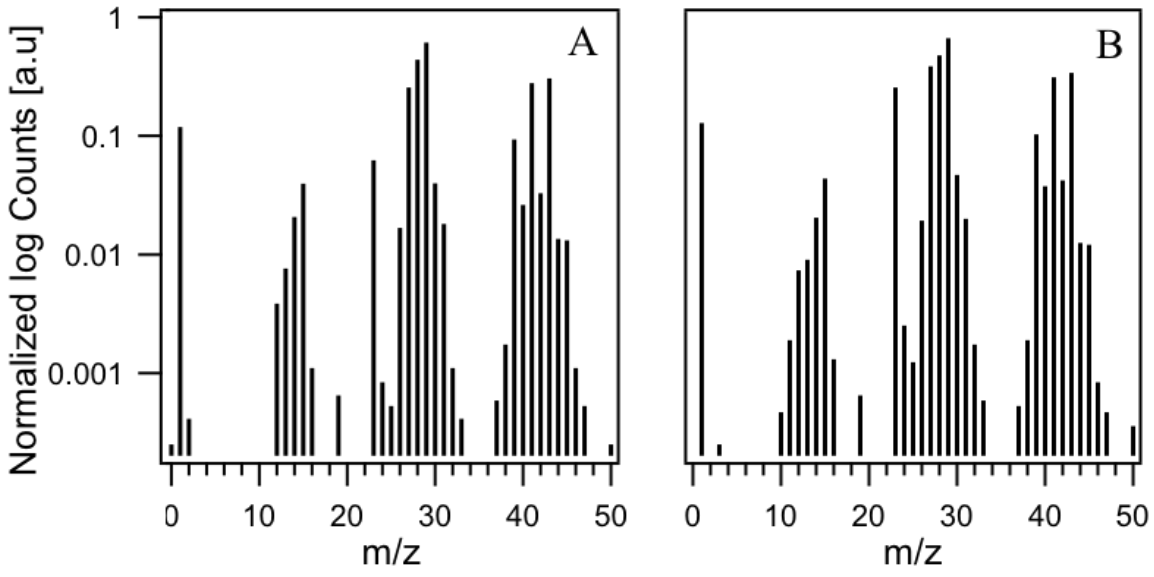

Figure 3.4. ToF-SIMS spectra of bilayers formed from 9:1 mixture of DMPC/DMPG lipids in 0.01 M Tris buffer, 0.1 M NaCl at 23 ºC, pH 7.4 (A) before exposure to LiCl (B) after exposure to 1.0 mg/L LiCl in 0.01 M Tris buffer with 0.1M NaCl at pH 7.4 and rinse with 0.01 M Tris buffer solution in the presence of 0.1 M NaCl at 23 ºC, and pH 7.4.

We also employed SEM/EDS to provide further evidence of nanosheets on the bilayer after rinsing. Figure 3.5 shows the SEM image and the corresponding EDS spectra on different spots of an ultraflat SiO_2 wafer with a bilayer prepared from a 9:1 mixture of DMPC/DMPG lipids. Following nanosheet exposure and rinse, localized regions of the bilayer contained $LiCoO_2$ nanosheets which were observed by SEM/EDS. Figure 3.5 shows that $LiCoO_2$ nanosheets have distinct flake-like structures, which can be easily distinguished from larger cubic structures of NaCl. EDS spectrum 1 in Figure 3.5 shows that the cubic structures exhibit Na (1.04 keV) and Cl (2.62 keV) signals in EDS, further confirming our ability to distinguish the difference between nanosheets and salt. EDS spectrum 2 in Figure 3.5 shows that in a region void of nanosheets or salt features, only Si (1.84 keV) and O (0.52 keV) signals originating from the underlying SiO_2 substrate are detected. EDS spectrum 3 in Figure 3.5 shows that the region of $LiCoO_2$ nanosheets exhibits Co signals (0.79 and 7.65 keV). The identity of the peak at 3.4-3.5 keV that is evident in the EDS spectra is not known. It is too far from Ca (3.69 keV) and K (3.312) to be either of those elements. Evidence from ToF-SIMS data presented in Figure 3.3 and SEM/EDS data in Figure 3.5 clearly show that our rinsing procedures do not remove the $LiCoO_2$ nanosheets.

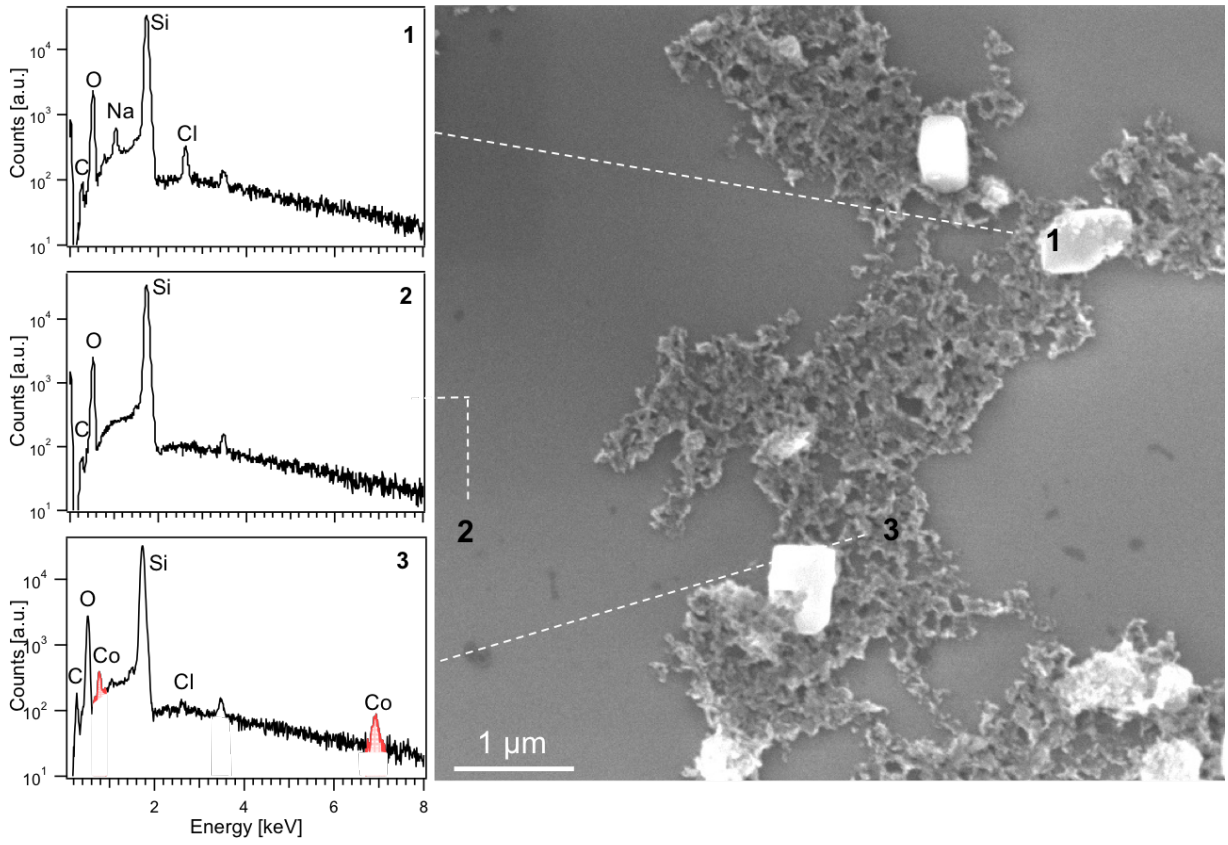

Figure 3.5. SEM/EDS image of a bilayer formed from 9:1 mixture of DMPC/DMPG in 0.01 M Tris buffer, 0.1 M NaCl at 23 ºC and pH 7.4 upon exposure to $LiCoO_2$ nanosheets and rinsing. The large particle ("1") is NaCl, ("2") is the ultraflat SiO_2 substrate, and the finer material ("3") consists of $LiCoO_2$ nanosheets.

3.3.2 $LiCoO_2$ Nanosheets Elicit Increases in SFG Signal Intensity from SLBs Made from 9:1 Mixtures of DMPC/DMPG Lipids

Having shown that $LiCoO_2$ nanosheets are likely to be present at the membrane surface, we applied SFG spectroscopy to study their impact on molecular order along the lipid carbon chains by using our recently described approach.[33] Specifically, we applied SFG to probe the structural changes among the methyl groups of the alkyl tails upon interaction with 5 mg/L of $LiCoO_2$. A representative SFG spectrum of a 9:1 DMPC/DMPG bilayer in 0.01 M Tris buffer in the presence of 0.1 M NaCl at pH 7.4 is shown in Figure 3.6A. As we reported earlier,[33] we typically observe three vibrational features centered at 2875, 2907, and 2950 cm^{-1} remain invariant with ionic strength between 0.001 and 0.1 M NaCl concentration. To probe the structural changes of the bilayer, we monitor the 2875 cm^{-1} peak, which can be attributed to the CH_3 symmetric stretch of the alkyl tails, as suggested by Liu and co-workers.[18, 40] Upon interaction with the $LiCoO_2$ nanosheet solution, the SFG spectrum of the bilayer shown in Figure 3.6B shows higher intensity at 2875 cm^{-1} relative to the signal of the bilayer before introduction of the nanosheets. The spectral differences were determined by calculating the area under the 2875 cm^{-1} peak.[35] This result is robust over five measurements and consistently shows SFG signal intensity differences of a factor of 2.0 ± 0.7.

We further investigated the effect of nanosheet concentration on the observed SFG responses. As detailed in the publication, 1 mg/L solution of $LiCoO_2$ does not significantly alter the SFG intensity at the 2875 cm^{-1} peak, while 10 mg/L solution increases the SFG signal intensity by a factor of 1.5 ± 0.6. The observed SFG responses are concentration-dependent with 5 mg/L concentration having the highest impact on the bilayer structure.

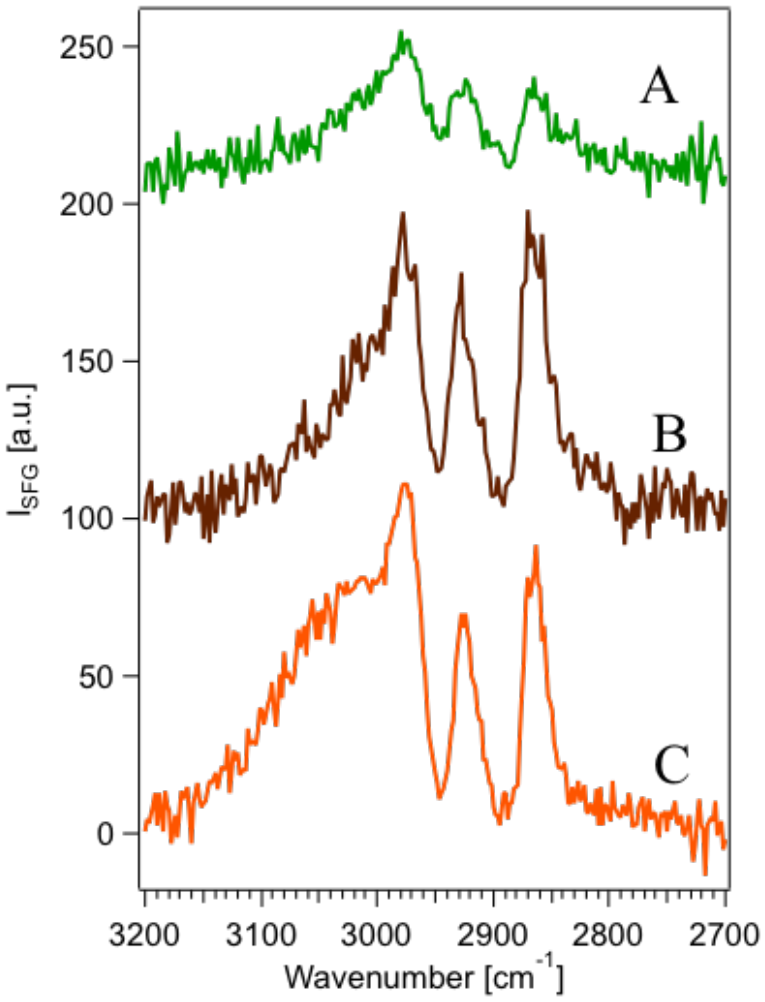

Figure 3.6. Representative ssp-polarized SFG spectra of bilayers formed from a 9:1 DMPC/DMPG in 0.01 M Tris buffer, 0.1 M NaCl at 23 ºC and pH 7.4 (A) before the addition of nanosheets, (B) upon exposure to 5 mg/L of $LiCoO_2$ nanosheets solution (C) upon exposure to 5 mg/L of delithiated $LiCoO_2$ nanosheet solution.

$LiCoO_2$ nanosheets have no C–H oscillators that would contribute to the SFG signal intensity. Therefore, changes in the signal intensity are due solely to the structural changes occurring at the bilayer surface upon nanosheet attachment. The measured SFG intensity depends on the number of SFG-active C–H oscillators and their orientational average (Eqs. 2.2.7 and 2.2.9, see Chapter 2). Provided that lipids do not leave the bilayer, probing the SFG intensity differences for a certain vibrational mode yields information about changes in bilayer symmetry. Single-component supported lipid bilayers give readily detectable SFG signals due to the fact that proximal leaflet borders the solid support and the distal leaflet borders the electrical double layer, extending into solution. Yet, more SFG signal intensity is obtained from bilayers containing upper and lower leaflets with different densities or lipid composition, as discussed by Anglin and Conboy.[41] The results shown here suggest that leaflet asymmetry may be induced upon addition of the $LiCoO_2$ nanosheets to the bilayers formed from the 9:1 mixture of DMPC/DMPG. Additional experiments to test this hypothesis are outlined below.

3.3.3. Delithiated $LiCoO_2$ Nanosheets Also Exhibit Strong SFG Responses from SLBs Made from a 9:1 Mixture of DMPC/DMPG Lipids

Delithiated $LiCoO_2$ nanosheets elicit similar SFG response as the $LiCoO_2$ nanosheets (Figure 3.6B). Although the delithiated nanosheets exhibit a near neutral ζ-potential (+0.5 ± 1.2) in contrast to the positive ζ-potential of $LiCoO_2$ (+12.9 ± 0.6 mV) at pH 7.4 (0.01 M Tris) in 0.1 M NaCl, adding them to the bilayers appears to elicit statistically similar increases in the SFG responses (factor of 1.7 ± 0.6 over three measurements).

Computational studies investigating the interactions between charged nanoparticles and lipid bilayers with zwitterionic headgroups suggest that nonspecific adsorption of charged nanoparticles onto phospholipid bilayers may lead to a change in the local phase (gel *vs* liquid

crystalline) of the bilayer.[42-44] According to these simulations, positively charged particles are predicted to raise the effective transition temperature of the bilayer by creating a less dense upper leaflet. This situation is attributed to the van der Waals interactions between the positively charged particles (Table 3.1) and the zwitterionic headgroups of the lipids. Wang and co-workers offered a similar interpretation using data obtained from fluorescence microscopy,[45-46] which may however have been influenced by the label-specific response modifications of supported lipid bilayers that have been well established for some spin labels by Conboy and co-workers.[41]

The gel-to-liquid crystalline phase transition temperatures for DMPC and DMPG are 24 and 23 ºC, respectively. In this study, the spectra are collected at 22 ± 1 ºC, where the gel and the liquid crystalline phases coexist.[18] However, it is not clear whether the observed response is a consequence of a phase transition. The observed increases in the SFG signal intensity upon nanosheet addition could also be due to bilayer asymmetry induced by rearrangement of the negatively charged DMPG lipids upon the addition of positively charged nanosheets. The portion of neutral or negatively charged nanosheets in the delithiated batch (recall the ζ-potential of +0.5 ± 1.2 mV, Table 3.1) may not interact with the bilayer, or the interaction may be dominated by entropic contributions from solvent reorganization and is the subject of future studies. The impact of the bilayer composition and the PG-specific effect on interaction will be discussed further in the following two sections.

3.3.4. SLBs Made from Pure DMPC Lipids Resist Apparent Asymmetry Induction

To determine the effect of the negatively charged PG group on the SFG response from the bilayers, we investigated the interaction of lithiated and delithiated $LiCoO_2$ nanosheets with bilayers composed of only zwitterionic DMPC lipids (no DMPG present). Before the addition of

the nanosheets, the pure DMPC bilayers exhibit vibrational features comparable to those obtained from the bilayers formed from the 9:1 mixture of DMPC/DMPG.

As shown in Figure 3.7A, the SFG intensity observed for the pure DMPC bilayer changes little upon exposure to $LiCoO_2$ nanosheets. This result indicates that, unlike the bilayers made from 9:1 DMPC/DMPG mixtures, the nanosheets do not induce structural change in the bilayer prepared from the purely zwitterionic PC lipids, at least as viewed by SFG spectroscopy under the conditions of our experiment, and no interaction occurs between the pure DMPC bilayer and the $LiCoO_2$ nanosheets. Although the bilayers remain intact in all cases, the observation that structural anisotropy, as measured by SFG spectroscopy, occurs only in the presence of DMPG indicates that the PG headgroup plays an important role in the interaction. Our experiment using bilayers prepared from pure DMPC (the zwitterionic lipids) effectively rules out a possible density difference between the distal and proximal leaflets as a sole mechanism for bilayer asymmetry, provided that the nanosheets are indeed present.

3.3.5. SLBs Containing DMPC/DMPS Lipids Elicit Similar Responses to SLBs Containing DMPC/DMPG Lipids

A similar response was observed when the DMPG lipids were substituted with DMPS lipids in bilayers (Figure 3.7C). $LiCoO_2$ nanosheets were observed to increase the SFG signal intensity from the 9:1 mixture of bilayers made of DMPC/DMPS lipids by a factor of 1.9 ± 0.5 over three measurements. In the plasma membrane, phosphatidylserine (PS) lipids are restricted predominately to the cytosolic leaflet, and the appearance of PS at the outer leaflet is associated with apoptosis.[47-49] Therefore, induced transbilayer movement of PS lipids from the inner to outer leaflet is particularly important in eukaryotic cellular membranes as it signals the macrophages to phagocytosize the cell.

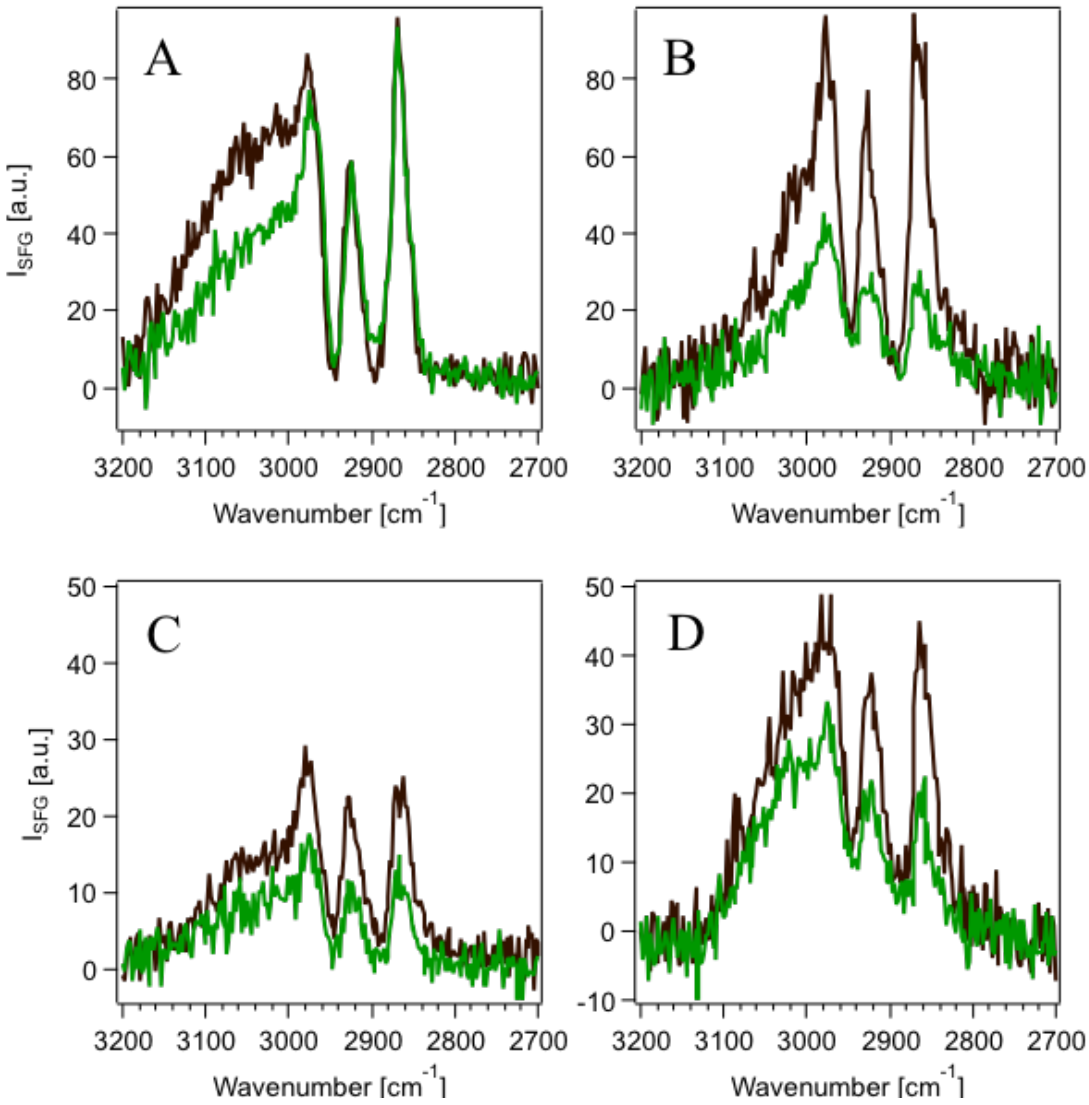

Figure 3.7. ssp-Polarized SFG spectra of bilayers formed from (A) 100% DMPC lipids, (B) 9:1 mixture of DMPC/DMPG lipids, (C) 9:1 mixture of DMPC/DMPS lipids (D) 8:2 mixture of DMPC/DMPG lipids, before (green) and after (brown) exposure to 5 mg/L of $LiCoO_2$ in 0.01 M Tris buffer, 0.1 M NaCl at 23 ºC and pH 7.4.

3.3.6. SLBs Made from an 8:2 Mixture of DMPC/DMPG Lipids Are Also Prone to Nanosheet-Induced Asymmetrization

Our findings presented in previous sections for the bilayers prepared from the 9:1 mixture of DMPC/DMPG and DMPC/DMPS led us to propose a mechanism in which the concentration of the negatively charged PG (or PS) lipids within each leaflet changes upon nanosheet addition. The resultant difference in the PG (or PS) concentration within the proximal *vs* the distal leaflet would then constitute enough of a compositional asymmetry that the SFG signal increases could be explained. To test this hypothesis, we increased the PG ratio in the bilayers. Figure 3.7D shows that once $LiCoO_2$ nanosheets are added, bilayers formed from 8:2 mixtures of DMPC/DMPG exhibit SFG signal intensity increases (a factor of 1.6 ± 0.3 over three measurements).

Anglin and Conboy previously showed that the zwitterionic PC and the phosphatidylethanolamine (PE) groups are susceptible to fast lipid flip-flop near the T_m.[41] It has also been shown that lipids having negatively charged PG headgroups are associated with activation energy barrier lower than that of PC- and PE-terminated lipids which brings the phospholipid headgroup in the hydrophobic interior of the bilayer,[50-51] thus making negatively charged DMPG lipids more prone to flip-flop when compared to zwitterionic lipids. It is our interpretation that the electrostatic attraction between the positively charged $LiCoO_2$ nanosheets and the negatively charged PG headgroups causes the DMPG lipids in the leaflet proximal to the fused silica support (proximal leaflet and away from nanosheets) to flip to the distal leaflet (close to nanosheets). This situation leaves the distal leaflet enriched in DMPG relative to the proximal leaflet, thus leading to compositional asymmetry in the bilayer and a rationale for the observed SFG signal intensity increases. A similar phenomenon of bilayer asymmetry induced by a surface-associated polypeptide was earlier demonstrated by Brown and Conboy,[40] and here we show that

the effect also occurs with lithiated and delithiated cobalt oxide nanosheets. Yet, there may be a limit to leaflet enrichment with the negatively charged DMPG lipids.

The nanosheet-induced mechanism of compositional asymmetry in the bilayers also explains why the SFG signal observed at around 2875 cm^{-1} does not return–on average–to the original intensity (factor of 1.4 ± 0.8 over eight measurements) after rinsing with nanosheet-free buffer solution (only three out of eight runs show that the SFG signal intensity returns back to the original bilayer intensity). This result may be attributable to the negative charges on the fused silica surface that may inhibit the negatively charged PG headgroups from returning to the proximal leaflet. Yet, the more likely reason for the disruption of lipid order to persist after rinsing is that the $LiCoO_2$ nanosheets are still present at the membrane following rinsing, as shown in the ToF-SIMS spectra in Figure 3.3 and the SEM image in Figure 3.5. The latter interpretation is relevant for biological cell membranes because they are not supported by silica substrates. Finally, we note that the SFG signal above 3000 cm^{-1}, which arises from the beginning of the O−H stretching continuum of interfacial water molecules, becomes stronger upon addition of the nanosheets. We attribute this response to differences in the interfacial water environment at the bilayer surface[52] before and after addition of the nanosheets, whose investigation is outside the scope of the present study.

3.3.7. NMC Nanosheets with Similar Crystal Structure Do Not Induce Apparent Asymmetry

As mentioned in the introduction, we also examined the interactions of more complex lithium intercalation compounds with the supported lipid bilayers. Specifically, we used $LiNi_{1/3}Mn_{1/3}Co_{1/3}O_2$, which is a commercially available cathode material. Unlike the previously examined metal oxide nanosheets, we found that the SFG responses from bilayers formed from our 9:1 mixture of DMPC/DMPG lipids at the H_2O (0.1 M NaCl, 0.01 M Tris buffer, pH 7.4)/silica

interface are invariant with bilayer exposure to 5 mg/L of NMC nanosheets (Figure 3.8C, measurements made within 15 min of suspending the nanosheets). Although the NMC nanosheets are similar to the other lithium intercalation compounds in shape and crystal structure,[36] their ζ-potentials (−19.5 ± 1.4 mV) suggest that these nanosheets carry a negative surface charge. If the NMC nanomaterial were to attach to the 9:1 DMPC/DMPG bilayers, then the negatively charged DMPG lipids would avoid Coulomb repulsion by moving from the distal (close to NMC nanomaterial) to the proximal (close to solid support) leaflet, due to the negative charge of the SiO_2 substrate. This suggests that NMC does not interact with the 9:1 DMPC/DMPG bilayers under the solution conditions used in our experiments. To obtain additional insight on the possible environmental impact of NMC nanosheet formulations, we examined the role of phosphate in the interaction. Phosphates are found in surface coatings of battery materials and are also present in aquatic environments.[16,53] Figure 3.8D shows that the spectral features are retained for the bilayers formed from a 9:1 mixture of DMPC/DMPG in the presence of 88.1 μM phosphate, which is common to biological growth media. NMC exposure (5 mg/L) does not alter the SFG response in the presence of phosphate either. The lack of changes in the SFG spectra upon NMC addition, with or without phosphate present, suggests that structural and compositional rearrangements within the supported lipid bilayers studied here are associated with high energy barriers that are not overcome under the conditions of the experiments, or that NMC does not interact with the bilayer in the first place. For the former case, we caution that more work is needed to quantify the amount of NMC material at the interface, which is ongoing.

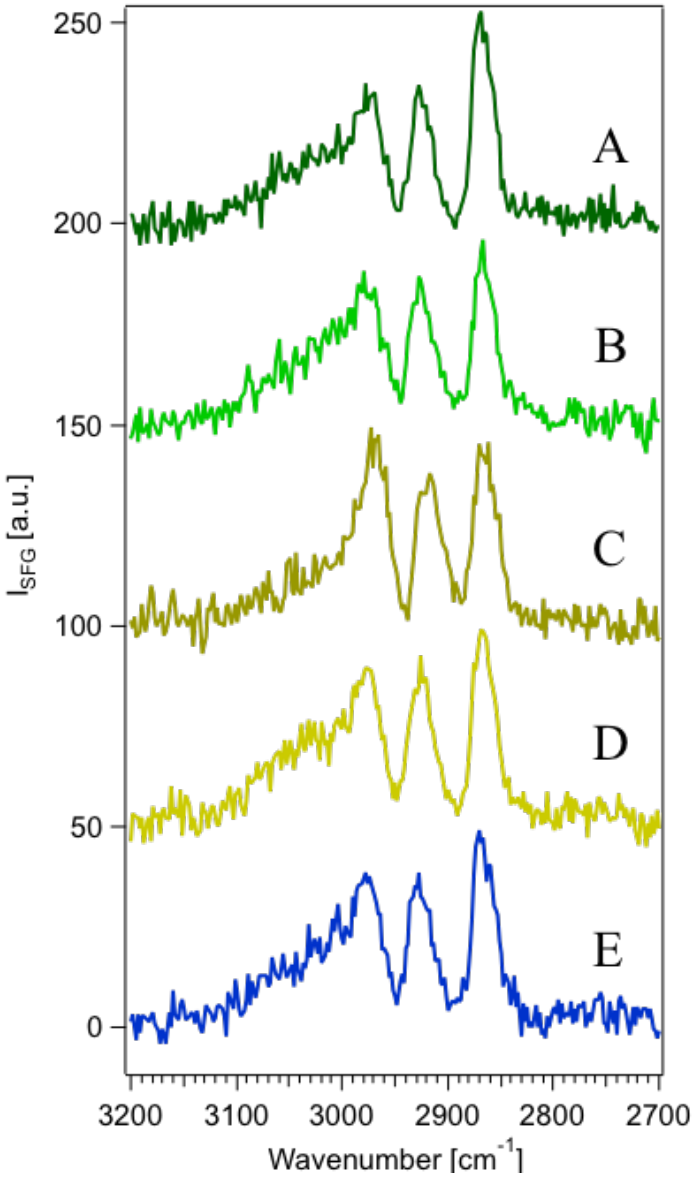

Figure 3.8. ssp-Polarized SFG spectra of bilayers formed from 9:1 DMPC/DMPG at 23 ºC, pH 7.4 (A) in 0.01 M Tris buffer, 0.1 M NaCl (B) in 0.01 M Tris buffer, 0.1 M NaCl, 88.1 µM Na_2HPO_4, (C) upon exposure of 5 mg/L of NMC nanosheets in 0.01 M Tris buffer, 0.1 M NaCl (D) upon exposure of 5 mg/L NMC nanosheets in 0.01 M Tris buffer, 0.1 M NaCl, 88.1 µM Na_2HPO_4 , and (E) after rinsing with 0.01 M Tris buffer, 0.1 M NaCl, 88.1 µM Na_2HPO_4. Spectra are offset for clarity.

3.4. Conclusions and Future Directions

In summary, we have presented experimental evidence for the induction of compositional asymmetrization upon interaction of supported lipid bilayers prepared from 9:1 and 8:2 mixtures of DMPC and DMPG with lithiated and delithiated $LiCoO_2$ nanosheets while maintaining 0.1 M NaCl concentration and pH 7.4 through the use of 0.01 M Tris buffer. We find that lithiated and delithiated $LiCoO_2$ nanosheets elicit increases in SFG signal intensity from 9:1 DMPC/DMPG bilayers, which we interpret to be due to the enrichment of negatively charged DMPG lipids in the bilayer leaflet closer to the positively charged $LiCoO_2$ nanosheets. Delithiated $LiCoO_2$ nanosheets also exhibit strong SFG intensity increases from 9:1 DMPC/DMPG bilayers. This enrichment process may be Coulomb-limited. Bilayers made from pure DMPC, in contrast, show no apparent asymmetry induction, as reported by SFG spectroscopy, isolating the role of the negatively charged DMPG lipids in inducing the attachment of these nanosheets and the concomitant bilayer asymmetrization, provided that the nanosheets are indeed present. Finally, we find that exposure of the bilayers to a related battery cathode material, NMC, does not result in changes to the SFG responses, independent of whether the common coanion phosphate is present.

Studying how emerging nanomaterials projected to be widely used in the near future interact with biologically relevant systems is key to understand the mechanisms of their interactions.[54] Doing so will enable the identification of possible negative consequences of introducing such materials at very large scales into the environment. Specifically, the insight that some cobalt oxide nanoformulations cause alterations to the compositional asymmetry in idealized model membranes may represent a first step toward assessing the biological consequences of their predicted widespread use. In addition, the findings presented herein contribute to molecular level insights that we argue are necessary for developing formulations enabling the sustainable use of

emerging nanotechnologies. Next, Chapter 4 will investigate how electrostatics and ion dissolution impact the interactions of $LiCoO_2$ nanosheet interactions with SLBs.

CHAPTER 4

Evidence for Considerable Metal Cation Concentrations from Lithium Intercalation Compounds in the Nano-Bio Interface Gap

Portions of this chapter are reproduced in part
with permission from the American Chemical Society:

Doğangün, M.; Hang, M. N.; Machesky, J.; McGeachy, A. C.; Dalchand, N.; Hamers, R. J.; Geiger, F. M. *J. Phys. Chem. C* **2017**, *121* (49), 27473–27482.

4.1. Introduction

In Chapter 3, we showed that lithium cobalt oxide ($LiCoO_2$) nanosheets induce alterations to the compositional asymmetry in two-component SLBs through electrostatic interactions. In Chapter 4, we further explore the charge interactions by altering the ζ-potential of nanosheets and changing the ionic strength of the solution. Yet, while many nanomaterials are poorly soluble in water, dissolution of some transition metal oxide nanoparticles, including those containing TiO_2, ZnO, and CuO, in aqueous environments may result in cellular toxicity due to the release of Ti^{2+}, Zn^{2+}, and Cu^{2+} ions into solution.[1-2] Indeed, previous work by Hang *et al*. demonstrated that the toxicity of nanoscale lithium nickel manganese cobalt oxide (NMC) to the Gram-negative bacterium *Shewanella oneidensis* MR-1 arises from the incongruent release of transition metal ions (specifically Ni^{2+} and Co^{2+}) into solution, as opposed to the nanoparticles themselves.[3] Specifically, that study showed that Co^{2+} significantly delayed the onset of exponential growth at sub mg/L concentrations, while Li^+ had no effect on bacterial growth.[3] For simultaneous exposure to both Li^+ and Co^{2+}, total oxygen consumption remained unchanged. Subsequent research investigated the impact of chemical composition of NMC on bacterial oxygen consumption,[4] and how the surface structure of $LiCoO_2$ nanosheets can be altered to enhance phosphate binding,[5] so as to decrease ion dissolution by an environmentally acquired surface coating.

In this Chapter, we aim to address the possible importance of ion dissolution from the $LiCoO_2$ nanosheets for the induction of compositional asymmetry in supported lipid bilayers (SLBs). To this end, we present results from vibrational SFG spectroscopy experiments sensitive to how the chemical composition of SLBs may or may not change upon exposure to aqueous Li^+ and Co^{2+} ions. This study provides empirical evidence for a locally high concentration of ions present at the bilayer-nanosheet gap and provide estimates for the dissolved ion concentrations at

the interfacial region, which may ultimately be helpful for to abating potential environmental impacts of nanomaterials used for energy storage.

4.2. Experimental Details

4.2.1. SLB Preparation

1,2-dimyristoyl-*sn*-glycero-3-phosphocholine (DMPC) and 1,2-dimyristoyl-*sn*-glycero3-phospho-(1-*rac*-glycerol) (DMPG) were purchased from Avanti Polar Lipids and used without further purification. Lipid bilayers from small unilamellar vesicles of pure DMPC as well as a lipid mixture containing 90 mol% DMPC and 10 mol% DMPG were prepared on 3mm thick IR-grade fused silica windows (ISP Optics) by the vesicle fusion method, as described in Chapter 3. Experiments were carried out at room temperature (22 ± 1 ^{o}C). All SLBs were formed in (1) 0.01 M Tris, 0.1 M NaCl in the presence of 0.005 M $CaCl_2{\cdot}2H_2O$, (2) 0.01 M HEPES buffer and 0.1 M NaCl in the presence of 0.005 M $CaCl_2{\cdot}2H_2O$, or (3) 0.01 M Tris, 0.001 M NaCl in the presence of 0.005 M $CaCl_2{\cdot}2H_2O$, at pH 7.40 ± 0.03, and rinsed with Ca-free buffer following bilayer formation.

4.2.2. Dynamic Light Scattering (DLS) of Nanosheets and Lipid Vesicles

Diffusion coefficients, electrophoretic mobilities, *z-A*verage hydrodynamic diameters (nm) and apparent ζ-potentials for fresh suspensions (5 mg/L) of $LiCoO_2$ nanosheets and vesicle solutions were determined using a Malvern Instruments Zetasizer Nano, with a He-Ne laser at 633 nm operating at a maximum of 5 mW. Electrophoretic mobilities determined from three measurements, each consisting of 20 runs, were converted to ζ-potential by the Smoluchowski model which simply assumes spherical particles.[6] We note that nanosheets have different aspect ratios that might lead to deviations in the absolute values. Reported *z-A*verage hydrodynamic

diameters are the averages of three measurements, each consisting of 15 runs. For DLS measurements, solutions (140 μL) were placed into low-volume, disposable cuvettes (Sarstedt, Part No. 67.758). For ζ-potential measurements, solutions (1 mL) were transferred into a clear, disposable folded capillary cell (Malvern Instruments, Part No. DTS1070).

Lipid vesicle stock suspensions were diluted to a concentration of 0.0625 mg/L in (1) 0.01 M Tris, 0.1 M NaCl, (2) 0.01 M HEPES buffer and 0.1 M NaCl, or (3) 0.01 M Tris, 0.001 M NaCl at pH 7.40 ± 0.03. Apparent ζ-potentials and *z*-average hydrodynamic diameters of small unilamaller vesicles used in this Chapter are shown in Table 4.1. Details of bilayer characterization have been reported in our previously published study.[1] $LiCoO_2$ nanosheets were synthesized by Dr. Mimi Hang in the Hamers group and $LiCoO_2$ nanosheet suspensions were freshly prepared before each experiment by sonicating in a solution of 0.01 M Tris or 0.01 M HEPES buffer in the presence of 0.1 M NaCl or 0.001 M NaCl, at pH 7.40 ± 0.03 for 10 minutes and vortexed for 30 seconds. DLS measurements were carried out within 10 min of suspending the nanosheets.

Table 4.1. Properties of small unilamellar vesicles (SUVs) of 9:1 mixtures of DMPC/DMPG lipids [a]

[NaCl] (M)	Buffering agent (0.01M)	Apparent ζ-Potential (mV)	*z*-Average Hydrodynamic Diameter (nm)
0.001	Tris	-18(2)	70(2)
0.1	Tris	-12(1)	82(1)
0.1	HEPES	-12(1)	83(1)

[a]All solutions were buffered to pH 7.4. Standard errors of the point estimates are given in the parentheses.

4.2.3. Nanosheet Imaging on SLBs

Leo Supra55 VP scanning electron microscope (SEM) coupled with a Thermo Scientific UltraDry energy-dispersive X-ray spectroscopy (EDS) detector was used to verify the attachment $LiCoO_2$ nanosheets on SLBs formed from unilamellar vesicles prepared from a 9:1 mix of DMPC/DMPG in Tris buffer on 5% thermal oxide ultraflat SiO_2 wafers.[7] In HEPES buffer, the nanosheet attachment to SLBs was probed by SEM (Hitachi SU8040) coupled with an Oxford Aztec X-max 80 EDS detector. The images were taken using 14 keV incident electron energy. Ultraflat SiO_2 wafers were cleaned with methanol, rinsed with Millipore water, and plasma cleaned for 10 min prior to bilayer exposure. A custom-made Teflon flow cell which has a volume of 1 mL with the tubing was used to prepare the substrates. Substrates were then left to air-dry before the measurements.

4.2.4. Metal Ion Dissolution from $LiCoO_2$ Nanosheets

A PerkinElmer Optima 2000 inductively couple plasma optical emission spectrometer (ICP-OES) was used to determine metal concentrations of the $LiCoO_2$ nanosheets in aqueous solutions held at 0.1M NaCl, 0.01M Tris and pH 7.4. To characterize metal ion release into the solution, triplicate sample suspensions of $LiCoO_2$ at 5 mg/L concentration was prepared. After 4 hours, the suspensions were centrifuged at 4,700g for 10 minutes to remove most of the $LiCoO_2$ nanoparticles in solution. The supernatants were then ultracentrifuged for 2 hours at 288,000g using a Beckman Coulter Optima Ultracentrifuge with a SW-41 Ti Rotor to ensure removal of any remaining $LiCoO_2$ nanoparticles. Concentrations of dissolved metal species in the resulting supernatants were measured by ICP-OES. Stock solutions of LiCl and $CoCl_2.6H_2O$ in 0.01 M Tris

buffer and 0.1 M NaCl at pH 7.4 at metal ion concentrations equivalent to those measured by ICP-OES were used as described in the Results and Discussion section.

4.2.5. Concentration of Metal Ions at the Nanosheet/SLB Interface

Second harmonic generation (SHG) $\chi^{(3)}$ spectroscopy is used to quantify the metal ion concentration at the interface. SHG studies reported here were carried out using the methods described previously,[8-9] using the s-in/all out polarization combination. Interfacial potential for the bilayers made from a mixture of 9:1 DMPC/DMPG lipids in 0.1M NaCl and 0.01 M Tris buffer at pH 7.4 was found using the Gouy-Chapman Equation[10-11]

$$\sigma = 0.1174\, I^{1/2} \sinh (19.46\, \Phi) \qquad \text{Eq. 4.1}$$

In our recent work by Troiano *et al*., the surface charge density (σ) was calculated to be – 0.11 ± 0.06 C/m^2 for the bilayer.[12] Thereon, the interfacial potential (Φ) is found to be – 0.177 V. By applying these values to the Eq. 4.1., the ratio of the adsorbed ion concentration to bulk ion concentrations, respectively, is found to be up to three orders of magnitude, for monovalent cations. This indicates that the Li^+ ion concentration at the nanosheet/bilayer interface is likely to be higher that the bulk solution concentration determined by ICP-OES measurements.

4.3. Results and Discussion

4.3.1. $LiCoO_2$ Nanosheet Interactions with SLBs Formed from 9:1 Mixtures of DMPC/DMPG Lipids Depend Critically on ζ-Potential at 0.1 M NaCl

We first examined the effect of buffer choice and ζ-potential on nanosheet-bilayer interactions (Table 4.2). While $LiCoO_2$ nanosheets suspended in 0.1M NaCl, 0.01 M Tris buffer exhibit positive ζ-potentials (+12.9 ± 0.6 mV),[7] they were found to exhibit negative ζ-potentials (−19.4 ± 1.8 mV) when suspended in solutions prepared using 0.1M NaCl and 0.01 M HEPES

buffer. This difference in ζ-potentials for the two different buffers is putatively attributed to the possibly surface-active nature of the Tris cation, which has been previously reported to be present at silica and bilayer surfaces.[7, 9] This finding also highlights the importance of buffer choice when studying oxide nanosheets at the nano-bio interface. Note that while the ζ-potentials of nanosheet suspensions show differences in the two different buffers, the ζ-potentials of the vesicles formed from the 9:1 mixture of DMPC/DMPG lipids used for preparing the supported lipid bilayers studied in this work remain invariant in the two buffers (Table 4.1).

Table 4.2. Apparent ζ-Potentials[a] for Fresh Suspensions (5mg/L) of $LiCoO_2$ Nanosheets in 0.001 M or 0.1 M NaCl and 0.01 M HEPES or Tris Buffer at pH 7.4 and Corresponding Observed Changes in SFG Signal Intensity Upon Exposure of SLBs Made from 9:1 Mixtures of DMPC/DMPG Lipids.

[NaCl] (M)	Buffering agent (0.01M)	Apparent ζ-Potential (mV)	ΔI_{SFG}
0.1	Tris	+12.9 ± 0.6	Increase by +2.0±0.7
0.1	HEPES	-19.4 ± 1.8	No change
0.001	Tris	-9.4 ± 0.8	No change
0.001	HEPES	-20.5 ± 0.3	Not measured

[a]Estimate assumes spherical particles.

We used SEM/EDS to provide evidence of $LiCoO_2$ nanosheet attachment to bilayers formed from the 9:1 mixture of DMPC/DMPG used in these experiments.[7] Figure 4.1A shows the SEM image and the corresponding EDS spectra of an ultraflat SiO_2 wafer with a bilayer prepared from a 9:1 mixture of DMPC/DMPG lipids in 0.1 M NaCl buffered at pH 7.4 using 0.01 M Tris buffer. Following nanosheet exposure and rinse, the EDS data reveals localized regions of the bilayer contained $LiCoO_2$ nanosheets, identified at 0.79 and 7.65 keV for cobalt, that are readily distinguished from Na (1.04 keV) and Cl (2.62 keV) signals originating from the cubic feature seen in the image and Si (1.74 keV) and O (0.52 keV) signals from the underlying SiO_2 substrate.

Switching from Tris to HEPES buffer would be expected to lead to some degree of Coulombic repulsion between the negatively charged bilayers and the $LiCoO_2$ nanosheets, which carry a negative potential in HEPES buffer.[9] Indeed, as shown in Figure 4.1B, the flake-like $LiCoO_2$ structures in HEPES buffer are present but in more confined regions compared to Tris. EDS data shows the presence of $LiCoO_2$ nanosheets in localized regions, identified at 0.78, 6.92 and 7.65 keV for cobalt. Signals originating from the cubic feature seen in the image are from Na (1.04 keV) and Cl (2.62 and 2.82 keV) and signals from the underlying SiO_2 substrate appear at 1.74 keV for Si and at 0.52 keV for O.

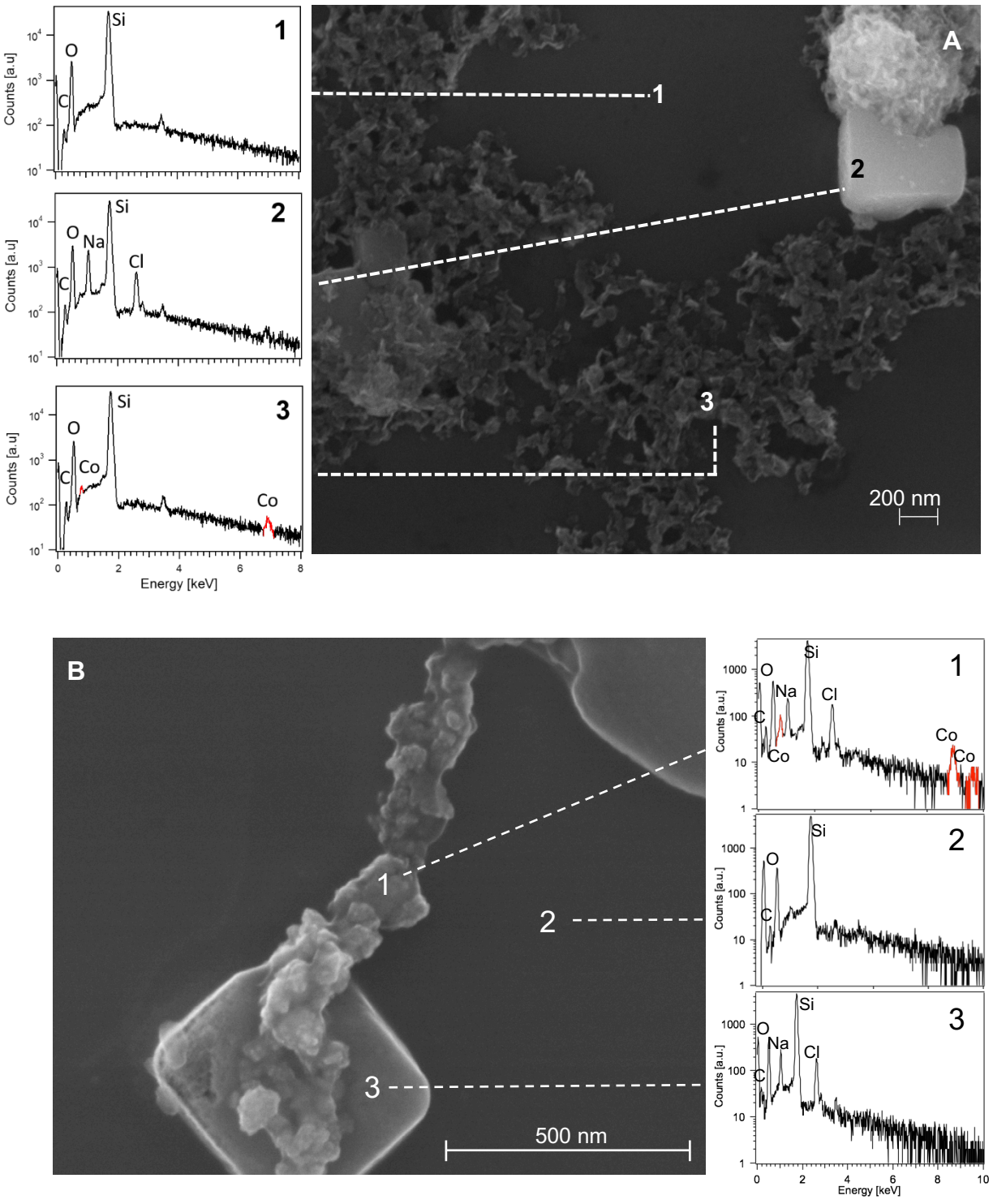

Figure 4.1. SEM images and EDS spectra from numbered areas indicated of bilayers formed from a 9:1 mixture of DMPC/DMPG in (A) 0.01 M Tris buffer, 0.1 M NaCl at 23°C and pH 7.4 upon exposure to $LiCoO_2$ nanosheets (5 mg/L) and rinsing, and (B) 0.01 M HEPES buffer, 0.1 M NaCl at 23°C and pH 7.4 upon exposure to $LiCoO_2$ nanosheets (5 mg/L) and rinsing.

To probe the nanosheet-bilayer interactions *in situ*, and under conditions of dynamically changing aqueous flow, we proceeded to record vibrational SFG spectra of the supported lipid bilayers before, during, and after exposure to the oxide nanosheets. Figures 4.2A and 4.2B show representative SFG spectra of 9:1 DMPC/DMPG bilayers maintained in 0.01 M Tris and in 0.01 M HEPES buffer, respectively, both in the presence of 0.1 M NaCl at pH 7.4. Before the addition of the $LiCoO_2$ nanosheets, the SLBs produce vibrational SFG spectra featuring comparable peak positions at *ca.* 2980, 2930, and 2875 cm^{-1}, where the 2875 cm^{-1} peak which is attributed to the CH_3 symmetric stretch of the alkyl tails and the other two features are presumably due to interference from the O−H stretches.[7, 13-15] The contributions from the O−H stretching region to the C−H stretching region will be discussed in Chapter 5.

We note that the relative signal intensities vary somewhat with choice of buffer. Unlike the previously examined $LiCoO_2$ nanosheets suspended in Tris buffer, which show SFG signal increases that are attributable to asymmetry induction in the membrane (Fig. 4.2A),[7] the SFG responses from the bilayer remain invariant upon exposing it to $LiCoO_2$ nanosheets suspended in 0.01M HEPES buffer (Fig. 4.2B). A similar lack of a signal intensity change was observed when NMC nanosheets, carrying a negative ζ-potential of -19.5 ± 1.4 mV in 0.01 M Tris buffer and 0.1 M NaCl were exposed to bilayers formed from 9:1 mixture of DMPC/DMPG at 0.1 M NaCl.[7] These two results suggest that negatively charged nanosheets do not induce compositional asymmetry in supported lipid bilayers formed from 9:1 mixtures of DMPC/DMPG under the solution conditions used in our experiments, a likely result of Coulombic repulsion, given that the bilayers studied here carry a negative surface potential under the conditions of our experiments.[9]

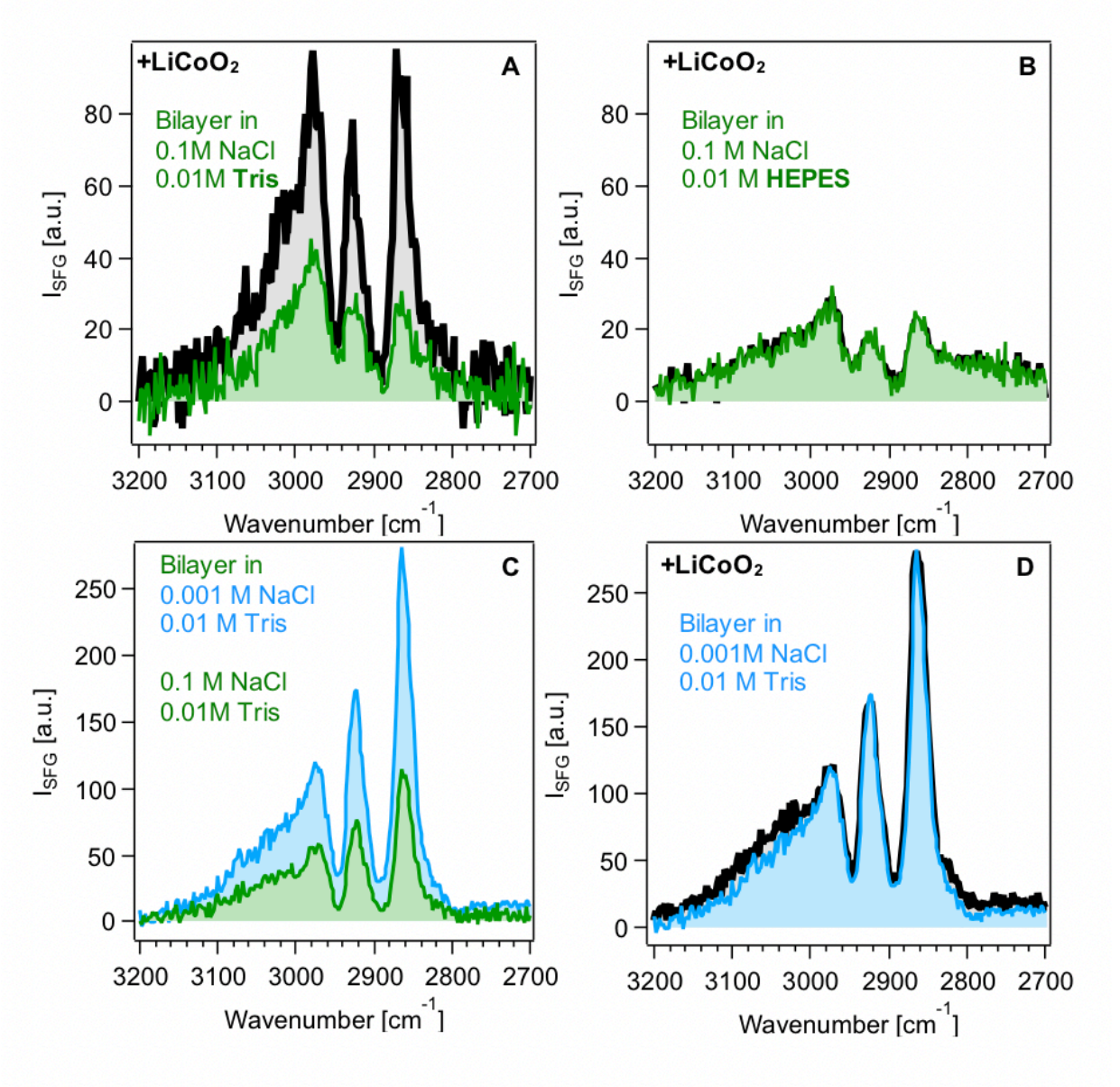

Figure 4.2. *ssp*-Polarized SFG spectra of bilayers formed from 9:1 mixture of DMPC/DMPG lipids at 22 °C and pH 7.4 in (A) 0.1 M NaCl, 0.01M Tris buffer before (green) and after (black) exposure to $LiCoO_2$ nanosheets (5 mg/L) (B) 0.1 M NaCl, 0.01M HEPES buffer before (green) and after (black) exposure to $LiCoO_2$ nanosheets (5 mg/L) (C) 0.1 M NaCl, 0.01 M Tris buffer (green), 0.01 M NaCl, 0.01M Tris buffer (blue) (D) 0.01 M NaCl, 0.01 M Tris buffer before (blue) and after (black) exposure to $LiCoO_2$ nanosheets (5 mg/L).

4.3.2. $LiCoO_2$ Nanosheets Do Not Disturb SLBs Formed from 9:1 Mixtures of DMPC/DMPG Lipids at Low Ionic Strength

To investigate the role of ionic strength on the oxide nanosheet-bilayer interactions, we rinsed bilayers formed in 0.1 M NaCl and 0.01 M Tris buffer with a solution of 0.001 M NaCl in 0.01 M Tris buffer and subsequently exposed them at that low ionic strength to $LiCoO_2$ nanosheets maintained in Tris buffer. Figure 4.2C shows that while the general lineshape of the SFG spectra obtained at high vs. low ionic strength in the presence of 0.01 M Tris buffer is invariant with salt concentration, the signal intensities tend to be higher at low salt concentration than at high salt concentration. Figure 4.2D shows that exposing the SLBs to $LiCoO_2$ nanosheets suspended in 0.001 M NaCl and 0.01 M Tris buffer at pH 7.4, conditions for which the nanosheet ζ-potential is -9.4 ± 0.8 mV (Table 4.2), leads only to insignificant SFG signal intensity changes. This outcome is attributable to the notion that despite reduced charge screening at low ionic strength, considerable charge-charge repulsion remains such that the oxide nanosheets cannot readily approach the bilayer to induce chemical asymmetry, as probed by SFG spectroscopy.

4.3.3. Dissolution of $LiCoO_2$ Nanosheets in Aqueous Solution Releases Li^+ and Co^{2+} Ions

Having established that $LiCoO_2$ nanosheets that carry a positive ζ-potential produce SFG signal intensity increases that indicate the induction of chemical asymmetry within supported lipid bilayers formed from 9:1 mixtures of DMPC/DMPG at 0.1 M NaCl, while those carrying a negative ζ-potential do not (even though they are still present at the bilayer, as evidenced by SEM, Fig. 4.1), we proceeded to further investigate the fundamental interactions that lead to chemical asymmetry in bilayers exposed to oxide nanosheets. Our prior work[7] established that bilayers prepared from purely zwitterionic lipids do not produce SFG signal intensity changes upon exposure to $LiCoO_2$ nanosheets under conditions of 0.1 M salt and 0.01 M Tris buffer, while those

prepared from mixes containing 10 mol% of the negatively charged lipids PS or PG do. This finding pointed to the importance of the lipids with negatively charged headgroups in the bilayer. Motivated by the extent of oxide dissolution reported for nanoscale lithium nickel manganese cobalt oxide by Hang *et al*.,[3] we asked whether the $LiCoO_2$ nanosheets studied in this present work could release metal cations directly into the membrane-nanosheet gap, where those metal cations (as opposed to the actual nanosheets) could interact with the lipids to produce the observed SFG signal intensity changes described here.

Incongruent oxide dissolution may release metal cations in amounts that depend on the intrinsic properties of the oxide (*e.g.*, chemical composition and particle size) as well as the aqueous solution conditions (*e.g.*, pH, temperature, ionic strength).[16] Under the conditions of our experiment (0.1 M salt, 0.01 M Tris buffer, pH 7.4, and room temperature), ICP-OES measurements (Table 4.3) carried out by Dr. Mimi Hang from the Hamers group show, for suspensions of 5 mg/L $LiCoO_2$ stirred for four hours, dissolved Li ions at 0.124 ± 0.002 mg/L and dissolved Co ions at 0.042 ± 0.001 mg/L. Table 4.3 also shows that the extent of dissolution is fairly comparable for conditions of 0.001 M salt and 0.01 M Tris buffer. Ion dissolution for the condition of using HEPES buffer is comparable to that of Tris buffer.

Given the above findings, any experiment testing whether the presence of dissolved ions from the $LiCoO_2$ nanosheets cause the observed SFG signal intensity increases produced by the bilayers upon exposure to the nanosheets should then start with sub-mg/L concentrations of Li and Co ions dissolved in 0.1 M salt solution maintained at pH 7.4 using 0.01 M Tris buffer. Controls for chloride and any minor changes in ionic strength would be provided by adding sub-mg/L amounts of NaCl to the 0.1 M salt solution while monitoring the SFG spectra obtained from the bilayers. The following two sections present the results from those experiments.

Table 4.3. Measured Concentrations of Ions Produced by Dissolution in a 5 mg/L Solution of $LiCoO_2$ Nanosheets.[a]

Buffer	Dissolved metal ion concentration (mg/L)			
	Li (mg/L)	Li (μM)	Co (mg/L)	Co (μM)
0.1 M NaCl, 0.01M Tris	0.124 ± 0.002	17.86 ± 0.29	0.042 ± 0.001	0.71 ± 0.01
0.001 M NaCl, 0.01M Tris	0.206 ± 0.001	29.68 ± 0.20	0.029 ± 0.001	0.49 ± 0.05
0.1 M NaCl, 0.01M HEPES	0.283 ± 0.004	40.77 ± 0.61	0.035 ± 0.004	0.59 ± 0.07

[a] The mean and standard deviation of three replicate samples are listed for the measured values.

4.3.4. Sub-mg/L Concentration of Aqueous Metal Ions Found in Bulk Nanosheet Solution Do Not Induce Apparent Bilayer Asymmetry from SLBs Formed from 9:1 Mixtures of DMPC/DMPG Lipids

As shown in Figures 4.3A and 4.3B, the presence of Li^+ and Co^{2+} ions at concentrations determined by ICP-OES to be relevant for $LiCoO_2$ nanosheet dissolution in high ionic strength does not produce significant SFG signal intensity increases in the spectra obtained from the bilayers. We further investigated possible combined ion effects by introducing a solution containing both Li^+ and Co^{2+} ions using the concentrations determined in the dissolution experiments. Figure 4.3C shows negligible changes in the SFG spectra upon exposing bilayers to aqueous solutions under those conditions as well. Controls shown in Figure 4.3D indicate no change in the spectral lineshape when adding even one mg/L NaCl to the aqueous solution.

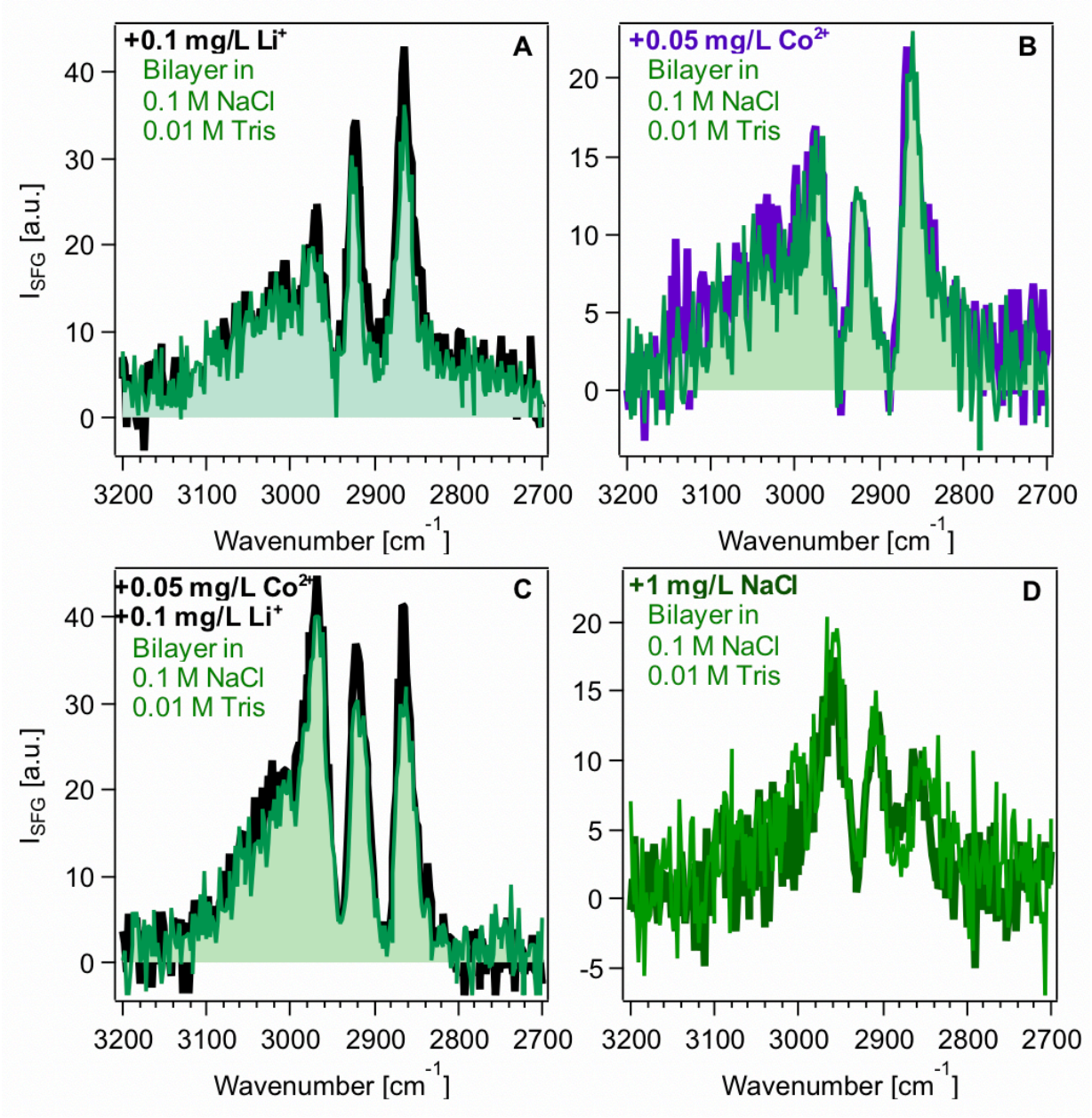

Figure 4.3. *ssp*-Polarized SFG spectra of bilayers formed from 9:1 mixture of DMPC/DMPG lipids before (green) and after exposure to (A) 0.1 mg/L Li^+ (black), (B) 0.05 mg/L Co^{2+} (purple), (C) a mixture of 0.1 mg/L Li^+ and 0.05 mg/L Co^{2+} (black), and (D) 1 mg/L NaCl (dark green), all in 0.01 M Tris buffer, 0.1 M NaCl, and at 22 °C and pH 7.4.

4.3.5. Elevated Concentrations of Aqueous Metal Ions Elicit Increases in SFG Signal Intensity from SLBs Formed from 9:1 Mixtures of DMPC/DMPG Lipids

Although ICP-OES measurements yield information about dissolved ion concentration in the solution phase, these concentrations do not necessarily correlate to the effective concentration of ions at the bilayer/nanosheet interface. We therefore exposed bilayers prepared from a 9:1 mixture of DMPC/DMPG to Li^+ and Co^{2+} ion concentrations 10 times above those determined in the nanosheet dissolution studies, at a total salt concentration of 0.1 M and at pH 7.4, maintained using 0.01 M Tris buffer. As shown in Figures 4.4A and 4.4B, the use of elevated ion concentrations indeed produced significant SFG signal intensity increases for the case of Li^+ and Co^{2+} ions. Again, these results are for solution conditions of 0.01 M Tris buffer and 0.1 M NaCl. This result is robust over three measurements.[17] Given the salt control (shown in Figure 4.3D), this outcome appears to point towards a role of ion specificity. The interaction appears to involve the negatively charged PG headgroup, as the introduction of 0.5 mg/L solution of Co^{2+} shown in Figure 4.4C respectively does not significantly alter the SFG signal intensity from bilayers composed of purely zwitterionic DMPC lipids, as shown in Figure 4.4C. Furthermore, Figure 4.4D shows that the increases in SFG signal intensity upon exposure to 0.5 mg/L Co^{2+} persist even upon rinsing.

Cation bonding to the backbone of peptides has been reported to depend on the hydration shell of the cation, with well-hydrated divalent cations showing stronger binding than weakly hydrated monovalent cations.[18] Similarly, the tendency of ions to interact with lipids in the bilayer membrane depends on the strength of their hydration shell,[19-20] with anionic lipids typically more prone to strong interactions with metal cations than zwitterionic lipids because of attractive Coulombic forces.[21] McLaughlin and coworkers showed that Co^{2+} forms strong complexes with

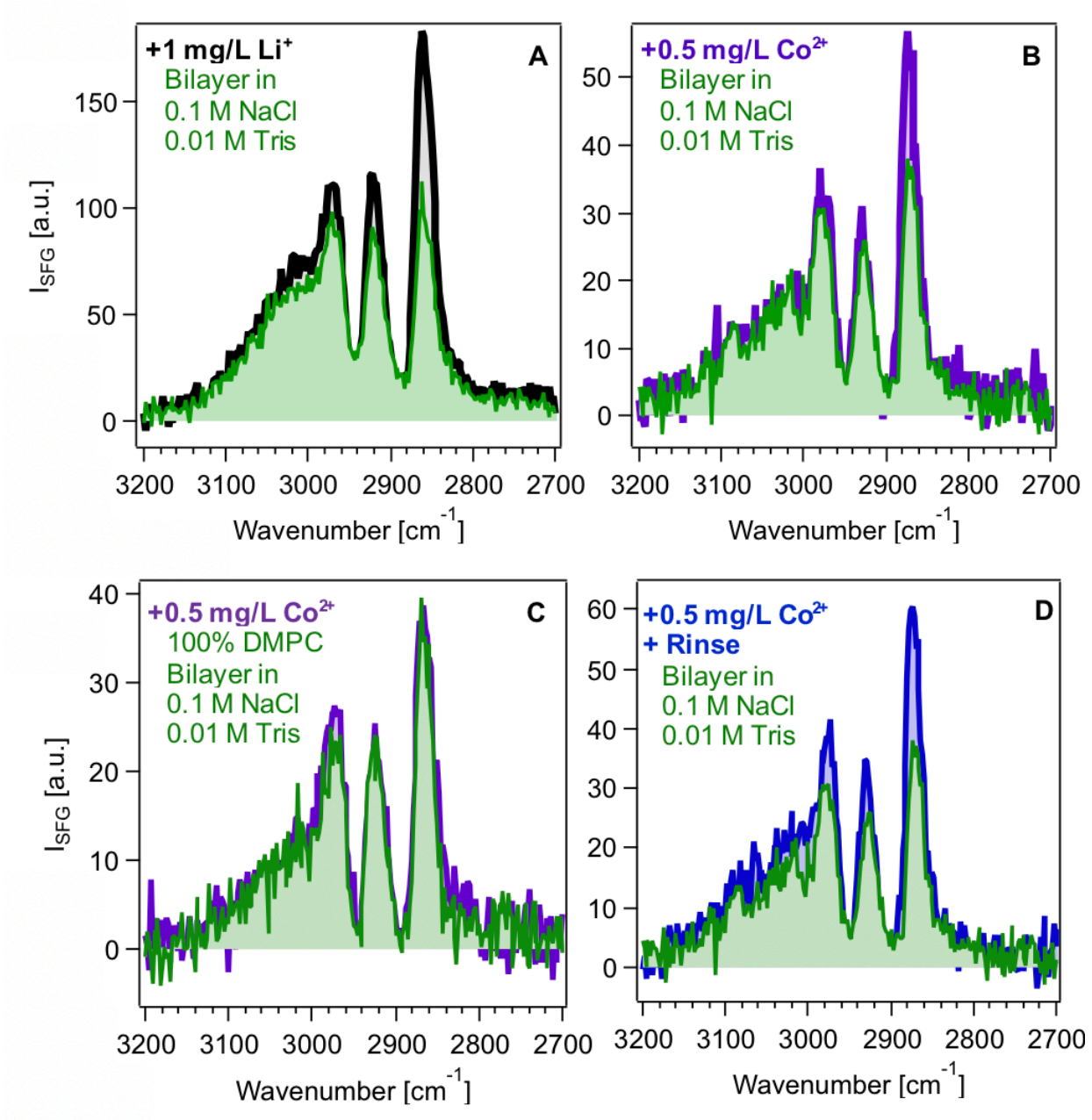

Figure 4.4. *ssp*-Polarized SFG spectra of bilayers formed from 9:1 mixture of DMPC/DMPG lipids before (green) and after exposure to (A) 1 mg/L Li^+ (black), (B) 0.5 mg/L Co^{2+} (purple). (C) *ssp*-Polarized SFG spectra of bilayer formed from 100% DMPC lipids before (green) and after exposure to 1 mg/L Li^+ (black). (D) *ssp*-Polarized SFG spectra of bilayers formed from 9:1 mixture of DMPC/DMPG lipids before (green) and after exposure to 0.5 mg Co^{2+} and rinsing. All data recorded in 0.01 M Tris buffer, 0.1 M NaCl, and at 22 °C and pH 7.4.

phoshatidylglycerol (PG) and phosphatidylserine (PS) lipids.[22-23] Li^+ also forms strong, high melting dehydrated metal ion-PS complexes and induces bilayer hydrocarbon chain crystallization at higher concentrations.[24-25] Since Co^{2+} is more strongly hydrated than Li^+, with hydration enthalpies of 2113 and 545 kJ/mol, respectively,[26] we expect a stronger interaction of Co^{2+} with negatively charged lipid headgroups or an interaction with the headgroup at a lower ion concentration. Yet, we observe compositional asymmetry induced by Co^{2+} at comparable ionic strengths under the conditions of our experiments. A more detailed analysis of the binding thermodynamics and electrostatics, including the determination of the number of cations bound per unit area within the nano-bio interface gap is found in Section 4.3.6.

4.3.6. Quantifying Co^{2+} Adsorption Thermodynamics and Electrostatics in the Nano-Bio-Interface Gap

As shown previously,[27-31] second harmonic generation (SHG) $\chi^{(3)}$ measurements can yield important information about binding thermodynamics and electrostatics.[12, 32-35] Fellow graduate students, Alicia McGeachy and Naomi Dalchand collected SHG spectroscopy adsorption isotherms (Figure 4.5A) in which the SH signal intensity is monitored as a function of Co^{2+} concentration in the presence of SLBs formed from DMPC and a 9:1 mixture of DMPC/DMPG at a constant salt concentration of 0.1 M allow us to explore the role of PG-lipids in promoting Co^{2+} adsorption, to estimate the adsorption Gibbs free energy and the interfacial charge density, and to investigate reversibility, thereby demonstrating the wide utility of the $\chi^{(3)}$ method for studying the nano-bio interface. Figure 4.5A shows the adsorption of Co^{2+} to single-component lipid bilayers formed solely from DMPC results in little change in the SHG intensity as the Co^{2+} concentration is raised. This finding is similar to the SFG spectroscopy result presented in Figure 4.4C, which

shows negligible SFG intensity changes upon exposure of bilayers formed from pure DMPC to Co^{2+} ions.

Figure 4.5A also shows the Co^{2+} adsorption isotherm to bilayers formed from a 9:1 mixture of DMPC and DMPG, revealing that the addition of just 10% of PG-terminated lipid leads to substantial SHG losses as the Co^{2+} concentration is raised. These results are consistent over triplicate measurements on individually formed bilayers of both compositions and consistent with previous studies that indicate divalent cations bind preferentially to anionic phospholipids.[22, 36-38] From the SHG adsorption isotherm and the extracted charge density, it is possible to determine the number of ions present at the interface at the concentration at which we observe the SFG signal intensity increases displayed in Figures 4.4B and 4.4D. At 100 mM salt concentration, charge densities are estimated from SHG adsorption isotherms using electrostatic and adsorption models like the combined Gouy-Chapman/Langmuir expression shown in Equation 4.1.[12]

$$I_{SHG} \propto |E_{SHG}|^2 \propto \left| A + B \sinh^{-1}\left[\left(\sigma_0 + \sigma_{ads}\left\{\frac{K_{ads}[M]}{1+K_{ads}[M]}\right\}\right)\left(\frac{8.44}{\sqrt{M+C_{elec}}}\right)\right]\right|^2 \qquad \text{Eq. 4.2}$$

Here, I_{SHG} and E_{SHG} are the second harmonic intensity and second harmonic electric field, respectively, $\sigma_0$is the charge density of the 9:1 DMPC/DMPG bilayer, σ_{ads} is the charge density of the adsorbed Co^{2+} at saturation coverage, K_{ads} is the apparent equilibrium constant of Co^{2+} adsorption in liters per mole, M is the bulk Co^{2+} concentration in moles per liter, and C_{elec} is the background electrolyte concentration (0.1 M NaCl) in moles per liter. As discussed in previously published work,[12] A and B, which contain the second- and third- order nonlinear susceptibilities of the system, and the incident electric field at the fundamental frequency and are treated as constants in our approximations and estimations. The applicability of the Langmuir adsorption

model in our case is justified by the observation of near quantitative reversibility in the Co^{2+}/bilayer interaction (Fig. 4.5B).

Fitting Equation 4.2 to the SHG adsorption data yields a Co^{2+} charge density of 0.1 ± 0.02 C/m^2, corresponding to roughly 3×10^{13} ions/cm^2 at maximum surface coverage if each ion carries a +2 charge. A charge density of 0.1 C/m^2 for Co^{2+} adsorption implies that the surface charge of the SLB is neutralized, as we have previously determined that SLBs formed from 9:1 DMPC/DMPG carry a surface charge density of approximately –0.1 C/m^2.[9, 12] Thus, cobalt ion adsorption to SLBs formed from 9:1 mixtures of DMPC and DMPG appears to result in charge neutralization at the interface. Using the equilibrium constant obtained from the SHG adsorption isotherm shown in Figure 4.5 (1760 ± 290 M^{-1}), and applying 55.5 M as the standard state for adsorption from solution,[39] ΔG^{Co2+}_{ads} is estimated to be –28 ± 0.4 kJ/mol. This value is comparable to our previous estimates for divalent metal ions binding to mineral oxide surfaces.[34, 40-41] While there are several studies exploring the adsorption behavior of Ca^{2+}, Ni^{2+}, and Mg^{2+} to phospholipids,[36-38, 42] and given the ultra-trace concentrations of cobalt in living systems,[43] little effort has been made to elucidate cobalt adsorption to phospholipid model systems or actual cells in terms of Gibbs free adsorption energies or quantitative surface coverages and electrostatics prior to this work.

From the Co^{2+} isotherm shown for the SLBs formed from 9:1 DMPC/DMPG (Fig. 4.5A), we estimate that *ca.* 2 x 10^{12} Co^{2+} ions per cm^2 are present at the interface under the conditions for which we observe the SFG signal intensity increases when the bilayer is exposed to 0.5 mg/L, or ~8.5 μM, $CoCl_2$ (Figure 4.4). Given the comparable SFG signal intensity increases when the bilayer is exposed to this $CoCl_2$ concentration and when it is exposed to 5 mg/L solutions of $LiCoO_2$ nanosheets under otherwise identical buffer and ionic strength conditions, then, we

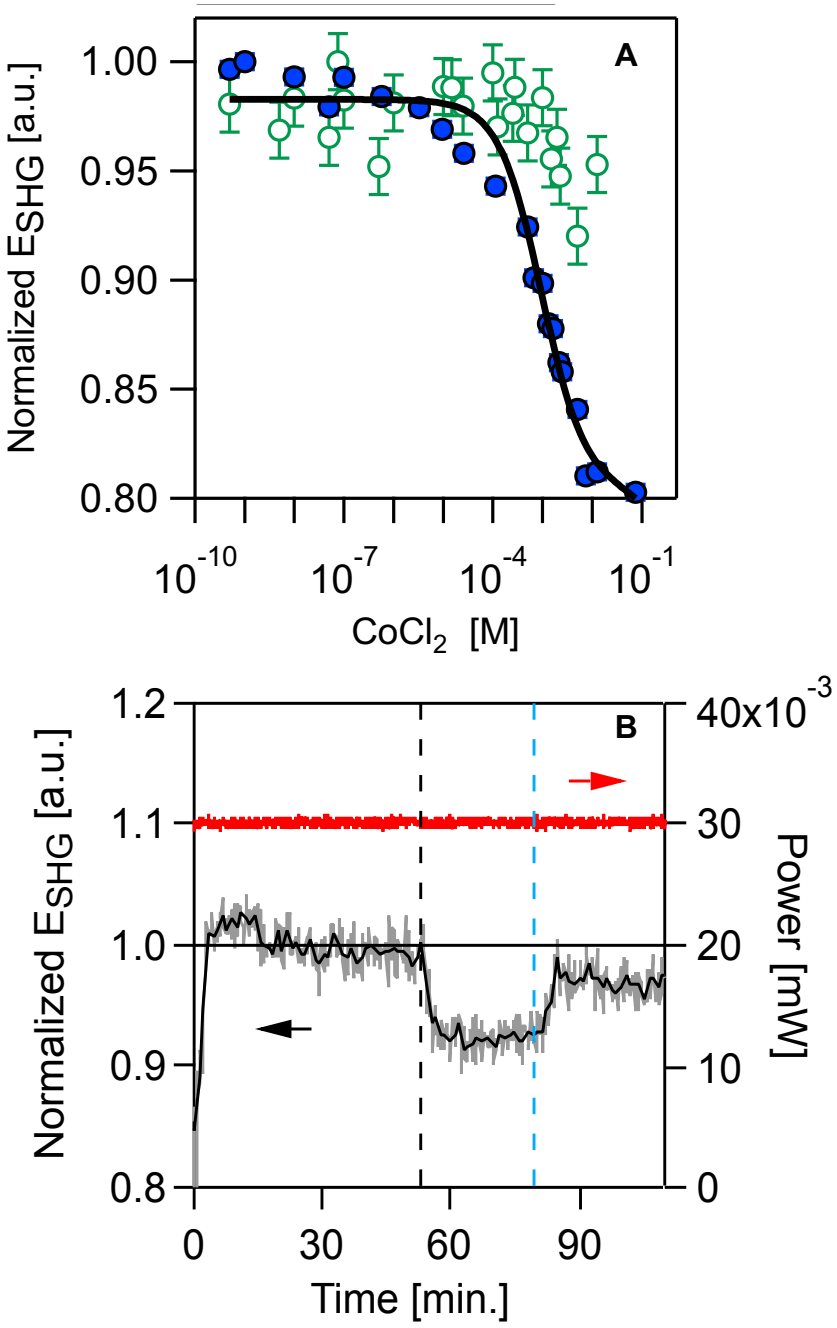

Figure 4.5. (A) Normalized SHG E-field as a function of bulk cobalt chloride concentration in the presence of supported lipid bilayers formed from DMPC (open circles) and 9:1 mixtures of DMPC and DMPG (filled circles) at 0.1 M NaCl (0.01 M Tris buffer, pH 7.4), and fit of the combined Gouy-Chapman and Langmuir model (solid black line). (B) Time trace of the normalized SHG E-field (left-axis) with a sliding average of 10 seconds (gray) and 50 seconds (black) and incident laser power (dots, right-axis) before and during the exposure of a SLB formed from a 9:1 mixture of DMPC and DMPG at 0.1 M NaCl (0.01 M Tris buffer, pH 7.4) to 0.001 M cobalt chloride at t=53 min, followed by rinsing in cobalt-free buffer at t=80 min.

estimate that a *ca.* ten-fold enhancement of Co^{2+} ions in the nano-bio interface gap when compared to the free Co^{2+} ion concentration in 5 mg/L solutions of $LiCoO_2$ nanosheets in 0.1 M salt and 0.01 M Tris buffer without bilayers present.

As stated above, Figure 4.5B reveals that cobalt adsorption to supported lipid bilayers formed from 9:1 mixtures of DMPC/DMPG lipids is nearly completely reversible under the conditions explored. In contrast, the SFG experiments we report do not show reversibility, as indicated by the retention in the spectral intensity and lineshapes shown in Figure 4.4D. These results, taken together, imply that while cobalt ions appear to reversibly adsorb to the bilayer surface, as monitored by SHG spectroscopy, the induced lipid asymmetry upon interaction persists, as revealed by SFG spectroscopy.

4.4. Conclusions and Future Directions

In conclusion, we have investigated the role of electrostatics on the interactions between redox active nanomaterials and supported lipid bilayers. We found that the interactions of $LiCoO_2$ nanosheets with bilayers formed from 9:1 mixtures of DMPC/DMPG depend critically on the ζ-potential of the nanosheets and the ionic strength. By studying metal ion dissolution from $LiCoO_2$ nanosheets, additional information on the mechanism of induced bilayer asymmetry was obtained. Specifically, we found that sub-mg/L concentrations of aqueous metal ions (Li^+ and Co^{2+}) found in bulk $LiCoO_2$ solution do not change the bilayer structure. However, elevated concentrations of aqueous metal ions in the 1 mg/L concentration regime were found to produce SFG signal intensity changes commensurate with induction of compositional asymmetry in the supported lipid bilayers studied here. This outcome is consistent with the notion that the induction of the bilayer asymmetry by $LiCoO_2$ nanosheets occurs through a non-contact mechanism that involves primarily the interaction of negatively charged lipids with dissolved ions concentrated within the electrical

double layers present at the nanosheet/bilayer gap. Surface coverage estimates of the Co^{2+} ions within this nano-bio interface gap were obtained by SHG spectroscopy and found to correspond to *ca.* 2 x 10^{12} Co^{2+} ions per cm^2 for the conditions of nanosheet concentrations that induce membrane asymmetry. SHG and SFG spectroscopy together indicate the observed effects to be specific to the negatively charged DMPG lipids, as bilayers formed purely from zwitterionic DMPC lipids show none of the effects described for the bilayers that contain DMPG. The observation that just 10% of DMPG lipids lead to the effects described here indicates the ion-lipid interactions are of considerable strength, which is the subject of ongoing work. Whether other lipid types have similar specific interactions with transition metal ions like Co^{2+} is the subject of ongoing work.

Our findings provide opportunities for mitigating non-contact interactions between natural and engineered nanomaterials and biological interfaces. Computational studies aimed at elucidating the thermodynamics of phosphate passivation of $LiCoO_2$ indicate that such an approach is in principle feasible.[5] We therefore suggest that reducing ion dissolution from lithium intercalation compounds, such as the one studied in this work, by intentional surface modifications may provide a path forward for enabling the design of new energy storage materials with reduced environmental impacts through controlled release mechanisms. Next, Chapter 5 will report vibrational SFG spectra in which the C–H stretches of lipid alkyl tails in fully hydrogenated single- and dual-component supported lipid bilayers are detected along with the O–H stretching continuum from water molecules located above the bilayer.

CHAPTER 5

Hydrogen Bond Networks Near Supported Lipid Bilayers from Vibrational Sum Frequency Generation Experiments and Atomistic Simulations

Portions of this chapter are reproduced in part
with permission from the American Chemical Society:

Doğangün, M.;[#] Ohno, P. E.;[#] Liang, D.;[#] McGeachy, A. C.; Bé, A. G.; Dalchand, N.; Li, T.; Cui, Q.; Geiger, F.M. *J. Phys. Chem. B* **2018**, *122* (18), 4870–4879.

5.1. Introduction

In the previous chapters, we focused on probing the C–H stretches of lipid alkyl tails to determine structural changes in SLBs. In this chapter, we report how to apply this approach to probe the C–H stretches of the alkyl tails in fully hydrogenated single- and dual-component SLBs along with the O–H stretching continuum of the H-bond network system in the electrical double layer to capture changes in the interfacial water structure.

The structure of water over lipid membranes is of interest for a variety of reasons that are rooted in fundamental scientific interest and connect all the way to biological function and technological applications.[1-6] Specific questions pertain to whether there exist populations of interfacial water molecules that can undergo hydrogen-bond (H-bond) interactions with certain membrane constituents that can be strengthened or weakened with variations in ionic strength, or, as indicated by molecular dynamics simulations,[2] whether some population of water molecules exists that may interact specifically with certain lipid headgroups over others.

While interface-specific vibrational spectroscopic approaches, particularly those that are based on sum frequency generation (SFG), are in principle well suited for probing water near membranes, this method has been largely limited to probing lipid monolayers[1, 7-19] chemically asymmetric bilayers,[20-22] or the use of D_2O as opposed to H_2O.[23-25] Indeed, the use of SFG spectroscopy for probing fully hydrogenated lipid bilayers is now just emerging. Part of the reason for this relatively new application of vibrational SFG spectroscopy to probe chemically unmodified lipid bilayers is rooted in the symmetry-breaking requirement of the method,[26] which has limited its use largely to asymmetric bilayers consisting of a deuterated and a hydrogenated leaflet, or lipid monolayers, as stated above. SFG signals generated by asymmetric membranes (deuterated leaflet on one side and hydrogenated leaflet on the other side, or aliphatic lipid tail on

one side and polar headgroup on the other) are strong enough to be detectable using low-repetition rate, low peak power laser systems most commonly used in the field. Two studies known to us also report SFG spectra of unlabeled symmetric lipid bilayers, demonstrating their low signal yields when compared to labeled bilayers.[27-28] The work presented in Chapters 3 and 4 have shown, in the C–H stretching region, that commercially available broadband optical parametric amplifier laser systems running at modest (kHz) repetition rates can overcome these limitations, [29-31] with reasonably high signal-to-noise ratios obtained in just a few minutes of spectral acquisition time.

The work presented in Chapter 5 probes lipid tail order and disorder while also informing on changes in the H-bond network strength that result from changes in the bulk ionic strength up 100 mM NaCl. Moreover, by varying the lipid bilayer composition from 100% zwitterionic lipid to an 8:2 mixture of zwitterionic and negatively charged lipids, we identify specific H-bond interactions between water molecules and the lipid headgroup choline moieties that manifest themselves in spectral intensity changes in the 3100 cm^{-1} to 3200 cm^{-1} range.

5.2. Experimental Details.

5.2.1. SFG Approach

Details of our SFG approach and experimental setup for probing condensed matter interfaces in the combined C–H and O–H stretching regions have been explained in Chapter 2. Further details regarding spectral acquisition and analysis procedures are also provided in Chapter 2. All SFG spectra were collected using the near total internal reflection geometry and the *ssp* polarization combination (*s*-polarized SFG, *s*-polarized 800 nm light, *p*-polarized IR light). All SFG spectra were recorded in triplicates and normalized to the *ppp*-polarized SFG response obtained from a gold window. To cover the full spectral range of interest, multiple spectra are collected at different IR center wavelengths before being combined into a single spectrum.

5.2.2. SLB Preparation

1,2-dimyristoyl-*sn*-glycero-3-phosphocholine (DMPC) and 1,2-dimyristoyl-*sn*-glycero-3-phospho-(1-*rac*-glycerol) (DMPG) were purchased from Avanti Polar Lipids and used without further purification. Lipid bilayers from small unilamellar vesicles of pure DMPC, lipid mixtures containing 90 mol% DMPC and 10 mol% DMPG, and 80 mol% DMPC and 20 mol% DMPG were prepared by the vesicle fusion method, as described earlier,[29, 31-34] on 3 mm thick calcium fluoride windows (ISP Optics, CF-W-25-3).

Experiments were carried out at room temperature (21 ± 2 ºC). All SLBs were formed at 0.01 M Tris buffer and 0.1 M NaCl in the presence of 0.005 M $CaCl_2 \cdot 2H_2O$ at pH 7.40 ± 0.03.[33] Following bilayer formation, SLBs were rinsed with Ca-free buffer to remove excess vesicles. The spectra were recorded at two different ionic strengths. Before the preparation of aqueous solutions, Millipore water was left overnight to equilibrate with atmospheric CO_2. The solution pH was measured for each salt concentration and the pH was adjusted to 7.4 with minimal NaOH and HCl before the solutions were flowed across the interface resulting in ionic strengths of ~10 μM and 0.1 M for the Millipore solution and NaCl solution, respectively.

5.2.3. FRAP Measurements

Two-dimensional diffusion coefficients, which can serve as a metric for bilayer quality, were estimated using fluorescence recovery after photobleaching (FRAP). FRAP measurements and sample preparation were carried out in a manner consistent with our previous approach.[29] The information for the experimental methods are detailed in the main text and supporting information of Doğangün *et al. J. Phys. Chem. B* **2018**, *122*, 4870. Here, we report the diffusion coefficients recorded by fellow graduate student Alicia McGeachy.

For SLBs formed from a 9:1 mixture of DMPC/DMPG lipids, we find diffusion coefficients on the order of 0.5 ± 0.2 $\mu m^2/s$ (13 replicates over two samples) after rinsing with 0.1 M NaCl, 0.01 M Tris buffer, which is consistent with our previously reported two-dimensional diffusion coefficients[29] and indicates that a well-formed bilayer is produced from the abovementioned method.[35-37] Upon rinsing with pH-adjusted Millipore water with no added salt, we find that the diffusion coefficient for SLBs formed from 9:1 mixtures of DMPC/DMPG lipids are on the order of 0.03 ± 0.01 $\mu m^2/s$ (6 replicates over 1 sample). The diffusion coefficient for SLBs formed from pure DMPC lipids on calcium fluoride is 0.4 ± 0.2 $\mu m^2/s$ (6 replicates over two samples) after rinsing with 0.1 M NaCl, 0.01 M Tris buffer. After rinsing with pH adjusted Millipore water, we find a diffusion coefficient of 0.07 ± 0.02 $\mu m^2/s$ (4 replicates over two samples). For SLBs formed from 8:2 mixtures of DMPC/DMPG lipids, the diffusion coefficient on calcium fluoride is 0.07 ± 0.04 $\mu m^2/s$ (6 replicates over one sample) after rinsing with 0.1 M NaCl, 0.01 M Tris buffer. These results indicate the bilayers transition between the gel and fluid phases, irrespective of the nature of the underlying substrates (CaF_2 vs fused silica).

5.2.4. Computational Methods

Molecular dynamics (MD) simulations for investigating the structure of the H-bond network near the lipid-water interface were performed by graduate student Dongyue Liang in the Cui group using the CHARMM-GUI[38] input generator to set up the DMPC and 9:1 DMPC/DMPG systems. The first and second moments of the distribution of water orientations was analyzed as a function of distance from the membrane-water interface. Given the importance of atomistic calculations in supporting the SFG experiments presented in this thesis, we will briefly discuss the results of the MD simulations. The details of the computational methods, the mass density

distribution, and the two-dimensional distribution plots can be found in Doğangün *et al. J. Phys. Chem. B* **2018**, *122*, 4870.

5.3. Results and Discussion

5.3.1. Single-Component Zwitterionic Supported Lipid Bilayers

Figure 5.1 shows the *ssp*-polarized SFG response from the pure DMPC bilayer without added salt. At this low ionic strength (~10 μM), we find clear spectral signatures from the C–H oscillators of the alkyl tails, [29, 31, 34] as well as broad contributions from the O–H stretches of the water molecules. The non-zero signals are due to the fact that the molecular environment above and below the bilayer is not fully symmetric, as would be expected for a suspended bilayer. Instead, symmetry breaking occurs due to the presence of the aqueous phase on one side and the solid support on the other. The frequencies corresponding to the signal peaks in the C–H stretching region shown in Figure 5.1 are comparable to the ones we observe for SLBs formed on fused silica substrates [29, 31, 34] The two broad features in the O–H stretching continuum located at ~3200 cm^{-1} and ~3400 cm^{-1} are associated with bandwidths (full width at half maximum) of about 200 cm^{-1}. The peak positions are within 50 cm^{-1} of what has been reported for water spectra obtained from symmetric bilayers prepared from negatively charged lipids on CaF_2.[28] The difference is attributed to the fact that our current experiments use bilayers formed from purely zwitterionic lipids.

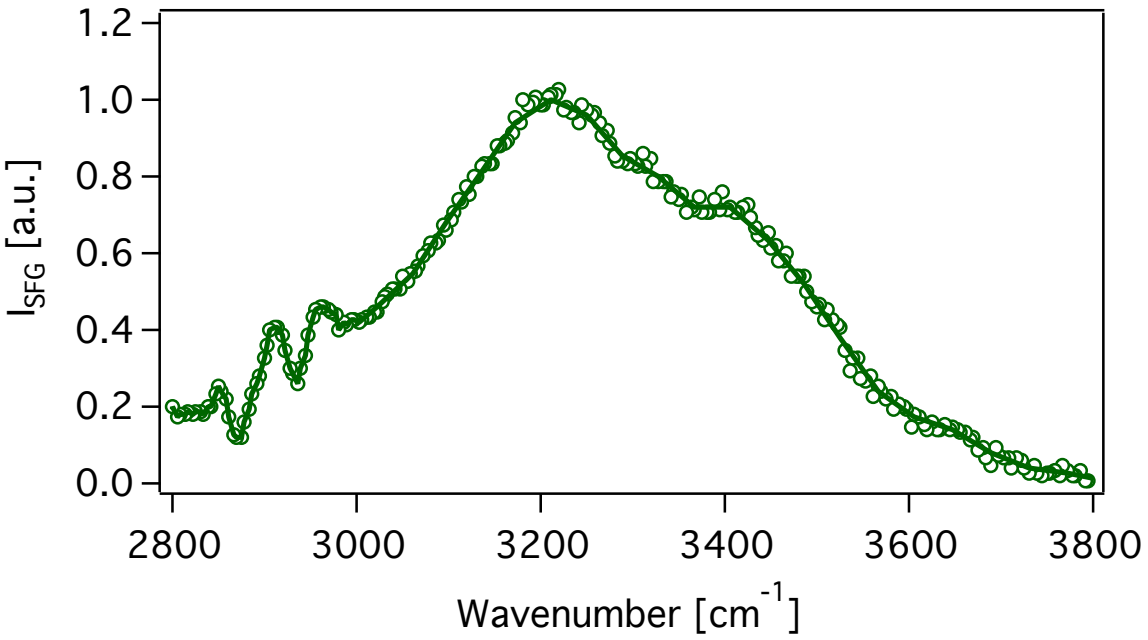

Figure 5.1. *ssp*-Polarized SFG spectrum of an SLB made from pure DMPC lipids in contact with low-ionic strength water adjusted to pH 7.4. The data below 3000 cm^{-1} have not been binned to preserve the C–H stretching region, while they were binned over nine points in x and y between 3000 cm^{-1} and 3800 cm^{-1}.

Replacing the H_2O phase with D_2O while maintaining low ionic strength, shown in Figure 5.2, leads to the C–H oscillators retaining their frequencies while the O–H stretching continuum is entirely absent. This experiment indicates that 1) there are no exogenous photon sources contributing to the SFG response from the bilayer under water (H_2O), and 2) that H_2O that may be possibly trapped between the bilayer and the substrate is readily exchanged or associated with too little SFG intensity to be detectable by our method. Control experiments assessing the possible role that CaF_2 dissolution could have on the spectra[48-49] (see Fig. 5.3) show that the presence of the bilayer eliminates any flow-dependent changes in the SFG signal intensity produced by the interfacial water molecules.

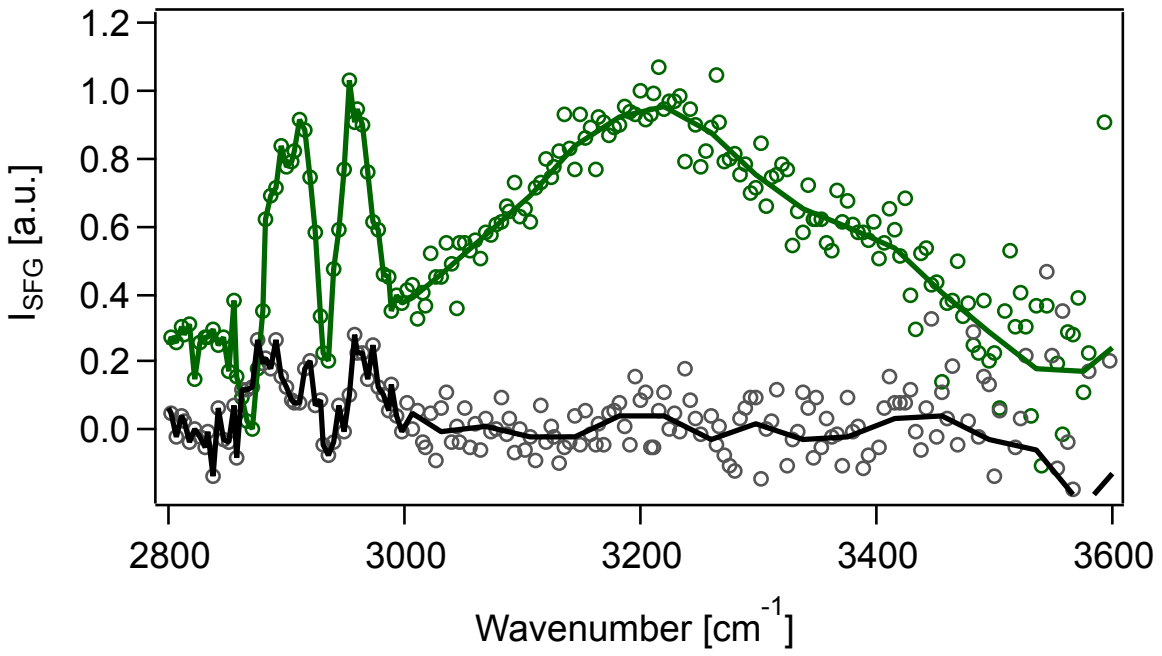

Figure 5.2. *ssp*-Polarized SFG spectra of an SLB made from a 9:1 mixture of DMPC/DMPG lipids in 0.1 M NaCl on a CaF_2 window in H_2O, pH 7.4 (green) and in D_2O, pD ~7-8 (black) at 21 ± 2 ºC. Lines represent spectra binned by over nine points in x and y between 2800 cm^{-1} and 3600 cm^{-1}.

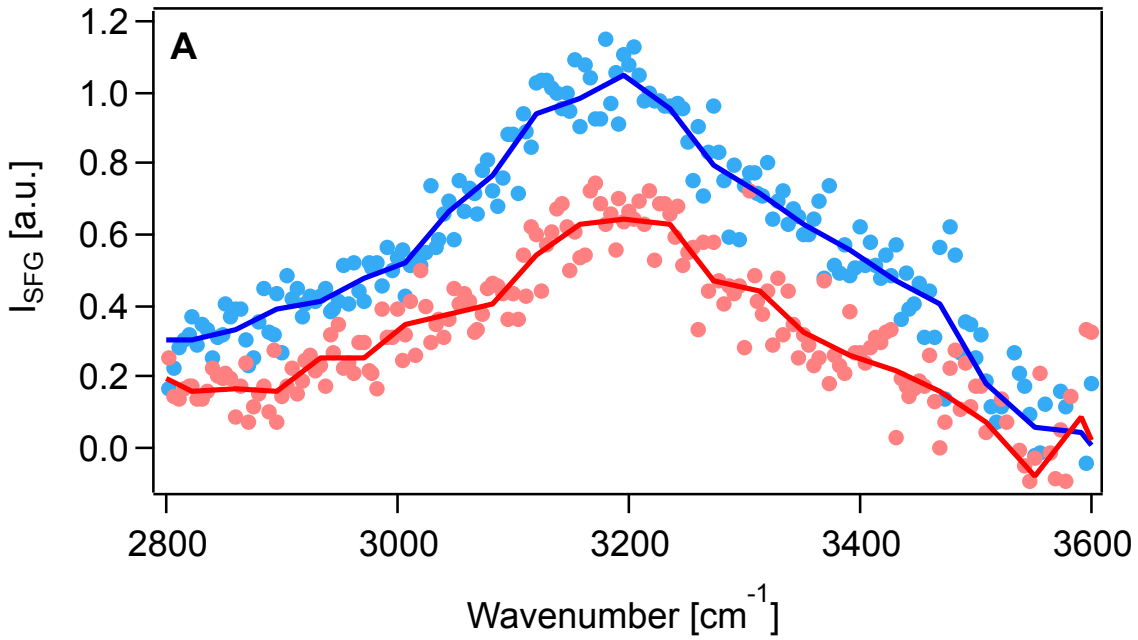

Figure 5.3: ssp-Polarized SFG spectrum of neat water adjusted to pH 7.4 with a flow rate of 1.5 mL/min (blue) and with no flow (red) (A) for CaF_2/water and (B) SLB/water interface (not-normalized).

The O–H stretching continuum can be viewed as a display of the various O-H···O distances sampled in the water network probed by the SFG spectrometer. As shown, for instance, by Lawrence and Skinner,[50] frequencies around 3200 cm^{-1} correspond to O–H stretches associated with water molecules in tighter H-bond networks, where distances between the donor hydrogen and acceptor oxygen atoms (H···O) are as short as 1.6 Å or less. Towards 3400 cm^{-1}, the spectrum samples water molecules in a considerably looser H-bond network, having H···O distances as long as 2.1 Å or so. Towards 3550 cm^{-1}, H···O distances can be as long as 2.4 Å or more. At the very end of the spectrum, near 3700 cm^{-1}, would be the O–H stretch of non-H-bonded water molecules, those that "straddle the interface".[51] Such signals are not identified within our signal-to-noise ratio, even though they have been reported to be present in Langmuir monolayers prepared from DPPC lipids.[52]

Figure 5.4 shows the SFG spectrum from the supported lipid bilayer in comparison with that of two other aqueous CaF_2 interfaces, namely that of bare CaF_2 in contact with ~10 μM ionic strength water adjusted to pH 7.4, as well as bare CaF_2 in contact with water vapor in He flow adjusted to 80% relative humidity. The SFG response from the bare CaF_2/water interface is in reasonable agreement with published data.[49, 53-54] We find that the peak positions from the bilayer/water interface is blue-shifted by around 25 cm^{-1} when compared to those obtained from the bare CaF_2/water interface. Additionally, the SFG spectrum from the CaF_2/water vapor interface exhibits a blue-shifted SFG spectrum when compared to the bilayer/water or CaF_2/water interfaces, consistent with the expectation that its hydrogen-bonding environment is looser than in the case of bulk water in contact with the solids.[55-56]

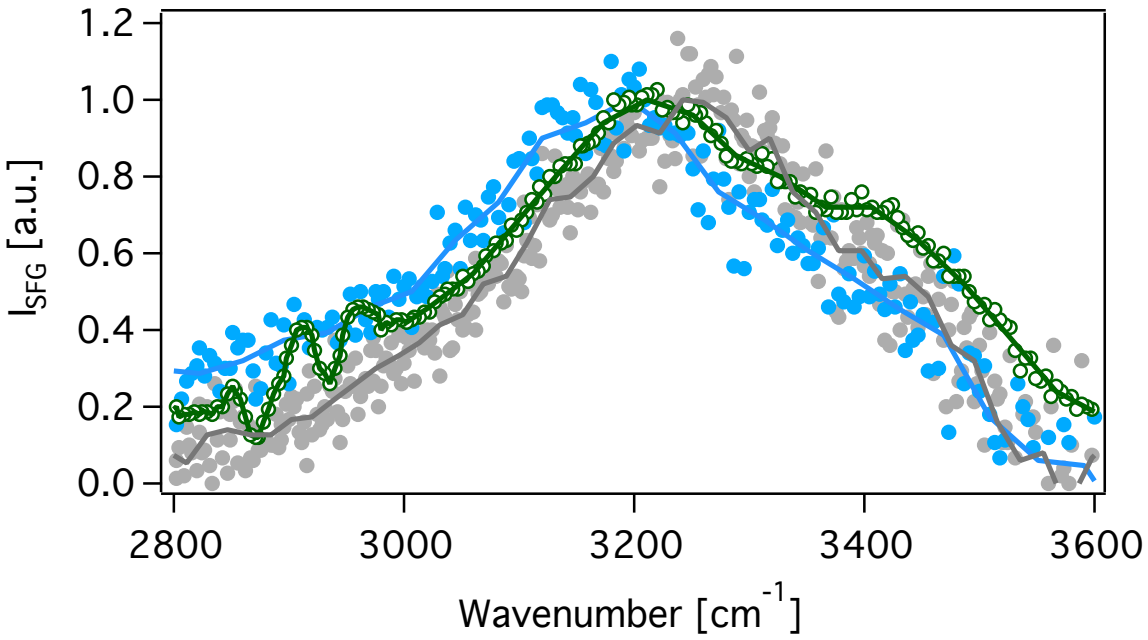

Figure 5.4. Comparison of *ssp*-polarized SFG spectra from the CaF_2/wet air interface (gray), the CaF_2/water interface (blue), and a CaF_2-supported SLB prepared from pure DMPC lipids (green). Lines represent spectra binned by over nine points in x and y between 2800 cm^{-1} and 3600 cm^{-1}.

Upon increasing the ionic strength in the bulk aqueous phase, the sodium and chloride ions can modify the H-bond network of water molecules in the bulk in ways that are the subject of much past and ongoing scientific attention and discussion.[57-58] NaCl, whose anion and cation fall right in the middle of the familiar Hofmeister series, are not necessarily expected to modify the H-bond network over lipid bilayers at the relatively modest concentrations (0.1 M) employed here. Moreover, ion-specific interactions with the lipids used in our work are unlikely to be strong under the conditions of our experiments. Indeed, Figure 5.5 shows that the spectral changes we observe in response to changes in the ionic strength are largely uniform over the entire frequency region probed in our experiment (1000 cm^{-1}). Between 3000 cm^{-1} and 3600 cm^{-1}, the ratio of the SFG spectral intensities at low (~10 μM) and high (0.1 M) ionic strength is computed to vary only slightly, from 1.7 at 3000 cm^{-1} to 2.3 at 3600 cm^{-1} and back to 2.0 at 3700 cm^{-1} (average of 2.1 ± 0.2 over all frequencies). We find this slight frequency dependence of the SFG intensity ratio to be indicative of a minor influence that the relatively modest salt concentrations used here even under what we term "high salt" have on the various contributors to the H-bond network. This interpretation is borne out in molecular dynamics simulations as well, which are summarized next.

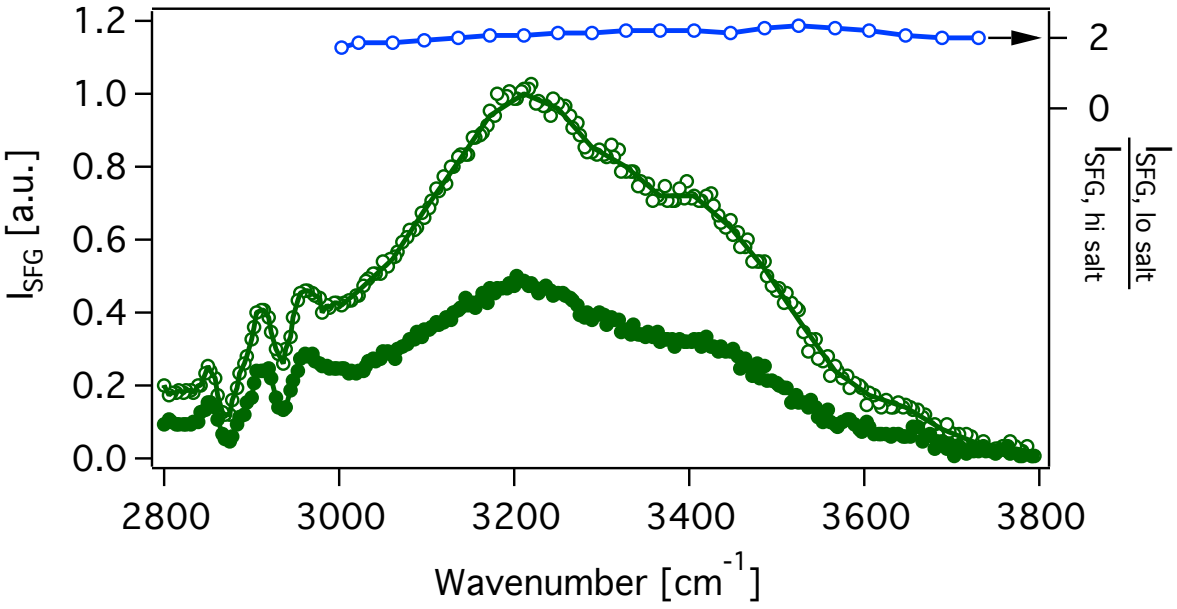

Figure 5.5: *ssp*-Polarized SFG spectrum of an SLB formed from pure DMPC lipids in Millipore water with no added salt (circles) and with 0.1 M NaCl (solid circles) at 21 ºC and pH 7.4. The lines represent the data that have been binned by over nine points in x and y between 3000 cm^{-1} and 3600 cm^{-1}.

To further explore the molecular details near the bilayer/water interface, in collaboration with graduate student Dongyue Liang from the Cui group, we performed MD simulations for a DMPC lipid bilayer with and without 0.15 M NaCl salt. We focus here on the analysis of the interfacial water structure, specifically the orientation of interfacial water molecules and the O···O distance of neighboring water molecules. According to the mass density distribution, the lipid-water interface is identified at z ~ 20 Å. In all cases studied, a small amount of water molecules penetrates below the lipid/water interface to interact with the lipid glycerol groups (for a snapshot, see Figure 5.6B). The distribution approaches the bulk value at ~8-10 Å away from the lipid-water interface. Nevertheless, the distribution of water orientation remains broad even at the interface, which is likely due to the dynamic nature of the lipid headgroup. As a result, no statistically significant difference is observed between the two DMPC cases studied, suggesting that the impact of salt on the water orientation at the interface is subtle compared to the effect of thermal fluctuations. Regarding the distributions of the nearest O···O distances among water molecules, which reports on the hydrogen bonding strength, our results suggest again that the impact of salt is small, supporting the observation from SFG analysis.

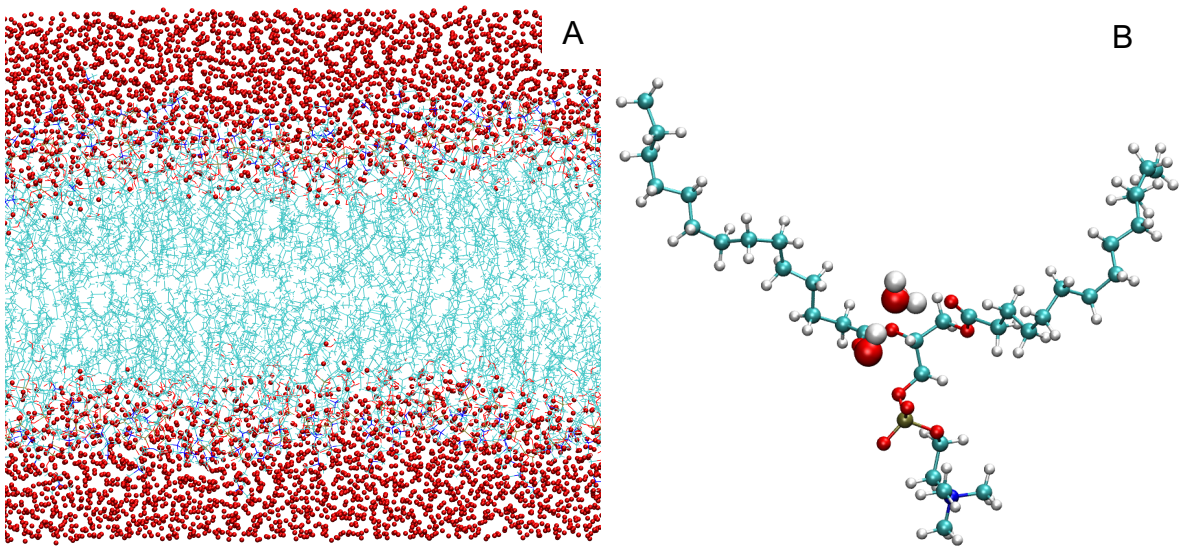

Figure 5.6. Snapshots from MD simulation of a solvated DMPC lipid bilayer system. (B) The snapshot illustrates the water molecules that penetrate below the phosphate-water interface and engage in hydrogen bonding interactions with the glycerol oxygen in the lipid (z~10 Å). Color representations: water oxygen – red, lipid nitrogen – blue, lipid phosphorus – tan, carbon – green, hydrogen – white.

The SFG signal intensity reductions observed across the frequency range investigated here as the salt concentration is raised from 10 μM to 0.1 M concentration levels are consistent with absorptive-dispersive mixing between $\chi^{(2)}$ and $\chi^{(3)}$ contributions to the SFG signal generation process, from charged interfaces according to[60-63]

$$\chi^{(2)}_{total} = \chi^{(2)}_{NR} + \chi^{(2)}_{surf} + \frac{\kappa}{\sqrt{\kappa^2+(\Delta k_z)^2}} e^{i\, arctan\left(\Delta k_z/\kappa\right)} \Phi(0)\chi^{(3)} \qquad \text{Eq. 5.2}$$

Here, the first two terms are the non-resonant and resonant 2nd-order susceptibility and the 3rd term is given by the inverse Debye screening length, κ, the inverse of the coherence length of the SFG process, Δk_z, and the interfacial potential, $\Phi(0)$, multiplied by the 3nd-order susceptibility. The $\chi^{(3)}$ phase angle $\varphi = arctan\left(\Delta k_z/\kappa\right)$ can be estimated from Gouy-Chapman theory: at the low (*resp*. high) salt concentration investigated here, κ is 1 x 10^7 (*resp*. 1 x 10^9) m^{-1}, while our experimental geometry leads to a Δk_z of 2.4 x 10^7 m^{-1}, which is invariant with salt concentration. The resulting phase angle, derived by fellow graduate student Paul Ohno, is shown in Figure 5.7A.

In the absence of phase-resolved measurements, which are proving to be considerably challenging at buried liquid-solid interfaces such as the ones studied here, it is difficult to quantitatively examine the interfacial potential, even if one uses the 3rd order ($\chi^{(3)}_{\text{bulk}}$) term recently reported by Wen et al.[60] that should be quite universally applicable for aqueous interfaces. Moreover, it is perhaps not possible to prepare, in an experiment, a truly "zero potential" reference state: even the fully protonated reference state of a carboxylic acid monolayer, commonly used as a reference state in surface potential measurements,[60, 64-65] is subject to dipolar potentials. In the absence of 1) phase resolved data and 2) a true zero potential – and/or zero charge density – reference state, quantitative knowledge of the interfacial potential at two different solution or bilayer conditions from which a difference in surface potential, i.e. $\Delta\Phi$, can be calculated is

difficult to obtain, though methods to acquire this knowledge remain a topic of keen interest to us that we will discuss in forthcoming work.

For now, we offer the following method for estimating surface potential changes from the second-order spectral lineshapes (in the O–H stretching region): an examination of Equation 5.2 reveals that even if, as suggested by the MD simulations discussed above, the H-bond network close to the interface remains invariant or nearly invariant (implying a constant $\chi^{(2)}_{\mathrm{surf}}$) upon changes in ionic strength, changes in the SFG signal intensity can still arise from the potential-dependent $\chi^{(3)}$ term. These changes take the form of a complex multiple of the $\chi^{(3)}_{\mathrm{bulk}}$ term, which is given mainly by the 3rd order optical properties of bulk water. Unfortunately, given the difficulties discussed above, our lack of phase-resolved measurements and our lack of access to a reference state of true $\Phi(0)=0$, precludes us from comprehensively accounting for the phase-angle dependent $\chi^{(2)}/\chi^{(3)}$ mixing, and thus quantitatively determining the interfacial potential from the SFG spectra reported here. Yet, surprisingly good qualitative agreement is obtained between the difference of the measured intensity spectra for the low and high salt conditions from Figure 5.5 and the calculated $\chi^{(3)}_{\mathrm{bulk}}$ intensity spectrum derived from the real and imaginary data reported by Wen *et al.* (see Fig. 5.7). This agreement supports our conclusion that the spectral changes are not indicative of large changes in the H-bonded network of water molecules but rather result from the $\chi^{(3)}$-potential dependent term. Moreover, under conditions where the SFG responses are dominated by the $\chi^{(3)}$ term, *i.e.* $\chi^{(3)}\,\Phi >> \chi^{(2)}$, an estimate of the difference in surface potential, $\Delta\Phi$, can be readily provided if the magnitude of the SFG intensity difference, ΔI_{SFG}, observed for conditions of varying ionic strength, bulk solution pH, analyte concentration, or surface composition, is known.

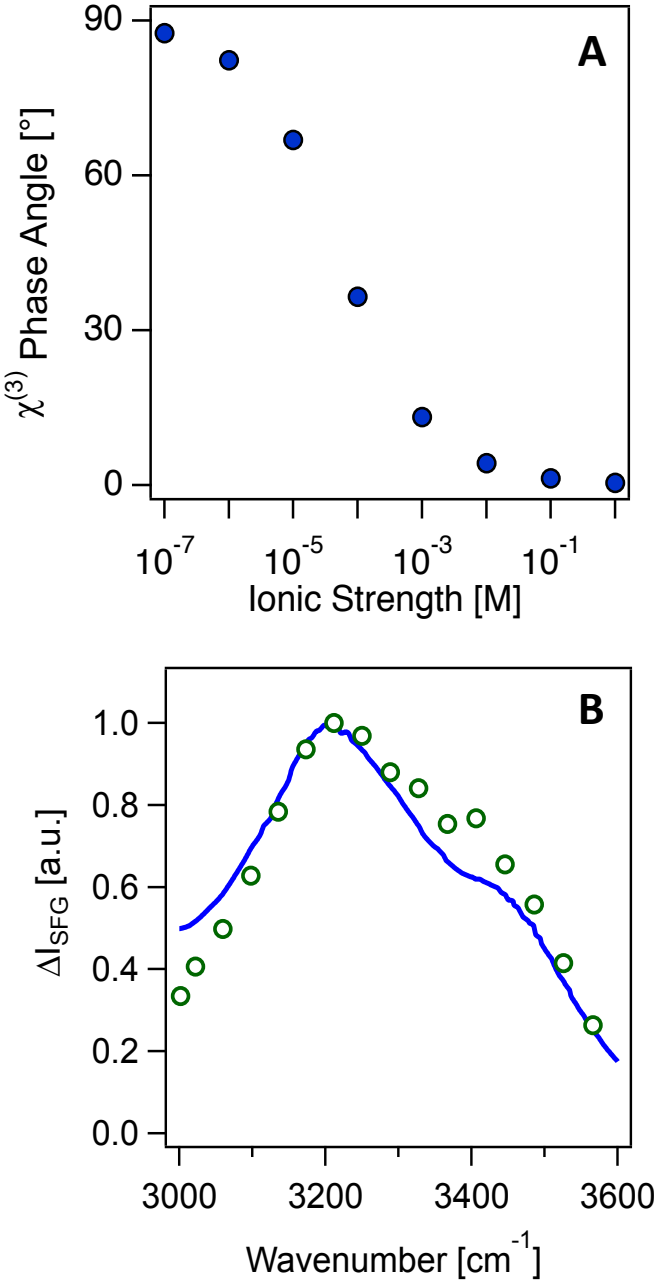

Figure 5.7. (A) Variation of the $\chi^{(3)}$ phase angle $\varphi = arctan\left(\Delta k_z / \kappa\right)$ with ionic strength under the conditions of our experiments. (B) Potential dependent $\chi^{(3)}$ effect: comparison between the difference between the low and high salt conditions from Figure 5.5 (green) and a calculated intensity spectrum derived from the $\chi^{(3)}$ spectra reported by Wen *et al.*[60] (blue). Even without comprehensively accounting for the absorptive-dispersive mixing controlled by the $\chi^{(3)}$ phase angle, φ, as per equation 5.2, which is not yet accessible through phase-resolved measurements at the solid/liquid interface, qualitative agreement is demonstrated.

5.3.2. Dual-Component Supported Lipid Bilayers Formed from Zwitterionic and Negatively Charged Lipids. Motivated by recent reports that the major contribution in the 3000 cm^{-1} to 3200 cm^{-1} frequency region originates from polarized water molecules that bridge phosphate and choline in the zwitterionic lipid headgroup (*n. b.*: that work focused on lipid monolayer/water interfaces as opposed to lipid bilayer/water interfaces, which are probed in the present study),[2] we proceeded to add negatively charged lipids to the zwitterionic system studied. Mixing in negatively charged lipids, such as DMPG, is then expected to reduce the population of polarized water molecules that interact specifically with the zwitterionic PC headgroup.

Figure 5.8 shows that this response is indeed observed. At 0.1 M NaCl, the three systems we surveyed (100% zwitterionic DMPC, 9:1 DMPC/DMPG, and 8:2 DMPC/DMPG) showed no significant changes in the 3400 cm^{-1} frequency region. Yet, as the percentage of negatively charged lipids increases, the SFG spectral intensity in the 3200 cm^{-1} region decreases, indicating the theoretical result obtained for lipid monolayer/water interfaces may also hold for lipid bilayer/water interfaces. Triplicate measurements can be found in the Supporting Information of Doğangün *et al. J. Phys. Chem. B* **2018**, *122*, 4870.

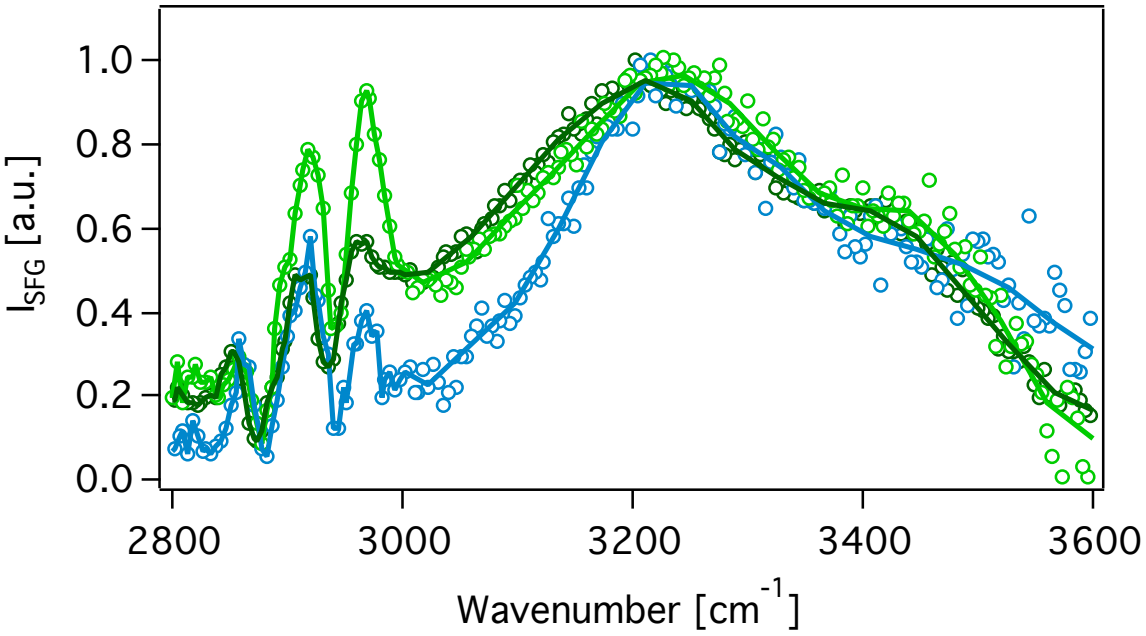

Figure 5.8. *ssp*-Polarized SFG spectrum of an SLB formed from pure DMPC (dark green), a 9:1 mixture of DMPC/DMPG (light green) and an 8:2 mixture of DMPC/DMPG (blue) lipids in 0.1 M NaCl (solid lines) at 22 ºC and pH 7.4. The circle markers represent the raw data while the darker lines represent the data that have been binned by over nine points in x and y between 3000 cm^{-1} and 3600 cm^{-1}.

Results from the MD simulation for 9:1 DMPC/DMPG with 0.15 M NaCl reveal similar trends when compared to the pure DMPC case, suggesting that the impact of a small amount (10%) of anionic lipids on the structure and orientation of water at the interface is minor, in the background of thermal fluctuations. Yet, computing the number of water molecules adjacent to lipid phosphate, choline, and those close to both phosphate and choline, in a manner consistent with the analysis by Morita and coworkers,[2] we find that mixing in DMPG lipids leads to a small, albeit statistically significant, decrease in the number of water molecule adjacent to both the lipid phosphate and choline moieties per area, as shown in Table 5.1. These computational results support the observations that the SFG signal intensities seen in the experimental spectra between 3100 cm^{-1} to 3200 cm^{-1} are due to local water molecules that specifically interact with the phosphate and choline moieties of the DMPC lipids.[2]

Table 5.1. Number of water molecules (per surface area) close to the lipid phosphate (labeled with "P"), close to choline (labeled with "N"), and close to both phosphate and choline groups (labeled with "NP") from atomistic MD simulations.[a]

Lipid composition	**DMPC**		**9:1 DMPC/DMPG**
[NaCl]	0 M	0.15 M	0.15 M
# H_2O@P (nm^{-2})	20.4 ± 0.3	20.5 ± 0.3	20.4 ± 0.2
# H_2O@N (nm^{-2})	19.4 ± 0.2	19.9 ± 0.3	18.6 ± 0.2
# H_2O@N&P (nm^{-2})	15.9 ± 0.3	16.1 ± 0.2	15.2 ± 0.2

[a]Following the work of Morita and co-workers,[2] the cutoff distance for water near phosphate is determined by the second minimum of the O–P radial distribution function; the cutoff distance for water near choline is determined by the first minimum of the O–N radial distribution function.

5.3. Conclusions

In conclusion, this chapter reports vibrational sum frequency generation spectra in which the C–H stretches of lipid alkyl tails in fully hydrogenated single- and dual-component supported lipid bilayers are detected along with the O–H stretching continuum of the hydrogen-bond network in the electrical double layer above the bilayers. Aided by atomistic simulations, we find that the hydrogen bond network over the purely zwitterionic bilayers is largely invariant with salt concentration between sub-micromolar and 100s of millimolar concentrations. The structure of the lipid tails is largely invariant with salt concentration as well, as indicated by a lack of relative spectral changes in the SFG responses observed in the C–H stretching region as salt concentration is varied. As the salt concentration is increased from ~10 μM to 0.1 M, the SFG intensities in the O–H stretching region decrease by a factor of 2. This observed salt concentration-dependent change in the SFG signal intensity is consistent with significant absorptive-dispersive mixing between $\chi^{(2)}$ and $\chi^{(3)}$ contributions to the SFG signal generation process from charged interfaces. Surprisingly good qualitative agreement is obtained between the difference of the measured intensity spectra for the low and high salt conditions from Figure 5.5 and the calculated $\chi^{(3)}_{\mathrm{bulk}}$ intensity spectrum derived from the real and imaginary data reported by Wen *et al.* (Figure 5.7). This agreement supports our conclusion that the spectral changes are not indicative of large changes in the H-bonded network of water molecules but rather result from the $\chi^{(3)}$-potential dependent term. Moreover, our analysis provides a method for estimating the difference in surface potential, $\Delta\Phi$, from the magnitude of the SFG intensity difference, ΔI_{SFG}, observed for conditions of varying ionic strength, bulk solution pH, analyte concentration, or surface composition, is known.

Specific interactions between water molecules and lipid headgroups are observed as well: Replacement of PC lipids with negatively charged PG lipids coincides with SFG signal intensity reductions in the 3100 cm^{-1} to 3200 cm^{-1} frequency region. Our atomistic simulations show that this outcome is consistent with a small, albeit statistically significant, decrease in the number of water molecules adjacent to both the lipid phosphate and choline moieties per unit area, supporting the SFG observations. This result further supports recent molecular dynamics simulations indicating that the major contribution in the 3000 cm^{-1} to 3200 cm^{-1} frequency region originates from polarized water molecules that bridge phosphate and choline in the zwitterionic lipid headgroup.[2]

5.4. Future Directions

Ultimately, the ability to probe H-bond networks over lipid bilayers in real time, *in situ,* holds the promise of opening paths for understanding, controlling, and predicting specific and non-specific interactions membranes with solutes such as ions and small molecules, peptides, polycations, proteins, and coated and uncoated nanomaterials. The studies explained in Chapters 3 and 4 can be expanded to investigate the water structure around SLBs upon exposure to nanoscale transition metal oxides and the ions dissolving from the nanomaterials. Investigating the alkyl tails of phospholipid bilayers along with the interfacial water structure has biological significance as water/membrane interactions will be relevant for many important biological processes in cellular membranes.

In addition to exploring the water structure over the SLBs upon exposure to nanomaterials and metal ions, future work will focus on making the model phospholipid bilayers more biologically relevant. This will involve the use of more biologically relevant phospholipids, incorporation of transmembrane proteins to SLBs and use of suspended lipid membranes. Chapter

6 reports preliminary experiments to incorporate lipopolysaccharides into SLBs mimicking the outer membrane of Gram-negative bacteria.

CHAPTER 6

Towards Using Model Membranes with Increased Complexity: Lipopolysaccharide Incorporated Supported Lipid Bilayers

6.1. Introduction

In Chapter 1, we established that cell membrane is the first point of contact between the cell and its external environment. Gram-negative bacteria, which are of particular biomedical and technological interest, are surrounded by an additional membrane layer, the outer membrane.[1-3] The outer membrane of Gram-negative bacteria is characteristically an asymmetric phospholipid bilayer.[1, 4] The inner leaflet resembles most cytoplasmic cell membranes, composed of phospholipids with membrane proteins, and the outer leaflet is predominantly composed of lipopolysaccharide (LPS) molecules.[4] LPSs have complex structures consisting of three parts (Fig. 6.1): (1) a particular lipid (Lipid-A) which tethers the LPS molecule to the outer membrane, (2) the core oligosaccharide region composed of sugars 3-deoxy-d-manno-octulsonic acid (Kdo) and l-glycero-d-manno-heptose (Hep) (inner core), hexoses, and hexosamines (outer core), and (3) the O-antigen region composed of a repeating chain of oligosaccharides variable across bacterial strains.[5-6] The O-antigen has a high variability in the number of repeating units. The phosphate groups of lipopolysaccharides increase the overall negative charge of the cell membrane and help to stabilize the structure. When LPS contains the complete core oligosaccharide and O-antigen regions, it is referred as smooth-LPS, whereas rough LPS is a shorter type of LPS that lacks the O-antigen with either complete or truncated core oligosaccharide regions.

Previous work has described the formation, structure, and physicochemical properties of LPS-containing SLBs.[6-8] Several studies have shown that the outer membrane of Gram-negative bacteria drives the interactions between the membrane and nanomaterials.[9-11] However, the underlying mechanisms are still unknown. Chapter 6 aims to investigate the sensitivity of vibrational SFG spectroscopy to lipid bilayer structures in increasing complexity. As a first step to

increase complexity of membrane models and gain molecular level insights into the bacterial outer membrane, we used smooth- and rough-LPS containing asymmetric SLBs.

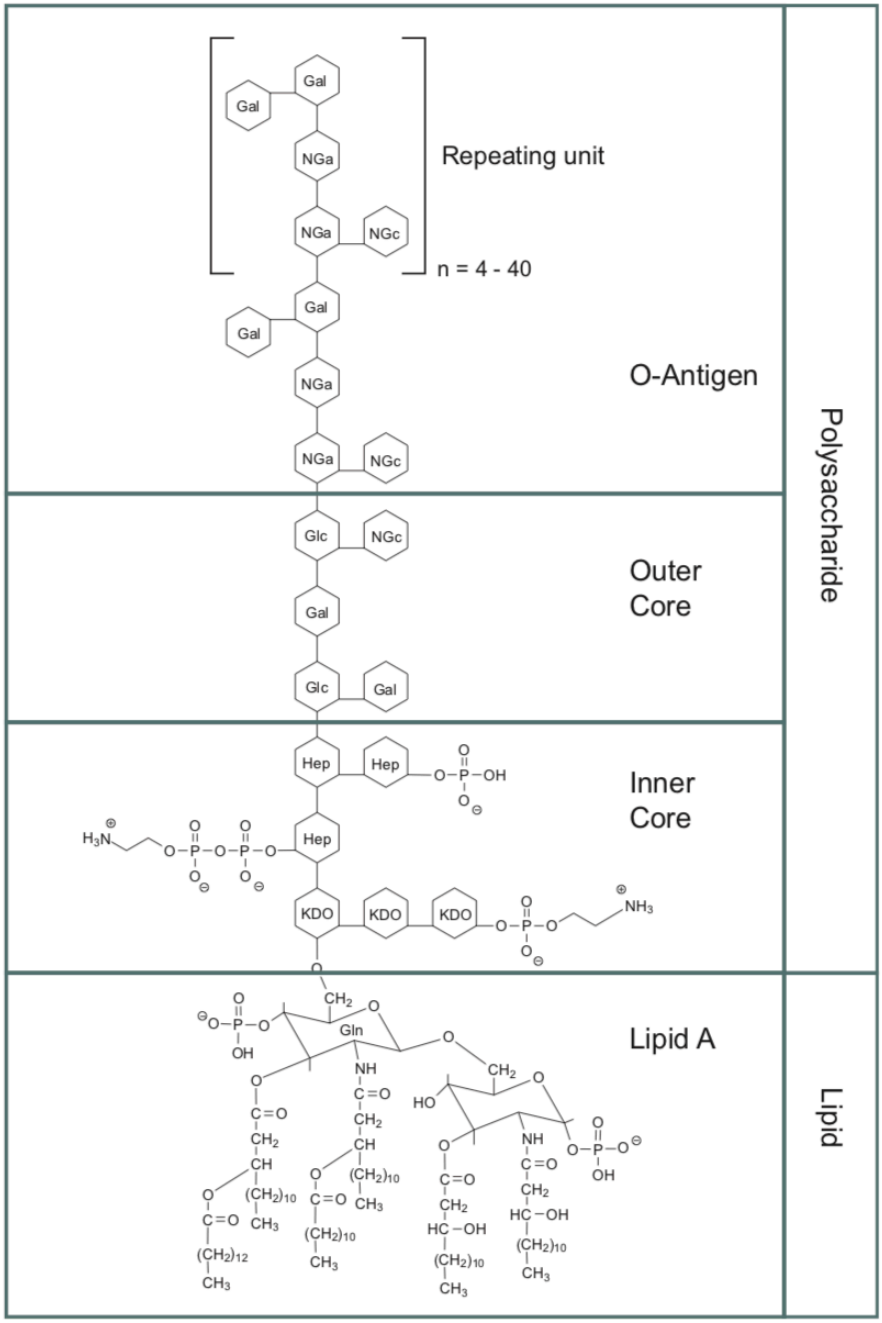

Figure 6.1. General structure for bacterial lipopolysaccharides.[12]
Abbreviations: KDO: 3-deoxy-α-D-mannooctulosonic acid; Hep: Heptulose (ketoheptose); NGa: Galactosamine; NGc: Glucosamine

6.2. Experimental Details

6.2.1. Materials

1-palmitoyl-2-oleoyl-*sn*-glycero-3-phosphocholine (POPC), 1,2-dioleoyl-*sn*-glycero-3-phosphocholine (DOPC), and 1,2-dimyristoyl-*sn*-glycero-3-phosphocholine (DMPC) were purchased from Avanti Polar Lipids, Inc. and used without further purification. Molecular structures of lipids are shown in Figure 6.2. The LPS molecules used in the vesicles were obtained from Sigma Aldrich and were purified from *Salmonella enterica serotype* minnesota (smooth strain) and *Salmonella enterica serotype* minnesota Re595 mutant (rough strain). The deep rough mutant LPS Re 595 is the shortest LPS molecule available, with both its outer core oligosaccharide and O-antigen regions shortened, leaving only the two sugars 3-deoxy-d-manno-octulsonic acid (Kdo) linked to the lipid A glucosamine headgroup.[13]

6.2.2. Supported Lipid Bilayer Preparation

Lipid vesicles were prepared by mixing solutions of POPC and DOPC with smooth and rough LPS in the 8:2 lipid/LPS mass ratio, and evaporating the solvent under a gentle stream of N_2 gas.[7] The lipid/LPS mixtures were then rehydrated in 0.150 M NaCl solution buffered with 0.002M HEPES at pH 7.4. The unilamellar vesicles were formed by extruding the lipid suspension through a 50 nm polycarbonate membrane filter (Whatman) 11 times using Avanti mini extruder kit. The lipid vesicles were introduced into the flow cell and allowed to spontaneously form an asymmetric membrane on the fused silica substrate. Following bilayer formation, the excess vesicles are rinsed with a 0.025 M NaCl solution buffered with 0.002M HEPES at pH 7.4.

Lipid A

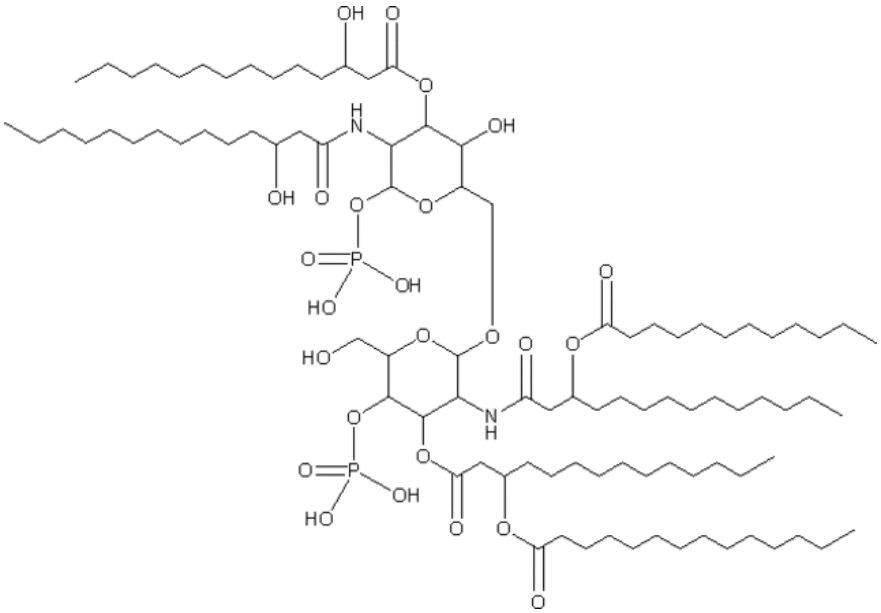

POPC

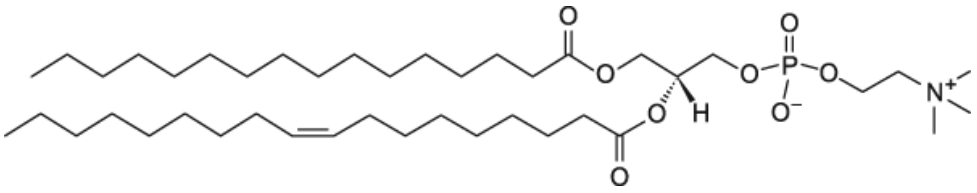

DOPC

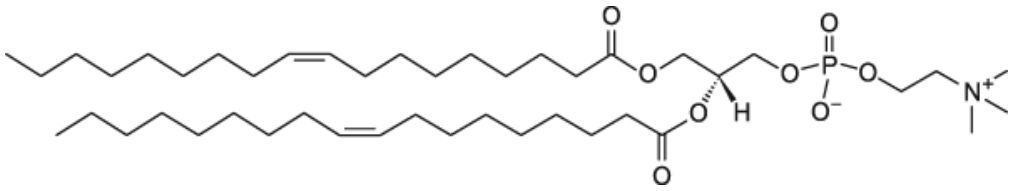

DMPC

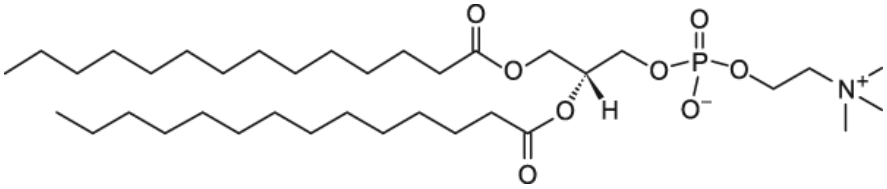

Figure 6.2. Molecular Structure of Lipid A of *Salmonella enterica serotype* Minnesota Re595, POPC, DOPC and DMPC lipids used in this chapter.
Abbreviations: POPC: 1-palmitoyl-2-oleoyl-*sn*-glycero-3-phosphocoline, DOPC: 1,2-dioleoyl-*sn*-glycero-3-phosphocholine, DMPC: 1,2-dimyristoyl-*sn*-glycero-3-phosphocholine

6.2.3 Sum Frequency Generation Spectroscopy in the C-H stretching region

The set-up and experimental details are described in Chapters 2 and 3. The *ssp*-polarization combination was used for all experiments. SFG was recorded with an integration time of 4 min and an average of 5 acquisitions.

6.3. Results and Discussion

As shown in Figure 6.3A, the SFG signal obtained from SLBs formed from 8:2 mixture of POPC/smooth-strain LPS show a broad peak in the C-H stretching region. Similarly, the shorter rough-strain LPS incorporated SLBs containing 80% POPC or 80% DOPC (Figures 6.3B and 6.3C), show only the presence of the peak at ~2980 cm^{-1}, which is subject to interference between the C-H and the O-H stretches from the aqueous phase.[14-16] Our previously published study discussed the role of lipid gel-to-liquid crystalline phase transition temperatures (T_m) on the SFG spectra obtained. Olenick *et al.* reports that the membranes having T_m's above the laboratory temperature exhibit SFG spectra with at least two additional peaks.[17] The T_m's of DOPC, POPC and DMPC are -18 ºC, -2 ºC, and 24 ºC, respectively, while the laboratory is maintained at 22 ± 2 ºC. Since the SLBs are composed primarily of POPC and DOPC which have T_m's below the laboratory temperature, it is reasonable that the SFG spectra reveal only one broad peak.[17-19]

Figure 6.3D shows the SFG signal obtained from SLBs formed from an 8:2 mixture of DMPC/rough-strain LPS where we obtain three sharp peaks, qualitatively similar to those from pure DMPC and 9:1 mixture of DMPC/DMPG presented in previous chapters. Considering that the T_m of DMPC is close to the laboratory temperature, we believe that it is reasonable that we see similar responses. LPS-incorporated DMPC spectrum was recorded to be able to make direct comparisons to previous work.[14, 17, 20-21] However, we note that low T_m lipids such as POPC and DOPC are more biologically relevant models for bacterial membranes.

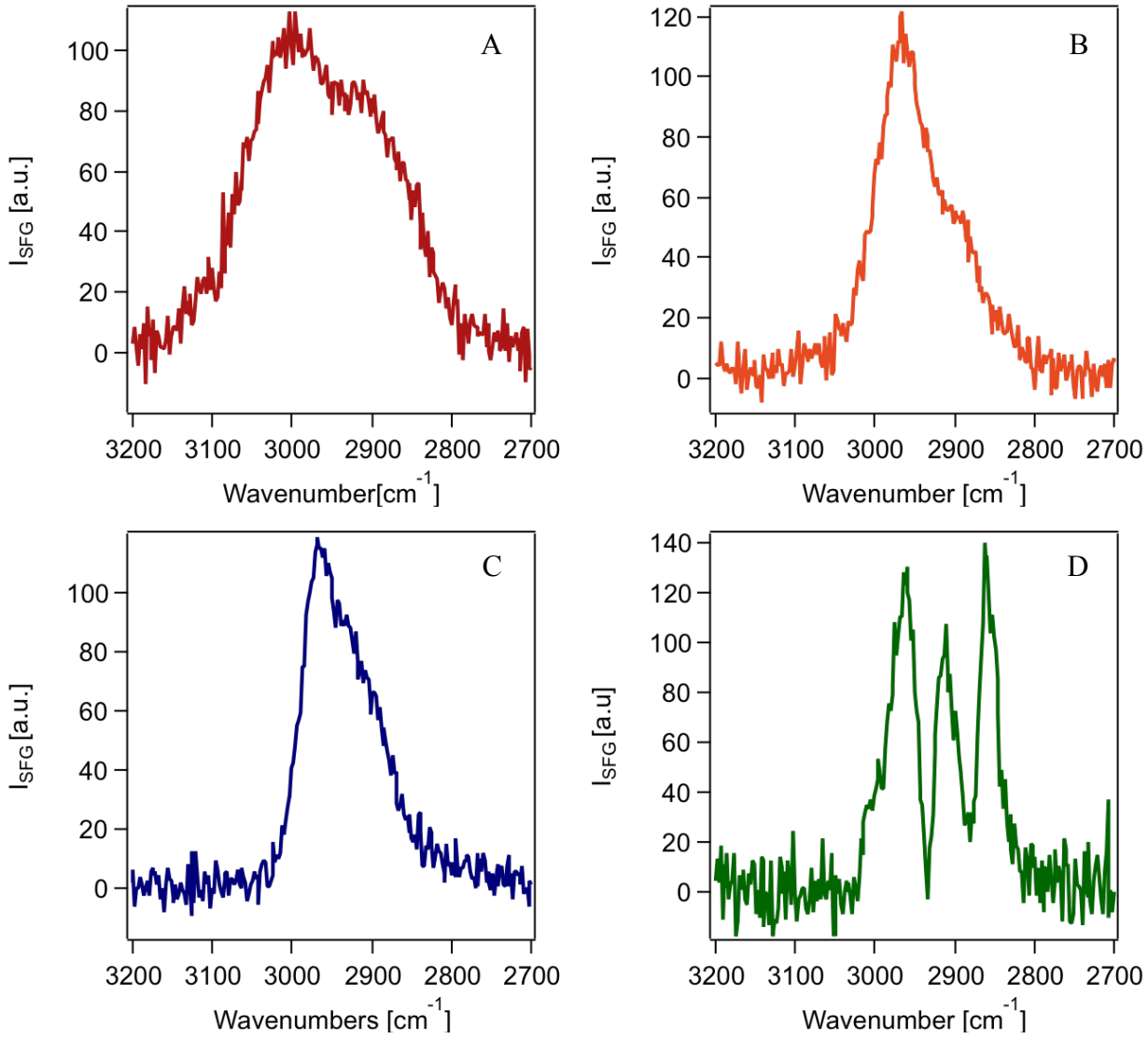

Figure 6.3. *ssp*-Polarized SFG spectra of an SLB formed from an 8:2 mixture of (A) POPC/rough-strain LPS (0.002 M HEPES, 0.025 M NaCl) (B) POPC/smooth-strain LPS (0.002 M HEPES, 0.025 M NaCl) (C) DOPC/rough-strain LPS (0.01 M Tris, 0.1 M NaCl) (D) DMPC/rough-strain LPS (0.01 M Tris, 0.1 M NaCl).

Provided that the LPS molecules are incorporated into the bilayers, the strong dependence of SFG spectra form LPS incorporated bilayers to the primary constituent lipid T_m reveal the presence of disordered alkyl chains from both smooth- and rough-strain LPS, resulting from the cancellation of net transition dipole moment. This outcome is consistent with previous work by Chen and coworkers,[22-23] where the SFG signal from the DPPG bilayers do not show significant differences upon incorporation of sections of LPS (Lipid A and Kdo2-lipid A from *Salmonella minnesota* Re595) in the C–H stretching region but reveal some changes in the water structure over the LPS which can be seen in the O–H stretching region.

6.4. Conclusions

Chapter 6 made a first step to investigate model membranes with increasing complexity by using LPS incorporated SLBs, intended to mimic the outer membrane of Gram-negative bacteria. Here, we have demonstrated the sensitivity of SFG to probe different lipid bilayer structures. Preliminary studies of LPS incorporated SLBs demonstrate that rough- and smooth-strain LPS that are bound to the SLB are fairly disordered such that they are aligned at the interface causing a cancellation of the net dipole moment. Thus, the SFG response of the LPS-incorporated SLBs resemble their lipid bilayer counterpart and LPS does not contribute in significant additional SFG signal in the C–H stretching region. LPS-incorporated SLBs having T_m's lower than the room temperature show only the presence of the peak at ~2980 cm^{-1}, which is subject to interference between the C–H and the O–H stretches from the aqueous phase.

6.5. Future Directions

Future research should include probing more complex models (supported lipid bilayers incorporating LPS, transmembrane proteins, and other biomolecules, as well as suspended lipid bilayers) in the O–H stretching region and investigate the water structure above the bilayer upon exposure to nanoscale transition metal oxides and the released metal ions. Exploring the interactions between more complex model systems and nanomaterials will open new doors to understand how cell surface structures and non-phospholipid components of cell membranes mediate interactions with nanomaterials. Improving the phospholipid membrane model will allow for better comparison to the responses observed in single- and multicellular organisms that are being carried out in the Center for Sustainable Nanotechnology.

Furthermore, future work should extend SFG spectroscopy to the C=O, N-H and PO_2^- stretching regions. Probing additional spectroscopic regions will allow for investigating more complex SLBs including LPS or transmembrane proteins, by probing their characteristic vibrations. Exploring the N-H and PO_2^- stretching region will allow for probing the orientation and structure of lipid headgroups which will lead to a better understanding of membrane interactions, when combined with the information obtained from the other spectroscopic regions.

Finally, given the fast-growing global demand for Li-ion batteries, scientists are pushing beyond the limits for developing new nanomaterials to achieve desired energy efficiency, performance, reliability, and lifetime. Future research should investigate the interactions of these emerging materials, such as $LiFePO_4$ and $LiNi_xCo_yAl_{1-x-y}O_2$. Correspondingly, inorganic coatings are widely used in commercially available cathode materials to enhance stability and durability while mitigating undesired reactivity (degradation, charging, ion dissolution). Understanding how

such coatings can alter environmental impact will be important in developing redesign strategies without altering performance.

The research presented in this thesis demonstrates that SFG spectroscopy, when combined with complementary techniques, is powerful in providing molecular insights into the nano-bio interface. By linking experimental and computational efforts to elucidate the molecular mechanisms of nanomaterial interactions with model membranes, we hope to develop a predictive understanding of the induced biological responses upon nanomaterial exposure and ultimately design nanomaterials to reduce adverse outcomes.

Chapter 1 References

1. Hochella, M. F.; Spencer, M. G.; Jones, K. L., Nanotechnology: Nature's Gift or Scientists' Brainchild? *Environ. Sci. Nano* **2015,** *2* (2), 114-119.

2. Tepe, N.; Bau, M., Importance of Nanoparticles and Colloids from Volcanic Ash for Riverine Transport of Trace Elements to the Ocean: Evidence from Glacial-Fed Rivers after the 2010 Eruption of Eyjafjallajökull Volcano, Iceland. *Sci. Total Environ.* **2014,** *488-489*, 243-251.

3. Sen, A.; Siekmann, F.; Krüger Heinz, U.; Zetzsch, C., Investigation of Atmospheric Nanoparticles: Impact of Sea Salt and Fate of Organic Molecules Adsorbed on Alumina. *Phys. Status Solidi B* **2006,** *243* (13), 3546-3550.

4. Howard, J. B.; Mckinnon, J. T.; Makarovsky, Y.; Lafleur, A. L.; Johnson, M. E., Fullerenes C60 and C70 in Flames. *Nature* **1991,** *352* (6331), 139-141.

5. Raiswell, R.; Benning, L. G.; Tranter, M.; Tulaczyk, S., Bioavailable Iron in the Southern Ocean: The Significance of the Iceberg Conveyor Belt. *Geochem. Trans.* **2008,** *9*.

6. Masciangioli, T.; Alper, J., *Challenges in Characterizing Small Particles: Exploring Particles from the Nano-to Microscales*. National Academies Press: 2012.

7. Griffin, S.; Masood, M.; Nasim, M.; Sarfraz, M.; Ebokaiwe, A.; Schäfer, K.-H.; Keck, C.; Jacob, C., Natural Nanoparticles: A Particular Matter Inspired by Nature. *Antioxidants* **2018,** *7* (1), 3.

8. Nel, A.; Xia, T.; Meng, H.; Wang, X.; Lin, S. J.; Ji, Z. X.; Zhang, H. Y., Nanomaterial Toxicity Testing in the 21st Century: Use of a Predictive Toxicological Approach and High-Throughput Screening. *Acc. Chem. Res.* **2013,** *46* (3), 607-621.

9. Chithrani, B. D.; Chan, W. C. W., Elucidating the Mechanism of Cellular Uptake and Removal of Protein-Coated Gold Nanoparticles of Different Sizes and Shapes. *Nano Lett.* **2007,** *7* (6), 1542-1550.

10. Sau, T. K.; Murphy, C. J., Room Temperature, High-Yield Synthesis of Multiple Shapes of Gold Nanoparticles in Aqueous Solution. *J. Am. Chem. Soc.* **2004,** *126* (28), 8648-8649.

11. Zhang, Y.; Chen, Y. S.; Westerhoff, P.; Hristovski, K.; Crittenden, J. C., Stability of Commercial Metal Oxide Nanoparticles in Water. *Water Res.* **2008,** *42* (8-9), 2204-2212.

12. Pązik, R.; Andersson, R.; Kępiński, L.; Nedelec, J.-M.; Kessler, V. G.; Seisenbaeva, G. A., Surface Functionalization of the Metal Oxide Nanoparticles with Biologically Active Molecules Containing Phosphonate Moieties. Case Study of Batio3. *J. Phys. Chem. C* **2011,** *115* (20), 9850-9860.

13. Nguyen, K. T.; Zhao, Y., Integrated Graphene/Nanoparticle Hybrids for Biological and Electronic Applications. *Nanoscale* **2014,** *6* (12), 6245-6266.

14. Choi, C.; Choi Moon, K.; Hyeon, T.; Kim, D. H., Nanomaterial-Based Soft Electronics for Healthcare Applications. *Chem. Nano Mat.* **2016,** *2* (11), 1006-1017.

15. Yu, S. H.; Lee Soo, H.; Lee Dong, J.; Sung, Y. E.; Hyeon, T., Conversion Reaction-Based Oxide Nanomaterials for Lithium Ion Battery Anodes. *Small* **2015,** *12* (16), 2146-2172.

16. McGillicuddy, E.; Murray, I.; Kavanagh, S.; Morrison, L.; Fogarty, A.; Cormican, M.; Dockery, P.; Prendergast, M.; Rowan, N.; Morris, D., Silver Nanoparticles in the Environment: Sources, Detection and Ecotoxicology. *Sci. Total Environ.* **2017,** *575*, 231-246.

17. Pereira, A. E. S.; Grillo, R.; Mello, N. F. S.; Rosa, A. H.; Fraceto, L. F., Application of Poly(Epsilon-Caprolactone) Nanoparticles Containing Atrazine Herbicide as an Alternative Technique to Control Weeds and Reduce Damage to the Environment. *J. Hazard. Mater.* **2014,** *268*, 207-215.

18. Kashyap, P. L.; Xiang, X.; Heiden, P., Chitosan Nanoparticle Based Delivery Systems for Sustainable Agriculture. *Int. J. Biol. Macromol.* **2015,** *77*, 36-51.

19. Servin, A.; Elmer, W.; Mukherjee, A.; De la Torre-Roche, R.; Hamdi, H.; White, J. C.; Bindraban, P.; Dimkpa, C., A Review of the Use of Engineered Nanomaterials to Suppress Plant Disease and Enhance Crop Yield. *J. Nanopart. Res.* **2015,** *17* (2).

20. Lu, J.; Chen, Z.; Ma, Z.; Pan, F.; Curtiss, L. A.; Amine, K., The Role of Nanotechnology in the Development of Battery Materials for Electric Vehicles. *Nat. Nanotechnol.* **2016,** *11*, 1031.

21. *Based on Iea Data from the Global Ev 2017 © Oecd/Iea 2016, https://Www.Iea.Org/Publications/Freepublications/Publication/Globalevoutlook2017.Pdf.*

22. Richa, K.; Babbitt, C. W.; Gaustad, G.; Wang, X., A Future Perspective on Lithium-Ion Battery Waste Flows from Electric Vehicles. *Resour. Conserv. Recycl.* **2014,** *83*, 63-76.

23. Hu, Y.; Cheng, H.; Tao, S., Retired Electric Vehicle (Ev) Batteries: Integrated Waste Management and Research Needs. *Environ. Sci. Technol.* **2017,** *51* (19), 10927-10929.

24. Liu, X.-Q.; Tang, R.-Z., Biological Responses to Nanomaterials: Understanding Nano-Bio Effects on Cell Behaviors. *Drug Deliv.* **2017,** *24* (2), 1-15.

25. Somorjai, G. A.; Li, Y., Impact of Surface Chemistry. *Proc. Natl. Acad. Sci.* **2011,** *108* (3), 917.

26. Somorjai, G. A.; Li, Y., *Introduction to Surface Chemistry and Catalysis*. 2nd Ed. ed.; Wiley: Hoboken, NJ, 2010.

27. Hoffman, J. B.; Alam, R.; Kamat, P. V., Why Surface Chemistry Matters for Qd–Qd Resonance Energy Transfer. *ACS Energy Lett.* **2017,** *2* (2), 391-396.

28. Friend, C. M.; Xu, B., Heterogeneous Catalysis: A Central Science for a Sustainable Future. *Acc. Chem. Res.* **2017,** *50* (3), 517-521.

29. Nel, A. E.; Madler, L.; Velegol, D.; Xia, T.; Hoek, E. M. V.; Somasundaran, P.; Klaessig, F.; Castranova, V.; Thompson, M., Understanding Biophysicochemical Interactions at the Nano-Bio Interface. *Nat. Mater.* **2009,** *8* (7), 543-557.

30. Elhafez, S. E. A.; Hamad, H. A.; Zaatout, A. A.; Malash, G. F., Management of Agricultural Waste for Removal of Heavy Metals from Aqueous Solution: Adsorption Behaviors, Adsorption Mechanisms, Environmental Protection, and Techno-Economic Analysis. *Environ. Sci. Pollut. Res. Int.* **2017,** *24* (2), 1397-1415.

31. Murphy, C. J.; Vartania, A. M.; Geiger, F. M.; Hamers, R. J.; Pedersen, J. A.; Cui, Q.; Haynes, C. L.; Carlson, E. E.; Hernandez, R.; Klaper, R. D.; Orr, G.; Rosenzweig, Z., Biological Responses to Engineered Nanomaterials: Needs for the Next Decade. *ACS Cent. Sci.* **2015,** *1*, 117-123.

32. Gatoo, M. A.; Naseem, S.; Arfat, M. Y.; Mahmood Dar, A.; Qasim, K.; Zubair, S., Physicochemical Properties of Nanomaterials: Implication in Associated Toxic Manifestations. *BioMed Res. Int.* **2014,** *2014*, 8.

33. Verma, A.; Stellacci, F., Effect of Surface Properties on Nanoparticle–Cell Interactions. *Small* **2010,** *6* (1), 12-21.

34. Georgieva, J. V.; Kalicharan, D.; Couraud, P.-O.; Romero, I. A.; Weksler, B.; Hoekstra, D.; Zuhorn, I. S., Surface Characteristics of Nanoparticles Determine Their Intracellular Fate in and Processing by Human Blood-Brain Barrier Endothelial Cells in Vitro. *Mol. Ther. 19* (2), 318-325.

35. Hang, M. N.; Gunsolus, I. L.; Wayland, H.; Melby, E. S.; Mensch, A. C.; Hurley, K. R.; Pedersen, J. A.; Haynes, C. L.; Hamers, R. J., Impact of Nanoscale Lithium Nickel Manganese Cobalt Oxide (Nmc) on the Bacterium Shewanella Oneidensis Mr-1. *Chem. Mater.* **2016,** *28* (4), 1092-1100.

36. Hoshino, A.; Fujioka, K.; Oku, T.; Suga, M.; Sasaki, Y. F.; Ohta, T.; Yasuhara, M.; Suzuki, K.; Yamamoto, K., Physicochemical Properties and Cellular Toxicity of Nanocrystal Quantum Dots Depend on Their Surface Modification. *Nano Lett.* **2004,** *4* (11), 2163-2169.

37. Kostarelos, K.; Lacerda, L.; Pastorin, G.; Wu, W.; WieckowskiSebastien; Luangsivilay, J.; Godefroy, S.; Pantarotto, D.; Briand, J.-P.; Muller, S.; Prato, M.; Bianco, A., Cellular Uptake of Functionalized Carbon Nanotubes Is Independent of Functional Group and Cell Type. *Nat. Nano* **2007,** *2* (2), 108-113.

38. Liu, W.-T., Nanoparticles and Their Biological and Environmental Applications. *J. Biosci. Bioeng.* **2006,** *102* (1), 1-7.

39. Marshall, A. T.; Haverkamp, R. G.; Davies, C. E.; Parsons, J. G.; Gardea-Torresdey, J. L.; van Agterveld, D., Accumulation of Gold Nanoparticles in Brassic Juncea. *Int. J. Phytoremediation* **2007,** *9* (3), 197-206.

40. Murphy, C. J.; Gole, A. M.; Stone, J. W.; Sisco, P. N.; Alkilany, A. M.; Goldsmith, E. C.; Baxter, S. C., Gold Nanoparticles in Biology: Beyond Toxicity to Cellular Imaging. *Acc. Chem. Res.* **2008,** *41* (12), 1721-1730.

41. Richter, R. P.; Bérat, R.; Brisson, A. R., Formation of Solid-Supported Lipid Bilayers: An Integrated View. *Langmuir* **2006,** *22* (8), 3497-3505.

42. Chan, Y.-H. M.; Boxer, S. G., Model Membrane Systems and Their Applications. *Curr. Opin. Chem. Biol.* **2007,** *11* (6), 581-587.

43. Hardy, G. J.; Nayak, R.; Zauscher, S., Model Cell Membranes: Techniques to Form Complex Biomimetic Supported Lipid Bilayers Via Vesicle Fusion. *Curr. Opin. Colloid Interface Sci.* **2013,** *18* (5), 448-458.

44. Liu, J.; Jiang, X.; Ashley, C.; Brinker, C. J., Electrostatically Mediated Liposome Fusion and Lipid Exchange with a Nanoparticle-Supported Bilayer for Control of Surface Charge, Drug Containment, and Delivery. *J. Am. Chem. Soc.* **2009,** *131* (22), 7567-7569.

45. Bayley, H.; Cremer, P. S., Stochastic Sensors Inspired by Biology. *Nature* **2001,** *413*, 226.

46. Nikoleli, G.-P.; Nikolelis, D.; Siontorou, G. C.; Karapetis, S., Lipid Membrane Nanosensors for Environmental Monitoring: The Art, the Opportunities, and the Challenges. *Sensors* **2018,** *18* (1).

47. Phillips, K. S.; Cheng, Q., Microfluidic Immunoassay for Bacterial Toxins with Supported Phospholipid Bilayer Membranes on Poly(Dimethylsiloxane). *Anal. Chem.* **2005,** *77* (1), 327-334.

48. Armanious, A.; Gerelli, Y.; Agnarsson, B.; Pace, H.; Micciulla, S.; Schneck, E.; Höök, F., A Holistic Approach to Study Interactions between Nanoparticles/Vesicles/Viruses and Supported Lipid Bilayers Using Qcm-D, Dual-Wavelength Spr, and Neutron Reflectometry. *Biophys. J. 114* (3), 279a.

49. Vafaei, S.; Tabaei Seyed, R.; Biswas Kabir, H.; Groves Jay, T.; Cho, N. J., Cell Adhesion: Dynamic Cellular Interactions with Extracellular Matrix Triggered by Biomechanical Tuning of Low-Rigidity, Supported Lipid Membranes (Adv. Healthcare Mater. 10/2017). *Adv. Healthc. Mater.* **2017,** *6* (10).

50. Larsson, C.; Rodahl, M.; Höök, F., Characterization of DNA Immobilization and Subsequent Hybridization on a 2d Arrangement of Streptavidin on a Biotin-Modified Lipid Bilayer Supported on Sio2. *Anal. Chem.* **2003,** *75* (19), 5080-5087.

51. Kam, L.; Boxer, S. G., Spatially Selective Manipulation of Supported Lipid Bilayers by Laminar Flow: Steps toward Biomembrane Microfluidics. *Langmuir* **2003,** *19* (5), 1624-1631.

52. Muñoz, J.; Montes, R.; Baeza, M., Trends in Electrochemical Impedance Spectroscopy Involving Nanocomposite Transducers: Characterization, Architecture Surface and Bio-Sensing. *TrAC, Trends Anal. Chem.* **2017,** *97*, 201-215.

53. Han, L.; Liu, P.; Petrenko, V. A.; Liu, A., A Label-Free Electrochemical Impedance Cytosensor Based on Specific Peptide-Fused Phage Selected from Landscape Phage Library. *Sci. Rep.* **2016,** *6*, 22199.

54. Kalmodia, S.; Parameswaran, S.; Yang, W.; Barrow, C. J.; Krishnakumar, S., Attenuated Total Reflectance Fourier Transform Infrared Spectroscopy: An Analytical Technique to Understand Therapeutic Responses at the Molecular Level. *Sci. Rep.* **2015,** *5*, 16649.

55. Baer, D. R.; Engelhard, M. H., Xps Analysis of Nanostructured Materials and Biological Surfaces. *J. Electron. Spectrosc. Relat. Phenom.* **2010,** *178-179*, 415-432.

56. Kenry; Geldert, A.; Liu, Y.; Loh, K. P.; Teck Lim, C., Nano-Bio Interactions between Carbon Nanomaterials and Blood Plasma Proteins: Why Oxygen Functionality Matters. *NPG Asia Mater.* **2017,** *9*, e422.

57. Xu, M.; Li, J.; Iwai, H.; Mei, Q.; Fujita, D.; Su, H.; Chen, H.; Hanagata, N., Formation of Nano-Bio-Complex as Nanomaterials Dispersed in a Biological Solution for Understanding Nanobiological Interactions. *Sci. Rep.* **2012,** *2*, 406.

58. Leroueil, P. R.; Hong, S.; Mecke, A.; Baker, J. R.; Orr, B. G.; Banaszak Holl, M. M., Nanoparticle Interaction with Biological Membranes: Does Nanotechnology Present a Janus Face? *Acc. Chem. Res.* **2007,** *40* (5), 335-342.

59. Tagaya, M., In Situ Qcm-D Study of Nano-Bio Interfaces with Enhanced Biocompatibility. *Polym. J.* **2015,** *47*, 599.

60. Troiano, J. M.; Olenick, L. L.; Kuech, T. R.; Melby, E. S.; Hu, D. H.; Lohse, S. E.; Mensch, A. C.; Doğangün, M.; Vartanian, A. M.; Torelli, M. D.; Ehimiaghe, E.; Walter, S. R.; Fu, L.; Anderton, C. R.; Zhu, Z. H.; Wang, H. F.; Orr, G.; Murphy, C. J.; Hamers, R. J.; Pedersen, J. A.; Geiger, F. M., Direct Probes of 4 Nm Diameter Gold Nanoparticles Interacting with Supported Lipid Bilayers. *J Phys Chem C* **2015,** *119* (1), 534-546.

61. Kim, S.-O.; Jackman, J. A.; Mochizuki, M.; Yoon, B. K.; Hayashi, T.; Cho, N.-J., Correlating Single-Molecule and Ensemble-Average Measurements of Peptide Adsorption onto Different Inorganic Materials. *Phys. Chem. Chem. Phys.* **2016,** *18* (21), 14454-14459.

62. Zhou, W. W., Z. L., *Scanning Microscopy for Nanotechnology Techniques and Applications*. Springer: New York, 2006.

63. Zhang, X.; Han, X.; Wu, F.; Jasensky, J.; Chen, Z., Nano-Bio Interfaces Probed by Advanced Optical Spectroscopy: From Model System Studies to Optical Biosensors. *Chin. Sci. Bull.* **2013,** *58* (21), 2537-2556.

64. Munteanu, B.; Harb, F.; Rieu, J. P.; Berthier, Y.; Tinland, B.; Trunfio-Sfarghiu, A. M., Charged Particles Interacting with a Mixed Supported Lipid Bilayer as a Biomimetic Pulmonary Surfactant. *Eur. Phys. J. E* **2014,** *37* (8), 72.

65. Ahmed, F. E.; Wiley, J. E.; Weidner, D. A.; Bonnerup, C.; Mota, H., Surface Plasmon Resonance (Spr) Spectrometry as a Tool to Analyze Nucleic Acid–Protein Interactions in Crude Cellular Extracts. *Cancer Genomics - Proteomics* **2010,** *7* (6), 303-309.

66. Jönsson, U.; Fägerstam, L.; Ivarsson, B.; Johnsson, B.; Karlsson, R.; Lundh, K.; Löfås, S.; Persson, B.; Roos, H.; Rönnberg, I., Real-Time Biospecific Interaction Analysis Using Surface Plasmon Resonance and a Sensor Chip Technology. *Biotechniques* **1991,** *11* (5), 620-627.

67. Messersmith, R. E.; Nusz, G. J.; Reed, S. M., Using the Localized Surface Plasmon Resonance of Gold Nanoparticles to Monitor Lipid Membrane Assembly and Protein Binding. *J. Phys. Chem. C* **2013,** *117* (50), 26725-26733.

68. Walker, R. A.; Gruetzmacher, J. A.; Richmond, G. L., Phosphatidylcholine Monolayer Structure at a Liquid−Liquid Interface. *J. Am. Chem. Soc.* **1998,** *120* (28), 6991-7003.

69. Shen, Y. R., Surface Properties Probed by Second-Harmonic and Sum-Frequency Generation. *Nature* **1989,** *337* (6207), 519-525.

70. Esenturk, O.; Walker, R. A., Surface Structure at Hexadecane and Halo-Hexadecane Liquid/Vapor Interfaces. *J. Phys. Chem. B* **2004,** *108* (30), 10631-10635.

71. Geiger, F. M., Second Harmonic Generation, Sum Frequency Generation, and X(3): Dissecting Environmental Interfaces with a Nonlinear Optical Swiss Army Knife. *Annu. Rev. Phys. Chem.* **2009,** *60* (1), 61-83.

72. Bain, C. D., Sum-Frequency Vibrational Spectroscopy of the Solid/Liquid Interface. *J. Chem. Soc., Faraday Trans.* **1995,** *91* (9), 1281-1296.

73. Richmond, G. L., Peer Reviewed: Vibrational Spectroscopy of Molecules at Liquid/Liquid Interfaces. *Anal. Chem.* **1997,** *69* (17), 536A-543A.

74. Yang, P.; Wu, F. G.; Chen, Z., Lipid Fluid-Gel Phase Transition Induced Alamethicin Orientational Change Probed by Sum Frequency Generation Vibrational Spectroscopy. *J. Phys. Chem. C* **2013,** *117* (33), 17039-17049.

75. Liu, J.; Conboy, J. C., Phase Transition of a Single Lipid Bilayer Measured by Sum-Frequency Vibrational Spectroscopy. *J. Am. Chem. Soc.* **2004,** *126* (29), 8894-8895.

76. Liu, J.; Conboy, J. C., 1,2-Diacyl-Phosphatidylcholine Flip-Flop Measured Directly by Sum-Frequency Vibrational Spectroscopy. *Biophys. J.* **2005,** *89* (4), 2522-2532.

77. Liu, J.; Conboy, J. C., Direct Measurement of the Transbilayer Movement of Phospholipids by Sum-Frequency Vibrational Spectroscopy. *J. Am. Chem. Soc.* **2004,** *126* (27), 8376-8377.

78. Anglin, T. C.; Cooper, M. P.; Li, H.; Chandler, K.; Conboy, J. C., Free Energy and Entropy of Activation for Phospholipid Flip-Flop in Planar Supported Lipid Bilayers. *J. Phys. Chem. B* **2010,** *114* (5), 1903-1914.

79. Brown, K. L.; Conboy, J. C., Electrostatic Induction of Lipid Asymmetry. *J. Am. Chem. Soc.* **2011,** *133* (23), 8794-8797.

80. Chen, X.; Chen, Z., Sfg Studies on Interactions between Antimicrobial Peptides and Supported Lipid Bilayers. *Biochim. Biophys. Acta Biomemb.* **2006,** *1758* (9), 1257-1273.

81. Wu, F. G.; Yang, P.; Zhang, C.; Li, B. L.; Han, X. F.; Song, M. H.; Chen, Z., Molecular Interactions between Amantadine and Model Cell Membranes. *Langmuir* **2014,** *30* (28), 8491-8499.

82. Kim, G.; Gurau, M. C.; Lim, S.-M.; Cremer, P. S., Investigations of the Orientation of a Membrane Peptide by Sum Frequency Spectroscopy. *J. Phys. Chem. B* **2003,** *107*, 1403-1409.

83. Walter, S. R.; Geiger, F. M., DNA on Stage: Showcasing Oligonucleotides at Surfaces and Interfaces with Second Harmonic and Vibrational Sum Frequency Generation. *J. Phys. Chem. Lett.* **2010,** *1* (1), 9-15.

84. Campen, R. K.; Ngo, T. T. M.; Sovago, M.; Ruysschaert, J.-M.; Bonn, M., Molecular Restructuring of Water and Lipids Upon the Interaction of DNA with Lipid Monolayers. *J. Am. Chem. Soc.* **2010,** *132* (23), 8037-8047.

85. Bordenyuk, A. N.; Weeraman, C.; Yatawara, A.; Jayathilake, H. D.; Stiopkin, I.; Liu, Y.; Benderskii, A. V., Vibrational Sum Frequency Generation Spectroscopy of Dodecanethiol on Metal Nanoparticles. *J. Phys. Chem. C* **2007,** *111* (25), 8925-8933.

86. Baer, D. R.; Gaspar, D. J.; Nachimuthu, P.; Techane, S. D.; Castner, D. G., Application of Surface Chemical Analysis Tools for Characterization of Nanoparticles. *Anal. Bioanal. Chem.* **2010,** *396* (3), 983-1002.

87. Roke, S.; Schins, J.; Müller, M.; Bonn, M., Vibrational Spectroscopic Investigation of the Phase Diagram of a Biomimetic Lipid Monolayer. *Physical Review Letters* **2003,** *90* (12), 128101.

88. Casper, C. B.; Verreault, D.; Adams, E. M.; Hua, W.; Allen, H. C., Surface Potential of Dppc Monolayers on Concentrated Aqueous Salt Solutions. *J. Phys. Chem. B* **2016,** *120* (8), 2043-2052.

89. Liu, J.; Conboy, J. C., Structure of a Gel Phase Lipid Bilayer Prepared by the Langmuir-Blodgett/Langmuir-Schaefer Method Characterized by Sum-Frequency Vibrational Spectroscopy. *Langmuir* **2005,** *21* (20), 9091-9097.

90. Watry, M. R.; Tarbuck, T. L.; Richmond, G. L., Vibrational Sum-Frequency Studies of a Series of Phospholipid Monolayers and the Associated Water Structure at the Vapor/Water Interface. *J. Phys. Chem. B* **2003,** *107* (2), 512-518.

Chapter 2 References

1. Richmond, G. L., Peer Reviewed: Vibrational Spectroscopy of Molecules at Liquid/Liquid Interfaces. *Anal. Chem.* **1997,** *69* (17), 536A-543A.

2. Du, Q.; Superfine, R.; Freysz, E.; Shen, Y. R., Vibrational Spectroscopy of Water at the Vapor Water Interface. *Phys. Rev. Lett.* **1993,** *70* (15), 2313-2316.

3. Moad, A. J.; Simpson, G. J., A Unified Treatment of Selection Rules and Symmetry Relations for Sum-Frequency and Second Harmonic Spectroscopies. *J. Phys. Chem. B* **2004,** *108* (11), 3548-3562.

4. Lambert, A. G.; Davies, P. B.; Neivandt, D. J., Implementing the Theory of Sum Frequency Generation Vibrational Spectroscopy: A Tutorial Review. *Appl. Spectrosc. Rev.* **2005,** *40* (2), 103-145.

5. Heinz, T. F., Second-Order Nonlinear Optical Effects at Surfaces and Interfaces. In *Nonlinear Surface Electromagnetic Phenomena*, Ponath, H.-E.; Stegeman, G. I., Eds. Elsevier Publishers: Amsterdam, 1991; p 353.

6. Shen, Y. R., Surface Properties Probed by Second-Harmonic and Sum-Frequency Generation. *Nature* **1989,** *337* (6207), 519-525.

7. Du, Q.; Freysz, E.; Shen, Y. R., Surface Vibrational Spectroscopic Studies of Hydrogen-Bonding and Hydrophobicity. *Science* **1994,** *264* (5160), 826-828.

8. Walker, R. A.; Gruetzmacher, J. A.; Richmond, G. L., Phosphatidylcholine Monolayer Structure at a Liquid−Liquid Interface. *J. Am. Chem. Soc.* **1998,** *120* (28), 6991-7003.

9. Wang, J.; Buck, S. M.; Even, M. A.; Chen, Z., Molecular Responses of Proteins at Different Interfacial Environments Detected by Sum Frequency Generation Vibrational Spectroscopy. *J. Am. Chem. Soc.* **2002,** *124* (44), 13302-13305.

10. Bain, C. D., Sum-Frequency Vibrational Spectroscopy of the Solid/Liquid Interface. *J. Chem. Soc., Faraday Trans.* **1995,** *91* (9), 1281-1296.

11. Gobrogge, E. A.; Woods, B. L.; Walker, R. A., Liquid Organization and Solvation Properties at Polar Solid/Liquid Interfaces. *Faraday Discuss.* **2013,** *167* (0), 309-327.

12. Buchbinder, A. M.; Weitz, E.; Geiger, F. M., Pentane, Hexane, Cyclopentane, Cyclohexane, 1-Hexene, 1-Pentene, Cis-2-Pentene, Cyclohexene, and Cyclopentene at Vapor/A-Alumina and Liquid/A-Alumina Interfaces Studied by Broadband Sum Frequency Generation. *J. Phys. Chem. C* **2010,** *114* (1), 554-566.

13. Upshur, M. A.; Chase, H. M.; Strick, B. F.; Ebben, C. J.; Fu, L.; Wang, H.; Thomson, R. J.; Geiger, F. M., Vibrational Mode Assignment of A-Pinene by Isotope Editing: One Down, Seventy-One to Go. *J. Phys. Chem. A* **2016,** *120* (17), 2684-2690.

14. Miranda, P. B.; Shen, Y. R., Liquid Interfaces: A Study by Sum-Frequency Vibrational Spectroscopy. *J. Phys. Chem. B* **1999,** *103* (17), 3292-3307.

15. Esenturk, O.; Walker, R. A., Surface Structure at Hexadecane and Halo-Hexadecane Liquid/Vapor Interfaces. *J. Phys. Chem. B* **2004,** *108* (30), 10631-10635.

16. Esenturk, O.; Walker, R. A., Surface Vibrational Structure at Alkane Liquid/Vapor Interfaces. *J. Chem. Phys.* **2006,** *125* (17), 12.

17. Eisenthal, K. B., Liquid Interfaces Probed by Second-Harmonic and Sum-Frequency Spectroscopy. *Chem. Rev.* **1996,** *96* (4), 1343-1360.

18. Bonn, M.; Bakker, H. J.; Backus, E. H., No Ice-Like Water at Aqueous Biological Interfaces. *Biointerphases* **2012,** *7*, 20.

19. Liljeblad, J. F. D.; Tyrode, E., Vibrational Sum Frequency Spectroscopy Studies at Solid/Liquid Interfaces: Influence of the Experimental Geometry in the Spectral Shape and Enhancement. *J. Phys. Chem. C* **2012,** *116* (43), 22893-22903.

20. Ishiyama, T.; Terada, D.; Morita, A., Hydrogen-Bonding Structure at Zwitterionic Lipid/Water Interface. *J. Phys. Chem. Lett.* **2016,** *7*, 216-220.

21. Chen, X.; Chen, Z., Sfg Studies on Interactions between Antimicrobial Peptides and Supported Lipid Bilayers. *Biochim. Biophys. Acta Biomemb.* **2006,** *1758* (9), 1257-1273.

22. Jung, S.-Y.; Lim, S.-M.; Albertorio, F.; Kim, G.; Gurau, M. C.; Yang, R. D.; Holden, M. A.; Cremer, P. S., The Vroman Effect: A Molecular Level Description of Fibrinogen Displacement. *J. Am. Chem. Soc.* **2003,** *125* (42), 12782-12786.

23. Mermut, O.; Phillips, D. C.; York, R. L.; McCrea, K. R.; Ward, R. S.; Somorjai, G. A., In Situ Adsorption Studies of a 14-Amino Acid Leucine-Lysine Peptide onto Hydrophobic Polystyrene and Hydrophilic Silica Surfaces Using Quartz Crystal Microbalance, Atomic Force Microscopy, and Sum Frequency Generation Vibrational Spectroscopy. *J. Am. Chem. Soc.* **2006,** *128* (11), 3598-3607.

24. Fu, L.; Liu, J.; Yan, E. C. Y., Chiral Sum Frequency Generation Spectroscopy for Characterizing Protein Secondary Structures at Interfaces. *J. Am. Chem. Soc.* **2011,** *133* (21), 8094-8097.

25. Fu, L.; Wang, Z.; Yan Elsa, C. Y., N-H Stretching Modes around 3300 Wavenumber from Peptide Backbones Observed by Chiral Sum Frequency Generation Vibrational Spectroscopy. *Chirality* **2014,** *26* (9), 521-524.

26. Liu, J.; Conboy, J. C., Asymmetric Distribution of Lipids in a Phase Segregated Phospholipid Bilayer Observed by Sum-Frequency Vibrational Spectroscopy. *J. Phys. Chem. C* **2007,** *111* (25), 8988-8999.

27. Roke, S.; Schins, J.; Müller, M.; Bonn, M., Vibrational Spectroscopic Investigation of the Phase Diagram of a Biomimetic Lipid Monolayer. *Phys. Rev. Lett.* **2003,** *90* (12), 128101.

28. Bordenyuk, A. N.; Weeraman, C.; Yatawara, A.; Jayathilake, H. D.; Stiopkin, I.; Liu, Y.; Benderskii, A. V., Vibrational Sum Frequency Generation Spectroscopy of Dodecanethiol on Metal Nanoparticles. *J. Phys. Chem. C* **2007,** *111* (25), 8925-8933.

29. Sovago, M.; Campen, R. K.; Wurpel, G. W. H.; Muller, M.; Bakker, H. J.; Bonn, M., Vibrational Response of Hydrogen-Bonded Interfacial Water Is Dominated by Intramolecular Coupling. *Phys. Rev. Lett.* **2008,** *100* (17).

30. Wu, F.-G.; Yang, P.; Zhang, C.; Han, X.; Song, M.; Chen, Z., Investigation of Drug–Model Cell Membrane Interactions Using Sum Frequency Generation Vibrational Spectroscopy: A Case Study of Chlorpromazine. *J. Phys. Chem. C* **2014,** *118* (31), 17538-17548.

31. Wu, F. G.; Yang, P.; Zhang, C.; Li, B. L.; Han, X. F.; Song, M. H.; Chen, Z., Molecular Interactions between Amantadine and Model Cell Membranes. *Langmuir* **2014,** *30* (28), 8491-8499.

32. Yang, P.; Wu, F. G.; Chen, Z., Lipid Fluid-Gel Phase Transition Induced Alamethicin Orientational Change Probed by Sum Frequency Generation Vibrational Spectroscopy. *J. Phys. Chem. C* **2013,** *117* (33), 17039-17049.

33. Roeters, S. J.; van Dijk, C. N.; Torres-Knoop, A.; Backus, E. H. G.; Campen, R. K.; Bonn, M.; Woutersen, S., Determining in Situ Protein Conformation and Orientation from the Amide-I Sum-Frequency Generation Spectrum: Theory and Experiment. *J. Phys. Chem. A* **2013,** *117* (29), 6311-6322.

34. Wang, J.; Even, M. A.; Chen, X.; Schmaier, A. H.; Waite, J. H.; Chen, Z., Detection of Amide I Signals of Interfacial Proteins in Situ Using Sfg. *J. Am. Chem. Soc.* **2003,** *125* (33), 9914-9915.

35. Chen, X.; Hua, W.; Huang, Z.; Allen, H. C., Interfacial Water Structure Associated with Phospholipid Membranes Studied by Phase-Sensitive Vibrational Sum Frequency Generation Spectroscopy. *J. Am. Chem. Soc.* **2010,** *132*, 11336-11342.

36. Ma, G.; Liu, J.; Fu, L.; Yan, E. C. Y., Probing Water and Biomolecules at the Air–Water Interface with a Broad Bandwidth Vibrational Sum Frequency Generation Spectrometer from 3800 to 900 Cm−1. *Appl. Spectrosc.* **2009,** *63* (5), 528-537.

37. Hore, D. K.; Beaman, D. K.; Richmond, G. L., Surfactant Headgroup Orientation at the Air/Water Interface. *J. Am. Chem. Soc.* **2005,** *127* (26), 9356-9357.

38. Boyd, R. W., *Nonlinear Optics, 3rd Edition*. Elsevier Academic Press Inc: San Diego, 2008; p 1-613.

39. Yan, E. C. Y.; Fu, L.; Wang, Z.; Liu, W., Biological Macromolecules at Interfaces Probed by Chiral Vibrational Sum Frequency Generation Spectroscopy. *Chem. Rev.* **2014,** *114* (17), 8471-8498.

40. Akamatsu, N.; Domen, K.; Hirose, C., Sfg Study of Two-Dimensional Orientation of Surface Methyl Groups on Cadmium Arachidate Langmuir-Blodgett Films. *J. Phys. Chem.* **1993,** *97* (39), 10070-10075.

41. Hayes, P. L.; Chen, E. H.; Achtyl, J. L.; Geiger, F. M., An Optical Voltmeter for Studying Cetyltrimethylammonium Interacting with Fused Silica/Aqueous Interfaces at High Ionic Strength. *J. Phys. Chem. A* **2009,** *113* (16), 4269-4280.

42. Troiano, J. M.; Olenick, L. L.; Kuech, T. R.; Melby, E. S.; Hu, D. H.; Lohse, S. E.; Mensch, A. C.; Doğangün, M.; Vartanian, A. M.; Torelli, M. D.; Ehimiaghe, E.; Walter, S. R.; Fu, L.; Anderton, C. R.; Zhu, Z. H.; Wang, H. F.; Orr, G.; Murphy, C. J.; Hamers, R. J.; Pedersen, J. A.; Geiger, F. M., Direct Probes of 4 Nm Diameter Gold Nanoparticles Interacting with Supported Lipid Bilayers. *J. Phys. Chem. C* **2015,** *119* (1), 534-546.

43. Stokes, G. Y.; Buchbinder, A. M.; Gibbs-Davis, J. M.; Scheidt, K. A.; Geiger, F. M., Heterogeneous Ozone Oxidation Reactions of 1-Pentene, 2-Hexene, Cyclopentene, Cyclohexene, and a Menthenol Derivative Studied by Sum Frequency Generation. *J. Phys. Chem. A* **2008,** *112*, 11688-11698.

44. Voges, A. B.; Al-Abadleh, H. A.; Musorrariti, M. J.; Bertin, P. A.; Nguyen, S. T.; Geiger, F. M., Carboxylic Acid- and Ester-Functionalized Siloxane Scaffolds on Glass Studied by Broadband Sum Frequency Generation. *J. Phys. Chem. B* **2004,** *108* (48), 18675-18682.

45. Buchbinder, A. M.; Weitz, E.; Geiger, F. M., When the Solute Becomes the Solvent: Orientation, Ordering, and Structure of Binary Mixtures of 1-Hexanol and Cyclohexane over the (0001) Alpha-Al2o3 Surface. *J. Am. Chem. Soc.* **2010,** *132* (41), 14661-14668.

46. Buchbinder, A. M.; Weitz, E.; Geiger, F. M., Pentane, Hexane, Cyclopentane, Cyclohexane, 1-Hexene, 1-Pentene, Cis-2-Pentene, Cyclohexene, and Cyclopentene at Vapor/A-Alumina and Liquid/A-Alumina Interfaces Studied by Broadband Sum Frequency Generation. *J. Phys. Chem. C* **2009,** *114* (1), 554-566.

47. Zhuang, X.; Miranda, P. B.; Kim, D.; Shen, Y. R., Mapping Molecular Orientation and Conformation at Interfaces by Surface Nonlinear Optics. *Phys. Rev. B* **1999,** *59* (19), 12632-12640.

48. Szoka, F.; Papahadjopoulos, D., Comparative Properties and Methods of Preparation of Lipid Vesicles (Liposomes). *Annu. Rev. Biophys. Bioeng.* **1980,** *9*, 467-508.

49. Castellana, E. T.; Cremer, P. S., Solid Supported Lipid Bilayers: From Biophysical Studies to Sensor Design. *Surf. Sci. Rep.* **2006,** *61* (10), 429-444.

50. Schonherr, H.; Johnson, J. M.; Lenz, P.; Frank, C. W.; Boxer, S. G., Vesicle Adsorption and Lipid Bilayer Formation on Glass Studied by Atomic Force Microscopy. *Langmuir* **2004,** *20* (26), 11600-11606.

Chapter 3 References

1. Shao-Horn, Y.; Croguennec, L.; Delmas, C.; Nelson, E. C.; O'Keefe, M. A., Atomic Resolution of Lithium Ions in Licoo2. *Nat. Mater.* **2003,** *2* (7), 464-467.

2. Xia, H.; Wan, Y.; Assenmacher, W.; Mader, W.; Yuan, G.; Lu, L., Facile Synthesis of Chain-Like Licoo2 Nanowire Arrays as Three-Dimensional Cathode for Microbatteries. *NPG Asia Mater.* **2014,** *6*, e126.

3. Gulbinska, M. K., *Lithium-Ion Battery Materials and Engineering: Current Topics and Problems from the Manufacturing Perspective*. Springer London: 2014.

4. Xiao, X. L.; Yang, L. M.; Zhao, H.; Hu, Z. B.; Li, Y. D., Facile Synthesis of Licoo2 Nanowires with High Electrochemical Performance. *Nano Res.* **2012,** *5* (1), 27-32.

5. Wei, T.; Zeng, R.; Sun, Y. M.; Huang, Y. H.; Huang, K. V., A Reversible and Stable Flake-Like Licoo2 Cathode for Lithium Ion Batteries. *Chem. Commun.* **2014,** *50* (16), 1962-1964.

6. Belharouak, I.; Sun, Y. K.; Liu, J.; Amine, K., Li(Ni1/3co1/3mn1/3)O-2 as a Suitable Cathode for High Power Applications. *J. Power Sources* **2003,** *123* (2), 247-252.

7. Conry, T. E.; Mehta, A.; Cabana, J.; Doeff, M. M., Structural Underpinnings of the Enhanced Cycling Stability Upon Al-Substitution in Lini0.45mn0.45co0.1-Yalyo2 Positive Electrode Materials for Li-Ion Batteries. *Chem. Mater.* **2012,** *24* (17), 3307-3317.

8. Goodenough, J. B.; Kim, Y., Challenges for Rechargeable Li Batteries. *Chem. Mater.* **2010,** *22* (3), 587-603.

9. Kang, K. S.; Meng, Y. S.; Breger, J.; Grey, C. P.; Ceder, G., Electrodes with High Power and High Capacity for Rechargeable Lithium Batteries. *Science* **2006,** *311* (5763), 977-980.

10. Kang, D. H. P.; Chen, M.; Ogunseitan, O. A., Potential Environmental and Human Health Impacts of Rechargeable Lithium Batteries in Electronic Waste. *Environ. Sci. Technol.* **2013,** *47* (10), 5495-5503.

11. Poizot, P.; Laruelle, S.; Grugeon, S.; Dupont, L.; Tarascon, J. M., Nano-Sized Transition-Metaloxides as Negative-Electrode Materials for Lithium-Ion Batteries. *Nature* **2000,** *407* (6803), 496-499.

12. Lu, Z. H.; MacNeil, D. D.; Dahn, J. R., Layered Li Nixco1-2xmnx O-2 Cathode Materials for Lithium-Ion Batteries. *Electrochem. Solid State Lett.* **2001,** *4* (12), A200-A203.

13. Ruffo, R.; Wessells, C.; Guggins, R. A.; Cui, Y., Electrochemical Behavior of Licoo2 as Aqueous Lithium-Ion Battery Electrodes. *Electrochem. Comm.* **2009,** *11*, 247-249.

14. Voet, D.; Voet, J. G., *Biochemistry*. 3rd ed.; Wiley Text Books: New York, NY, 2004.

15. Okubo, M.; Hosono, E.; Kim, J.; Enomoto, M.; Kojima, N.; Kudo, T.; Zhou, H.; Honma, I., Nanosize Effect on High-Rate Li-Ion Intercalation in Licoo2 Electrode. *J. Am. Chem. Soc.* **2007,** *129* (23), 7444-7452.

16. Tarascon, J. M.; Armand, M., Issues and Challenges Facing Rechargeable Lithium Batteries. *Nature* **2001,** *414* (6861), 359-367.

17. Nel, A. E.; Madler, L.; Velegol, D.; Xia, T.; Hoek, E. M. V.; Somasundaran, P.; Klaessig, F.; Castranova, V.; Thompson, M., Understanding Biophysicochemical Interactions at the Nano-Bio Interface. *Nat. Mater.* **2009,** *8* (7), 543-557.

18. Liu, J.; Conboy, J. C., Asymmetric Distribution of Lipids in a Phase Segregated Phospholipid Bilayer Observed by Sum-Frequency Vibrational Spectroscopy. *J. Phys. Chem. C* **2007,** *111* (25), 8988-8999.

19. Stanglmaier, S.; Hertrich, S.; Fritz, K.; Moulin, J.-F.; Haese-Seiller, M.; Raedler, J. O.; Nickel, B., Asymmetric Distribution of Anionic Phospholipids in Supported Lipid Bilayers. *Langmuir* **2012,** *28*, 10818-10821.

20. Rossetti, F. F.; Textor, M.; Reviakine, I., Asymmetric Distribution of Phosphatidyl Serine in Supported Phospholipid Bilayers on Titanium Dioxide. *Langmuir* **2006,** *22*, 3467-3473.

21. Allhusen, J. S.; Conboy, J. C., The Ins and Outs of Lipid Flip-Flop. *Acc. Chem. Res.* **2017,** *50* (1), 58-65.

22. Bretscher, M. S., Membrane Structure: Some General Principles. *Science* **1973,** *181* (4100), 622-629.

23. Lygre, H.; Moe, G.; Skalevik, R.; Holmsen, H., Interaction of Triclosan with Eukaryotic Membrane Lipids. *Eur. J. Oral Sci.* **2003,** *111* (3), 216-222.

24. Lambert, A. G.; Davies, P. B.; Neivandt, D. J., Implementing the Theory of Sum Frequency Generation Vibrational Spectroscopy: A Tutorial Review. *Appl. Spectrosc. Rev.* **2005,** *40* (2), 103-145.

25. Geiger, F. M., Second Harmonic Generation, Sum Frequency Generation, and Chi((3)): Dissecting Environmental Interfaces with a Nonlinear Optical Swiss Army Knife. *Annu. Rev. Phys. Chem.* **2009,** *60*, 61-83.

26. Richmond, G. L., Peer Reviewed: Vibrational Spectroscopy of Molecules at Liquid/Liquid Interfaces. *Anal. Chem.* **1997,** *69* (17), 536A-543A.

27. Esenturk, O.; Walker, R. A., Surface Structure at Hexadecane and Halo-Hexadecane Liquid/Vapor Interfaces. *J. Phys. Chem. B* **2004,** *108* (30), 10631-10635.

28. Zhu, X. D.; Suhr, H. J.; Shen, Y. R., Surface Vibrational Spectroscopy by Infrared-Visible Sum-Frequency Generation. *J. Opt. Soc. Am B: Opt. Soc.* **1986,** *3* (8), P252-&.

29. Wang, H. F.; Gan, W.; Lu, R.; Rao, Y.; Wu, B. H., Quantitative Spectral and Orientational Analysis in Surface Sum Frequency Generation Vibrational Spectroscopy (Sfg-Vs). *Int. Rev. Phys. Chem.* **2005,** *24* (2), 191-256.

30. Moad, A. J.; Simpson, G. J., A Unified Treatment of Selection Rules and Symmetry Relations for Sum-Frequency and Second Harmonic Spectroscopies. *J. Phys. Chem. B* **2004,** *108* (11), 3548-3562.

31. Liu, J.; Conboy, J. C., Phase Transition of a Single Lipid Bilayer Measured by Sum-Frequency Vibrational Spectroscopy. *J. Am. Chem. Soc.* **2004,** *126* (29), 8894-8895.

32. Castellana, E. T., Solid Supported Lipid Bilayers: From Biophysical Studies to Sensor Design. *Surf. Sci. Rep.* **2006**.

33. Troiano, J. M.; Olenick, L. L.; Kuech, T. R.; Melby, E. S.; Hu, D.; Lohse, S. E.; Mensch, A. C.; Doğangün, M.; Vartanian, A. M.; Torelli, M. D.; Ehimiaghe, E.; Walter, S. R.; Fu, L.; Anderton, C. R.; Zhu, Z.; Wang, H.-f.; Orr, G.; Murphy, C. J.; Hamers, R. J.; Pedersen, J. A.; Geiger, F. M., Direct Probes of 4 Nm Diameter Gold Nanoparticles Interacting with Supported Lipid Bilayers. *J. Phys. Chem. C* **2015,** *119* (1), 534-546.

34. Qian, D.; Hinuma, Y.; Chen, H.; Du, L.-S.; Carroll, K. J.; Ceder, G.; Grey, C. P.; Meng, Y. S., Electronic Spin Transition in Nanosize Stoichiometric Lithium Cobalt Oxide. *J. Am. Chem. Soc.* **2012,** *134* (14), 6096-6099.

35. Doğangün, M.; Hang, M. N.; Troiano, J. M.; McGeachy, A. C.; Melby, E. S.; Pedersen, J. A.; Hamers, R. J.; Geiger, F. M., Alteration of Membrane Compositional Asymmetry by Licoo2 Nanosheets. *ACS Nano* **2015,** *9*, 8755-8765.

36. Hang, M. N.; Gunsolus, I. L.; Wayland, H.; Melby, E. S.; Mensch, A. C.; Hurley, K. R.; Pedersen, J. A.; Haynes, C. L.; Hamers, R. J., Impact of Nanoscale Lithium Nickel Manganese Cobalt Oxide (Nmc) on the Bacterium Shewanella Oneidensis Mr-1. *Chem. Mater.* **2016,** *28* (4), 1092-1100.

37. Willey, K. F.; Vorsa, V.; Braun, R. M.; Winograd, N., Postionization of Molecules Desorbed from Surfaces by Kev Ion Bombardment with Femtosecond Laser Pulses. *Rapid Commun. Mass Spectrom.* **1998,** *12* (18), 1253-1260.

38. Sostarecz, A. G.; Cannon, D. M.; McQuaw, C. M.; Sun, S.; Ewing, A. G.; Winograd, N., Influence of Molecular Environment on the Analysis of Phospholipids by Time-of-Flight Secondary Ion Mass Spectrometry. *Langmuir* **2004,** *20* (12), 4926-4932.

39. Vaezian, B.; Anderton, C. R.; Kraft, M. L., Discriminating and Imaging Different Phosphatidylcholine Species within Phase-Separated Model Membranes by Principal Component Analysis of Tof-Secondary Ion Mass Spectrometry Images. *Anal. Chem.* **2010,** *82* (24), 10006-10014.

40. Brown, K. L.; Conboy, J. C., Electrostatic Induction of Lipid Asymmetry. *J. Am. Chem. Soc.* **2011,** *133* (23), 8794-8797.

41. Anglin, T. C.; Conboy, J. C., Kinetics and Thermodynamics of Flip-Flop in Binary Phospholipid Membranes Measured by Sum-Frequency Vibrational Spectroscopy. *Biochem.* **2009,** *48* (43), 10220-10234.

42. Ramalho, J. P. P.; Gkeka, P.; Sarkisov, L., Structure and Phase Transformations of Dppc Lipid Bilayers in the Presence of Nanoparticles: Insights from Coarse-Grained Molecular Dynamics Simulations. *Langmuir* **2011,** *27* (7), 3723-3730.

43. Grillo, D.; de la Cruz, M. O.; Szleifer, I., Theoretical Studies of the Phase Behavior of Dppc Bilayers in the Presence of Macroions. *Soft Matter* **2011,** *7* (10), 4672-4679.

44. Van Lehn, R. C.; Alexander-Katz, A., Membrane-Embedded Nanoparticles Induce Lipid Rearrangements Similar to Those Exhibited by Biological Membrane Proteins. *J. Phys. Chem. B* **2014,** *118* (44), 12586-12598.

45. Munteanu, B.; Harb, F.; Rieu, J. P.; Berthier, Y.; Tinland, B.; Trunfio-Sfarghiu, A. M., Charged Particles Interacting with a Mixed Supported Lipid Bilayer as a Biomimetic Pulmonary Surfactant. *Eur. Phys. J. E* **2014,** *37* (8).

46. Wang, B.; Zhang, L. F.; Bae, S. C.; Granick, S., Nanoparticle-Induced Surface Reconstruction of Phospholipid Membranes. *Proc. Natl. Acad. Sci. USA* **2008,** *105* (47), 18171-18175.

47. Devaux, P. F., Static and Dynamic Lipid Asymmetry in Cell Membranes. *Biochem. US* **1991,** *30* (5), 1163-1173.

48. Schlegel, R. A.; Williamson, P., Phosphatidylserine, a Death Knell. *Cell Death Differ.* **2001,** *8* (6), 551-563.

49. Vermes, I.; Haanen, C.; Steffensnakken, H.; Reutelingsperger, C., A Novel Assay for Apoptosis - Flow Cytometric Detection of Phosphatidylserine Expression on Early Apoptotic Cells Using Fluorescein-Labeled Annexin-V. *J. Immunol. Methods* **1995,** *184* (1), 39-51.

50. Kol, M. A.; van Laak, A. N. C.; Rijkers, D. T. S.; Killian, J. A.; de Kroon, A. I. P. M.; de Kruijff, B., Phospholipid Flop Induced by Transmembrane Peptides in Model Membranes Is Modulated by Lipid Composition. *Biochem.* **2003,** *42* (1), 231-237.

51. Homan, R.; Pownall, H. J., Transbilayer Diffusion of Phospholipids: Dependence on Headgroup Structure and Acyl Chain Length. *Biochim. Biophys. Acta Biomemb.* **1988,** *938* (2), 155-166.

52. Du, Q.; Superfine, R.; Freysz, E.; Shen, Y. R., Vibrational Spectroscopy of Water at the Vapor Water Interface. *Phys. Rev. Lett.* **1993,** *70* (15), 2313-2316.

53. Nel, A. E.; Madler, L.; Velegol, D.; Xia, T.; Hoek, E. M. V.; Somasundaran, P.; Klaessig, F.; Castranova, V.; Thompson, M., Understanding Biophysicochemical Interactions at the Nano-Bio Interface. *Nat. Mater.* **2009,** *8* (7), 543-557.

54. Murphy, C. J.; Vartanian, A. M.; Geiger, F. M.; Hamers, R. J.; Pedersen, J.; Cui, Q.; Haynes, C. L.; Carlson, E. E.; Hernandez, R.; Klaper, R. D.; Orr, G.; Rosenzweig, Z. e., Biological Responses to Engineered Nanomaterials: Needs for the Next Decade. *ACS Cent. Sci.* **2015,** *1* (3), 117-123.

Chapter 4 References

1. Xia, T.; Kovochich, M.; Liong, M.; Mädler, L.; Gilbert, B.; Shi, H.; Yeh, J. I.; Zink, J. I.; Nel, A. E., Comparison of the Mechanism of Toxicity of Zinc Oxide and Cerium Oxide Nanoparticles Based on Dissolution and Oxidative Stress Properties. *ACS Nano* **2008,** *2* (10), 2121-2134.

2. Franklin, N. M.; Rogers, N. J.; Apte, S. C.; Batley, G. E.; Gadd, G. E.; Casey, P. S., Comparative Toxicity of Nanoparticulate Zno, Bulk Zno, and Zncl2 to a Freshwater Microalga (Pseudokirchneriella Subcapitata): The Importance of Particle Solubility. *Environ. Sci. Technol.* **2007,** *41* (24), 8484-8490.

3. Hang, M. N.; Gunsolus, I. L.; Wayland, H.; Melby, E. S.; Mensch, A. C.; Hurley, K. R.; Pedersen, J. A.; Haynes, C. L.; Hamers, R. J., Impact of Nanoscale Lithium Nickel Manganese Cobalt Oxide (Nmc) on the Bacterium Shewanella Oneidensis Mr-1. *Chem. Mater.* **2016,** *28* (4), 1092-1100.

4. Gunsolus, I. L.; Hang, M. N.; Hudson-Smith, N. V.; Buchman, J. T.; Bennett, J. W.; Conroy, D.; Mason, S. E.; Hamers, R. J.; Haynes, C. L., Influence of Nickel Manganese Cobalt Oxide Nanoparticle Composition on Toxicity toward Shewanella Oneidensis Mr-1: Redesigning for Reduced Biological Impact. *Environ. Sci. Nano* **2017**.

5. Huang, X.; Bennett, J. W.; Hang, M. N.; Laudadio, E. D.; Hamers, R. J.; Mason, S. E., Ab Initio Atomistic Thermodynamics Study of the (001) Surface of Licoo2 in a Water Environment and Implications for Reactivity under Ambient Conditions. *J. Phys. Chem. C* **2017**.

6. Smoluchowski, M. V., *Physikalische Zeitschrift* **1905,** *6*, 529-531.

7. Doğangün, M.; Hang, M. N.; Troiano, J. M.; McGeachy, A. C.; Melby, E. S.; Pedersen, J. A.; Hamers, R. J.; Geiger, F. M., Alteration of Membrane Compositional Asymmetry by Licoo2 Nanosheets. *ACS Nano* **2015,** *9*, 8755-8765.

8. Geiger, F. M., Second Harmonic Generation, Sum Frequency Generation, and Chi((3)): Dissecting Environmental Interfaces with a Nonlinear Optical Swiss Army Knife. *Annu. Rev. Phys. Chem.* **2009,** *60*, 61-83.

9. Troiano, J. M.; Olenick, L. L.; Kuech, T. R.; Melby, E. S.; Hu, D.; Lohse, S. E.; Mensch, A. C.; Doğangün, M.; Vartanian, A. M.; Torelli, M. D.; Ehimiaghe, E.; Walter, S. R.; Fu, L.; Anderton, C. R.; Zhu, Z.; Wang, H.; Orr, G.; Murphy, C. J.; Hamers, R. J.; Pedersen, J. A.; Geiger, F. M., Direct Probes of 4 Nm Diameter Gold Nanoparticles Interacting with Supported Lipid Bilayers. *J. Phys. Chem. C* **2015,** *119* (1), 534-546.

10. Adamson, A., *Physical Chemistry of Surfaces*. 5th ed ed.; John Wiley & Sons:: New York, 1990.

11. Stumm, W. M., J. J., *Aquatic Chemistry: Chemical Equilibria and Rates in Natural Waters*. 3rd ed ed.; John Wiley & Sons, Inc., 1996.

12. Troiano, J. M.; McGeachy, A. C.; Olenick, L. L.; Fang, D.; Liang, D. Y.; Hong, J. W.; Kuech, T. R.; Caudil, E. R.; Pedersen, J. A.; Cui, Q.; Geiger, F. M., Quantifying the Electrostatics of Polycation-Lipid Bilayer Interactions. *J. Am. Chem. Soc.* **2017,** *139* (16), 5808-5816.

13. Liu, J.; Conboy, J. C., 1,2-Diacyl-Phosphatidylcholine Flip-Flop Measured Directly by Sum-Frequency Vibrational Spectroscopy. *Biophys. J.* **2005,** *89* (4), 2522-2532.

14. Olenick, L. L. C., H. M.; Fu, L.; Zhang, Y.; McGeachy, A. C.;; Doğangün, M. W., S. R.; Wang, H-f.; Geiger, F. M., Single-Component Supported Lipid Bilayers Probed Using Broadband Nonlinear Optics. *Phys. Chem. Chem. Phys.* **2018,** *20*, 3063-3072.

15. Wen, Y. C.; Zha, S.; Liu, X.; Yang, S. S.; Guo, P.; Shi, G. S.; Fang, H. P.; Shen, Y. R.; Tian, C. S., Unveiling Microscopic Structures of Charged Water Interfaces by Surface-Specific Vibrational Spectroscopy. *Phys. Rev. Lett.* **2016,** *116* (1).

16. Sajid, M.; Ilyas, M.; Basheer, C.; Tariq, M.; Daud, M.; Baig, N.; Shehzad, F., Impact of Nanoparticles on Human and Environment: Review of Toxicity Factors, Exposures, Control Strategies, and Future Prospects. *Environ. Sci. Pollut. Res. Int.* **2015,** *22* (6), 4122-4143.

17. Doğangün, M.; Hang, M. N.; Machesky, J. E.; McGeachy, A. C.; Dalchand, N.; Hamers, R. J.; Geiger, F. M., Evidence for Considerable Metal Cation Concentrations from Lithium Intercalation Compounds in the Nano–Bio Interface Gap. *J. Phys. Chem. C* **2017,** *121* (49), 27473-27482.

18. Okur, H. I.; Kherb, J.; Cremer, P. S., Cations Bind Only Weakly to Amides in Aqueous Solutions. *J. Am. Chem. Soc.* **2013,** *135* (13), 5062-5067.

19. Zimmermann, R.; Küttner, D.; Renner, L.; Kaufmann, M.; Werner, C., Fluidity Modulation of Phospholipid Bilayers by Electrolyte Ions: Insights from Fluorescence Microscopy and Microslit Electrokinetic Experiments. *J. Phys. Chem. A* **2012,** *116* (25), 6519-6525.

20. Collins, K. D.; Neilson, G. W.; Enderby, J. E., Ions in Water: Characterizing the Forces That Control Chemical Processes and Biological Structure. *Biophys. Chem.* **2007,** *128* (2–3), 95-104.

21. Binder, H.; Zschornig, O., The Effect of Metal Cations on the Phase Behavior and Hydration Characteristics of Phospholipid Membranes. *Chem. Phys. Lipids* **2002,** *115* (1-2), 39-61.

22. Lau, A.; McLaughlin, A.; McLaughlin, S., The Adsorption of Divalent Cations to Phosphatidylglycerol Bilayer Membranes. *Biochim. Biophys. Acta* **1981,** *645* (2), 279-292.

23. McLaughlin, A. C., The Interaction of Cobalt with Glycerophosphoryl Glycerol and Phosphatidyl Glycerol Bilayer Membranes. *Journal of Magnetic Resonance (1969)* **1982,** *49* (2), 246-256.

24. Hauser, H.; Shipley, G. G., Interactions of Divalent Cations with Phosphatidylserine Bilayer Membranes. *Biochem.* **1984,** *23* (1), 34-41.

25. López Cascales, J. J.; Garcia de la Torre, J., Effect of Lithium and Sodium Ions on a Charged Membrane of Dipalmitoylphosphatidylserine: A Study by Molecular Dynamics Simulation. *Biochim. Biophys. Acta Biomemb.* **1997,** *1330* (2), 145-156.

26. *Royal Society of Chemistry Data Book: Hydration Enthalpies of Selected Ions*. RSC: 2006.

27. Chen, E. H.; Hayes, P. L.; Nguyen, S. T.; Geiger, F. M., Zinc Interactions with Glucosamine-Functionalized Fused Silica/Water Interfaces. *J. Phys. Chem. C* **2010,** *114* (45), 19483-19488.

28. Hayes, P. L.; Malin, J. N.; Jordan, D. S.; Geiger, F. M., Get Charged Up: Nonlinear Optical Voltammetry for Quantifying the Thermodynamics and Electrostatics of Metal Cations at Aqueous/Oxide Interfaces. *Chem. Phys. Lett.* **2010,** *499* (4-6), 183-192.

29. Ohno, P. E.; Saslow, S. A.; Wang, H.-f.; Geiger, F. M.; Eisenthal, K. B., Phase-Referenced Nonlinear Spectroscopy of the A-Quartz/Water Interface. *Nat. Comm.* **2016,** *7*, 13587.

30. Ohno, P. E.; Wang, H. F.; Geiger, F. M., Second-Order Spectral Lineshapes from Charged Interfaces. *Nat. Comm.* **2017,** *8*.

31. Ong, S. W.; Zhao, X. L.; Eisenthal, K. B., Polarization of Water-Molecules at a Charged Interface - 2nd Harmonic Studies of the Silica Water Interface. *Chem. Phys. Lett.* **1992,** *191* (3-4), 327-335.

32. Achtyl, J. L.; Vlassiouk, I. V.; Surwade, S. P.; Fulvio, P. F.; Dai, S.; Geiger, F. M., Interaction of Magnesium Ions with Pristine Single-Layer and Defected Graphene/Water Interfaces Studied by Second Harmonic Generation. *J. Phys. Chem. B* **2014,** *118* (28), 7739-7749.

33. Malin, J. N.; Geiger, F. M., Uranyl Adsorption and Speciation at the Fused Silica/Water Interface Studied by Resonantly Enhanced Second Harmonic Generation and the Chi((3)) Method. *J. Phys. Chem. A* **2010,** *114* (4), 1797-1805.

34. Malin, J. N.; Hayes, P. L.; Geiger, F. M., Interactions of Ca, Zn, and Cd Ions at Buried Solid/Water Interfaces Studied by Second Harmonic Generation. *J. Phys. Chem. C* **2009,** *113* (6), 2041-2052.

35. Troiano, J. M.; Kuech, T. R.; Vartanian, A. M.; Torelli, M. D.; Sen, A.; Jacob, L. M.; Hamers, R. J.; Murphy, C. J.; Pedersen, J. A.; Geiger, F. M., On Electronic and Charge Interference in Second Harmonic Generation Responses from Gold Metal Nanoparticles at Supported Lipid Bilayers. *J. Phys. Chem. C* **2016,** *120* (37), 20659-20667.

36. Javanainen, M.; Melcrova, A.; Magarkar, A.; Jurkiewicz, P.; Hof, M.; Jungwirth, P.; Martinez-Seara, H., Two Cations, Two Mechanisms: Interactions of Sodium and Calcium with Zwitterionic Lipid Membranes. *Chem. Commun.* **2017,** *53* (39), 5380-5383.

37. Lehrmann, R.; Seelig, J., Adsorption of Ca2+ and La3+ to Bilayer-Membranes - Measurement of the Adsorption Enthalpy and Binding Constant with Titration Calorimetry. *Biochimica Et Biophysica Acta-Biomembranes* **1994,** *1189* (1), 89-95.

38. Melcrova, A.; Pokorna, S.; Pullanchery, S.; Kohagen, M.; Jurkiewicz, P.; Hof, M.; Jungwirth, P.; Cremer, P. S.; Cwiklik, L., The Complex Nature of Calcium Cation Interactions with Phospholipid Bilayers. *Sci. Rep.* **2016,** *6*.

39. Adamson, A. W., *Physical Chemistry of Surfaces*. 5th ed.; John Wiley & Sons: New York, 1990.

40. Chen, E. H.; Saslow, S. A.; Nguyen, S. T.; Geiger, F. M., Zinc Ion-Hydroxyl Interactions at Undecanol-Functionalized Fused Silica/Water Interfaces Using the Eisenthal Chi((3)) Technique. *J. Phys. Chem. C* **2012,** *116* (12), 7016-7020.

41. Hayes, P. L.; Malin, J. N.; Konek, C. T.; Geiger, F. M., Interaction of Nitrate, Barium, Strontium and Cadmium Ions with Fused Quartz/Water Interfaces Studied by Second Harmonic Generation. *J. Phys. Chem. A* **2008,** *112* (4), 660-668.

42. Mclaughlin, A.; Grathwohl, C.; Mclaughlin, S., Adsorption of Divalent-Cations to Phosphatidylcholine Bilayer Membranes. *Biochim. Biophys. Acta* **1978,** *513* (3), 338-357.

43. Okamoto, S.; Eltis, L. D., The Biological Occurrence and Trafficking of Cobalt. *Metallomics* **2011,** *3* (10), 963-970.

Chapter 5 References

1. Nojima, Y.; Suzuki, Y.; Yamaguchi, S., Weakly Hydrogen-Bonded Water inside Charged Lipid Monolayer Observed with Heterodyne-Detected Vibrational Sum Frequency Generation Spectroscopy. *J. Phys. Chem. C* **2017,** *121*, 2173-2180.

2. Ishiyama, T.; Terada, D.; Morita, A., Hydrogen-Bonding Structure at Zwitterionic Lipid/Water Interface. *J. Phys. Chem. Lett.* **2016,** *7*, 216-220.

3. Fayer, M. D., Dynamics of Water Interacting with Interfaces, Molecules, and Ions. *Acc. Chem. Res.* **2012,** *45*, 3-14.

4. Lopez, C. F.; Nielsen, S. O.; Klein, M. L.; Moore, P. B., Hydrogen Bonding Structure and Dynamics of Water at the Dimyristoylphosphatidylcholine Lipid Bilayer Surface from a Molecular Dynamics Simulation. *J. Phys. Chem. B* **2004,** *108*, 6603-6610.

5. Nagata, Y.; Mukamel, S., Vibrational Sum-Frequency Generation Spectroscopy at the Water/Lipid Interface: Molecular Dynamics Simulation Study. *J. Am. Chem. Soc.* **2010,** *132*, 6434-6442.

6. Bonn, M.; Bakker, H. J.; Backus, E. H., No Ice-Like Water at Aqueous Biological Interfaces. *Biointerphases* **2012,** *7*, 20.

7. Chen, X.; Hua, W.; Huang, Z.; Allen, H. C., Interfacial Water Structure Associated with Phospholipid Membranes Studied by Phase-Sensitive Vibrational Sum Frequency Generation Spectroscopy. *J. Am. Chem. Soc.* **2010,** *132*, 11336-11342.

8. Fu, L.; Liu, J.; Yan, E. C. Y., Chiral Sum Frequency Generation Spectroscopy for Characterizing Protein Secondary Structures at Interfaces. *J. Am. Chem. Soc.* **2011,** *133* (21), 8094-8097.

9. Fu, L.; Ma, G.; Yan, E. C. Y., In Situ Misfolding of Human Islet Amyloid Polypeptide at Interfaces Probed by Vibrational Sum Frequency Generation. *J. Am. Chem. Soc.* **2010,** *132* (15), 5405-5412.

10. Roke, S.; Schins, J.; Müller, M.; Bonn, M., Vibrational Spectroscopic Investigation of the Phase Diagram of a Biomimetic Lipid Monolayer. *Phys. Rev. Lett.* **2003,** *90* (12), 128101.

11. Smits, M.; Sovago, M.; Wurpel, G. W. H.; Kim, D.; Müller, M.; Bonn, M., Polarization-Resolved Broad-Bandwidth Sum-Frequency Generation Spectroscopy of Monolayer Relaxation. *J. Phys. Chem. C* **2007,** *111* (25), 8878-8883.

12. Sung, W.; Seok, S.; Kim, D.; Tian, C. S.; Shen, Y. R., Sum-Frequency Spectroscopic Study of Langmuir Monolayers of Lipids Having Oppositely Charged Headgroups. *Langmuir* **2010,** *26* (23), 18266-18272.

13. Walker, R. A.; Gruetzmacher, J. A.; Richmond, G. L., Phosphatidylcholine Monolayer Structure at a Liquid−Liquid Interface. *J. Am. Chem. Soc.* **1998,** *120* (28), 6991-7003.

14. Allgeyer, E. D.; Sterling, S. M.; Gunewardene, M. S.; Hess, S. T.; Neivandt, D. J.; Mason, M. D., Combining Total Internal Reflection Sum Frequency Spectroscopy Spectral Imaging and Confocal Fluorescence Microscopy. *Langmuir* **2015,** *31*, 987-994.

15. Kim, G.; Gurau, M. C.; Lim, S.-M.; Cremer, P. S., Investigations of the Orientation of a Membrane Peptide by Sum Frequency Spectroscopy. *J. Phys. Chem. B* **2003,** *107*, 1403-1409.

16. Livingston, R. A.; Zhang, Z.; Piatkowski, L.; Bakker, H. J.; Hunger, J.; Bonn, M.; Backus, E. H., Water in Contact with a Cationic Lipid Exhibits Bulklike Vibrational Dynamics. *J. Phys. Chem. B* **2016,** *120*, 10069-11008.

17. Mondal, J. A.; Nihonyanagi, S.; Yamaguchi, S.; Tahara, T., Three Distinct Water Structures at a Zwitterionic Lipid/Water Interface Revealed by Heterodyne-Detected Vibrational Sum Frequency Generation. *J. Am. Chem. Soc.* **2012,** *134* (18), 7842-7850.

18. Mondal, J. A.; Nihonyanagi, S.; Yamaguchi, S.; Tahara, T., Structure and Orientation of Water at Charged Lipid Monolayer/Water Interfaces Probed by Heterodyne-Detected Vibrational Sum Frequency Generation Spectroscopy. *J. Am. Chem. Soc.* **2010,** *132* (31), 10656-10657.

19. Inoue, K.-i.; Singh, P. C.; Nihonyanagi, S.; Yamaguchi, S.; Tahara, T., Cooperative Hydrogen-Bond Dynamics at a Zwitterionic Lipid/Water Interface Revealed by 2d Hd-Vsfg Spectroscopy. *J. Phys. Chem. Lett.* **2017,** *8* (20), 5160-5165.

20. Marrapu, P.; Cheng, Y.; Carmichael, G.; Beig, G.; Spak, S. In *Local and Regional Interactions between Air Quality and Climate in New Delhi - a Sector Based Analysis*, AGU Annual Meeting, Dec. 2011.

21. Liu, J.; Conboy, J. C., Structure of a Gel Phase Lipid Bilayer Prepared by the Langmuir−Blodgett/Langmuir-Schaefer Method Characterized by Sum-Frequency Vibrational Spectroscopy. *Langmuir* **2005,** *21* (20), 9091-9097.

22. Brown, K. L.; Conboy, J. C., Electrostatic Induction of Lipid Asymmetry. *J. Am. Chem. Soc.* **2011,** *133* (23), 8794-8797.

23. Watry, M. R.; Tarbuck, T. L.; Richmond, G. L., Vibrational Sum-Frequency Studies of a Series of Phospholipid Monolayers and the Associated Water Structure at the Vapor/Water Interface. *J. Phys. Chem. B* **2002,** *107* (2), 512-518.

24. Brown, M. G.; Raymond, E. A.; Allen, H. C.; Scatena, L. F.; Richmond, G. L., The Analysis of Interference Effects in the Sum Frequency Spectra of Water Interfaces†. *J. Phys. Chem. A* **2000,** *104* (45), 10220-10226.

25. Singh, P. C.; Inoue, K. i.; Nihonyanagi, S.; Yamaguchi, S.; Tahara, T., Femtosecond Hydrogen Bond Dynamics of Bulk-Like and Bound Water at Positively and Negatively Charged Lipid Interfaces Revealed by 2d Hd-Vsfg Spectroscopy. *Angew. Chem. Int. Ed.* **2016,** *55* (36), 10621-10625.

26. Boyd, R. W., *Nonlinear Optics, 3rd Edition*. Elsevier Academic Press Inc: San Diego, 2008; p 1-613.

27. Liu, J.; Conboy, J. C., Asymmetric Distribution of Lipids in a Phase Segregated Phospholipid Bilayer Observed by Sum-Frequency Vibrational Spectroscopy. *J. Phys. Chem. C* **2007,** *111* (25), 8988-8999.

28. Chen, X.; Chen, Z., Sfg Studies on Interactions between Antimicrobial Peptides and Supported Lipid Bilayers. *Biochim. Biophys. Acta - Biomemb.* **2006,** *1758* (9), 1257-1273.

29. Olenick, L. L.; Chase, H. M.; Fu, L.; Zhang, Y.; McGeachy, A. C.; Doğangün, M.; Walter, S. R.; Wang, H.-f.; Geiger, F. M., Single-Component Supported Lipid Bilayers Probed Using Broadband Nonlinear Optics. *Phys. Chem. Chem. Phys.* **2018,** *20* (5), 3063-3072.

30. Troiano, J. M.; McGeachy, A. C.; Olenick, L. L.; Fang, D.; Liang, D.; Hong, J.; Kuech, T. R.; Caudill, E. R.; Pedersen, J. A.; Cui, Q.; Geiger, F. M., Quantifying the Electrostatics of Polycation–Lipid Bilayer Interactions. *J. Am. Chem. Soc.* **2017,** *139*, 5808-5816.

31. Troiano, J. M.; Olenick, L. L.; Kuech, T. R.; Melby, E. S.; Hu, D. H.; Lohse, S. E.; Mensch, A. C.; Doğangün, M.; Vartanian, A. M.; Torelli, M. D.; Ehimiaghe, E.; Walter, S. R.; Fu, L.; Anderton, C. R.; Zhu, Z. H.; Wang, H. F.; Orr, G.; Murphy, C. J.; Hamers, R. J.; Pedersen, J. A.; Geiger, F. M., Direct Probes of 4 Nm Diameter Gold Nanoparticles Interacting with Supported Lipid Bilayers. *J. Phys. Chem. C* **2015,** *119* (1), 534-546.

32. Castellana, E. T.; Cremer, P. S., Solid Supported Lipid Bilayers: From Biophysical Studies to Sensor Design. *Surf. Sci. Rep.* **2006,** *61* (10), 429-444.

33. Doğangün, M.; Hang, M. N.; Troiano, J. M.; McGeachy, A. C.; Melby, E. S.; Pedersen, J. A.; Hamers, R. J.; Geiger, F. M., Alteration of Membrane Compositional Asymmetry by Licoo2 Nanosheets. *Acs Nano* **2015,** *9* (9), 8755-8765.

34. Doğangün, M.; Hang, M. N.; Machesky, J.; McGeachy, A. C.; Dalchand, N.; Hamers, R. J.; Geiger, F. M., Evidence for Considerable Metal Cation Concentrations from Lithium Intercalation Compounds in the Nano–Bio Interface Gap. *J. Phys. Chem. C* **2017,** *121* (49), 27473-27482.

35. Wu, E.; Jacobson, K.; Papahadjopoulos, D., Lateral Diffusion in Phospholipid Multibilayers Measured by Fluorescence Recovery after Photobleaching. *Biochem.* **1977,** *16* (17), 3936-3941.

36. Kalb, E.; Frey, S.; Tamm, L. K., Formation of Supported Planar Bilayers by Fusion of Vesicles to Supported Phospholipid Monolayers. *Biochim. Biophys. Acta Biomemb.* **1992,** *1103* (2), 307-316.

37. Vaz, W. L. C.; Clegg, R. M.; Hallmann, D., Translational Diffusion of Lipids in Liquid Crystalline Phase Phosphatidylcholine Multibilayers. A Comparison of Experiment with Theory. *Biochem.* **1985,** *24* (3), 781-786.

38. Jo, S.; Lim, J. B.; Klauda, J. B.; Im, W., Charmm-Gui Membrane Builder for Mixed Bilayers and Its Application to Yeast Membranes. *Biophys. J.* **2009,** *97* (1), 50-58.

39. Phillips, J. C.; Braun, R.; Wang, W.; Gumbart, J.; Tajkhorshid, E.; Villa, E.; Chipot, C.; Skeel, R. D.; Kale, L.; Schulten, K., Scalable Molecular Dynamics with Namd. *J. Comput. Chem.* **2005,** *26* (16), 1781-1802.

40. Klauda, J. B.; Venable, R. M.; Freites, J. A.; O'Connor, J. W.; Tobias, D. J.; Mondragon-Ramirez, C.; Vorobyov, I.; MacKerell Jr, A. D.; Pastor, R. W., Update of the Charmm All-Atom Additive Force Field for Lipids: Validation on Six Lipid Types. *J. Phys. Chem. B* **2010,** *114* (23), 7830-7843.

41. Venable, R. M.; Luo, Y.; Gawrisch, K.; Roux, B.; Pastor, R. W., Simulations of Anionic Lipid Membranes: Development of Interaction-Specific Ion Parameters and Validation Using Nmr Data. *J. Phys. Chem. B* **2013,** *117* (35), 10183-10192.

42. Darden, T.; York, D.; Pedersen, L., Particle Mesh Ewald: An N· Log (N) Method for Ewald Sums in Large Systems. *J. Chem. Phys.* **1993,** *98* (12), 10089-10092.

43. Andersen, H. C., Rattle: A "Velocity" Version of the Shake Algorithm for Molecular Dynamics Calculations. *J. Comp. Phys.* **1983,** *52* (1), 24-34.

44. Feller, S. E.; Zhang, Y.; Pastor, R. W.; Brooks, B. R., Constant Pressure Molecular Dynamics Simulation: The Langevin Piston Method. *J. Chem. Phys.* **1995,** *103* (11), 4613-4621.

45. Martyna, G. J.; Tobias, D. J.; Klein, M. L., Constant Pressure Molecular Dynamics Algorithms. *J. Chem. Phys.* **1994,** *101* (5), 4177-4189.

46. Lee, J.; Cheng, X.; Swails, J. M.; Yeom, M. S.; Eastman, P. K.; Lemkul, J. A.; Wei, S.; Buckner, J.; Jeong, J. C.; Qi, Y., Charmm-Gui Input Generator for Namd, Gromacs, Amber, Openmm, and Charmm/Openmm Simulations Using the Charmm36 Additive Force Field. *J. Chem. Theory Comput.* **2015,** *12* (1), 405-413.

47. Wu, E. L.; Cheng, X.; Jo, S.; Rui, H.; Song, K. C.; Dávila-Contreras, E. M.; Qi, Y.; Lee, J.; Monje-Galvan, V.; Venable, R. M., Charmm-Gui Membrane Builder toward Realistic Biological Membrane Simulations. *J. Comput. Chem.* **2014,** *35* (27), 1997-2004.

48. Becraft, K. A.; Richmond, G. L., In Situ Vibrational Spectroscopic Studies of the Caf2/H2o Interface. *Langmuir* **2001,** *17* (25), 7721-7724.

49. Lis, D.; Backus, E. H. G.; Hunger, J.; Parekh, S. H.; Bonn, M., Liquid Flow Along a Solid Surface Reversibly Alters Interfacial Chemistry. *Science* **2014,** *344* (6188), 1138.

50. Lawrence, C. P.; Skinner, J. L., Ultrafast Infrared Spectroscopy Probes Hydrogen-Bonding Dynamics in Liquid Water. *Chem. Phys. Lett.* **2003,** *369* (3), 472-477.

51. Scatena, L. F.; Brown, M. G.; Richmond, G. L., Water at Hydrophobic Surfaces: Weak Hydrogen Bonding and Strong Orientation Effects. *Science* **2001,** *292* (5518), 908.

52. Ma, G.; Chen, X.; Allen, H. C., Dangling Od Confined in a Langmuir Monolayer. *J. Am. Chem. Soc.* **2007,** *129*, 14053-14057.

53. Covert, P. A.; Jena, K. C.; Hore, D. K., Throwing Salt into the Mix: Altering Interfacial Water Structure by Electrolyte Addition. *J. Phys. Chem. Lett.* **2013,** *5* (1), 143-148.

54. Hopkins, A. J.; Schrödle, S.; Richmond, G. L., Specific Ion Effects of Salt Solutions at the CaF2/Water Interface. *Langmuir* **2010,** *26* (13), 10784-10790.

55. Kondo, T.; Nomura, K.; Gemmei-Ide, M.; Kitano, H.; Noguchi, H.; Uosaki, K.; Saruwatari, Y., Structure of Water at Zwitterionic Copolymer Film–Liquid Water Interfaces as Examined by the Sum Frequency Generation Method. *Coll. Surf. B Biointer.* **2014,** *113*, 361-367.

56. Bradley, L. C.; Dilworth, Z. R.; Barnette, A. L.; Hsiao, E.; Barthel, A. J.; Pantano, C. G.; Kim, S. H., Hydronium Ions in Soda-Lime Silicate Glass Surfaces. *J. Am. Ceram. Soc.* **2013,** *96* (2), 458-463.

57. Daly, C. A.; Streaker, L. M.; Sun, Y.; Pattenaude, S. R.; Hassanali, A. A.; Petersen, P. B.; Corcelli, S. A.; Ben-Amotz, D., Decomposition of the Experimental Raman and Infrared Spectra of Acidic Water into Proton, Special Pair, and Counterion Contributions. *J. Phys. Chem. Lett.* **2017,** *8*, 5246-5252.

58. Perera, P. N.; Browder, B.; Ben-Amotz, D., Perturbations of Water by Alkali Halide Ions Measured Using Multivariate Raman Curve Resolution. *J. Phys. Chem. B* **2009,** *113*, 1805-1809.

59. Roy, S.; Gruenbaum, S.; Skinner, J., Theoretical Vibrational Sum-Frequency Generation Spectroscopy of Water near Lipid and Surfactant Monolayer Interfaces. *J. Chem. Phys.* **2014,** *141* (18), 18C502.

60. Wen, Y.-C.; Zha, S.; Liu, X.; Yang, S.; Guo, P.; Shi, G.; Fang, H.; Shen, Y. R.; Tian, C., Unveiling Microscopic Structures of Charged Water Interfaces by Surface-Specific Vibrational Spectroscopy. *Phys. Rev. Lett.* **2016,** *116* (1), 016101.

61. Ohno, P. E.; Saslow, S. A.; Wang, H.-f.; Geiger, F. M.; Eisenthal, K. B., Phase-Referenced Nonlinear Spectroscopy of the Alpha-Quartz/Water Interface. *Nat. Comm.* **2016,** *7*, 13587.

62. Ohno, P. E.; Wang, H.-f.; Geiger, F. M., Second-Order Spectral Lineshapes from Charged Interfaces. *Nat. Comm.* **2017,** *8*, 1032.

63. Boamah, M. D.; Ohno, P. E.; Geiger, F. M.; Eisenthal, K. B., Relative Permittivity in the Electrical Double Layer from Nonlinear Optics. *arXiv 1702.02496 and J. Chem. Phys.* **2018,** *148*, 222808.

64. Konek, C. T.; Musorrafiti, M. J.; Al-Abadleh, H. A.; Bertin, P. A.; Nguyen, S. T.; Geiger, F. M., Interfacial Acidities, Charge Densities, Potentials, and Energies of Carboxylic Acid-Functionalized Silica/Water Interfaces Determined by Second Harmonic Generation. *J. Am. Chem. Soc.* **2004,** *126*, 11754-11755.

65. Gershevitz, O.; Sukenik, C. N., In Situ Ftir-Atr Analysis and Titration of Carboxylic Acid-Terminated Sams. *J. Am. Chem. Soc.* **2003,** *126* (2), 482-483.

Chapter 6 References

1. Clifton, L. A.; Skoda, M. W. A.; Daulton, E. L.; Hughes, A. V.; Le Brun, A. P.; Lakey, J. H.; Holt, S. A., Asymmetric Phospholipid: Lipopolysaccharide Bilayers; a Gram-Negative Bacterial Outer Membrane Mimic. *J. Royal Soc. Interface* **2013,** *10* (89).

2. Ruiz, N.; Kahne, D.; Silhavy, T. J., Transport of Lipopolysaccharide across the Cell Envelope: The Long Road of Discovery. *Nat. Rev. Microbiol.* **2009,** *7* (9), 677-683.

3. Osborn, M. J.; Rick, P. D.; Lehmann, V.; Rupprecht, E.; Singh, M., Structure and Biogenesis of the Cell Envelope of Gram-Negative Bacteria*. *Ann. N.Y. Acad. Sci.* **1974,** *235* (1), 52-65.

4. Silhavy, T. J.; Kahne, D.; Walker, S., The Bacterial Cell Envelope. *Cold Spring Harb. Perspect. Biol.* **2010,** *2* (5), a000414.

5. Nikaido, H., Molecular Basis of Bacterial Outer Membrane Permeability Revisited. *Microbiol. Mol. Biol. Rev.* **2003,** *67* (4), 593-656.

6. Erridge, C.; Bennett-Guerrero, E.; Poxton, I. R., Structure and Function of Lipopolysaccharides. *Microbes Infect.* **2002,** *4* (8), 837-851.

7. Jacobson, K. H.; Gunsolus, I. L.; Kuech, T. R.; Troiano, J. M.; Melby, E. S.; Lohse, S. E.; Hu, D.; Chrisler, W. B.; Murphy, C. J.; Orr, G.; Geiger, F. M.; Haynes, C. L.; Pedersen, J. A., Lipopolysaccharide Density and Structure Govern the Extent and Distance of Nanoparticle Interaction with Actual and Model Bacterial Outer Membranes. *Environ. Sci. Technol.* **2015,** *49* (17), 10642-10650.

8. Lind, T. K.; Wacklin, H.; Schiller, J.; Moulin, M.; Haertlein, M.; Pomorski, T. G.; Cárdenas, M., Formation and Characterization of Supported Lipid Bilayers Composed of Hydrogenated and Deuterated Escherichia Coli Lipids. *PLoS ONE* **2015,** *10* (12), e0144671.

9. Ivask, A.; ElBadawy, A.; Kaweeteerawat, C.; Boren, D.; Fischer, H.; Ji, Z.; Chang, C. H.; Liu, R.; Tolaymat, T.; Telesca, D.; Zink, J. I.; Cohen, Y.; Holden, P. A.; Godwin, H. A., Toxicity Mechanisms in Escherichia Coli Vary for Silver Nanoparticles and Differ from Ionic Silver. *ACS Nano* **2014,** *8* (1), 374-386.

10. Li, Y.; Shi, Z.; Radauer-Preiml, I.; Andosch, A.; Casals, E.; Luetz-Meindl, U.; Cobaleda, M.; Lin, Z.; Jaberi-Douraki, M.; Italiani, P.; Horejs-Hoeck, J.; Himly, M.; Monteiro-Riviere, N. A.; Duschl, A.; Puntes, V. F.; Boraschi, D., Bacterial Endotoxin (Lipopolysaccharide) Binds to the Surface of Gold Nanoparticles, Interferes with Biocorona Formation and Induces Human Monocyte Inflammatory Activation. *Nanotoxicol.* **2017,** *11* (9-10), 1157-1175.

11. Sondi, I.; Salopek-Sondi, B., Silver Nanoparticles as Antimicrobial Agent: A Case Study on E. Coli as A model for Gram-Negative Bacteria. *J. Colloid Interface Sci.* **2004,** *275* (1), 177-182.

12. Sigma, M., Lipopolysaccharides. In *Glycobiology Analysis Manual*, 2nd Ed. ed.

13. Raetz, C. R.; Guan, Z.; Ingram, B. O.; Six, D. A.; Song, F.; Wang, X.; Zhao, J., Discovery of New Biosynthetic Pathways: The Lipid a Story. *J. Lipid Res.* **2009,** *50 Suppl*, S103-108.

14. Troiano, J. M.; Olenick, L. L.; Kuech, T. R.; Melby, E. S.; Hu, D. H.; Lohse, S. E.; Mensch, A. C.; Doğangün, M.; Vartanian, A. M.; Torelli, M. D.; Ehimiaghe, E.; Walter, S. R.; Fu, L.; Anderton, C. R.; Zhu, Z. H.; Wang, H. F.; Orr, G.; Murphy, C. J.; Hamers, R. J.; Pedersen, J. A.; Geiger, F. M., Direct Probes of 4 Nm Diameter Gold Nanoparticles Interacting with Supported Lipid Bilayers. *J Phys Chem C* **2015,** *119* (1), 534-546.

15. Doğangün, M.; Ohno, P. E.; Liang, D.; McGeachy, A. C.; Be, A. G.; Dalchand, N.; Li, T.; Cui, Q.; Geiger, F. M., Hydrogen Bond Networks near Supported Lipid Bilayers from Vibrational Sum Frequency Generation Experiments and Atomistic Simulations. *arXiv:1803.01202* **2018**.

16. Du, Q.; Superfine, R.; Freysz, E.; Shen, Y. R., Vibrational Spectroscopy of Water at the Vapor Water Interface. *Phys. Rev. Lett.* **1993,** *70* (15), 2313-2316.

17. Olenick, L. L.; Chase, H. M.; Fu, L.; Zhang, Y.; McGeachy, A. C.; Doğangün, M.; Walter, S. R.; Wang, H.-f.; Geiger, F. M., Single-Component Supported Lipid Bilayers Probed Using Broadband Nonlinear Optics. *Phys. Chem. Chem. Phys.* **2018,** *20* (5), 3063-3072.

18. Liu, J.; Conboy, J. C., Phase Transition of a Single Lipid Bilayer Measured by Sum-Frequency Vibrational Spectroscopy. *J. Am. Chem. Soc.* **2004,** *126* (29), 8894-8895.

19. Liu, J.; Conboy, J. C., Structure of a Gel Phase Lipid Bilayer Prepared by the Langmuir-Blodgett/Langmuir-Schaefer Method Characterized by Sum-Frequency Vibrational Spectroscopy. *Langmuir* **2005,** *21* (20), 9091-9097.

20. Doğangün, M.; Hang, M. N.; Machesky, J. E.; McGeachy, A. C.; Dalchand, N.; Hamers, R. J.; Geiger, F. M., Evidence for Considerable Metal Cation Concentrations from Lithium Intercalation Compounds in the Nano–Bio Interface Gap. *J. Phys. Chem. C* **2017,** *121* (49), 27473-27482.

21. Doğangün, M.; Hang, M. N.; Troiano, J. M.; McGeachy, A. C.; Melby, E. S.; Pedersen, J. A.; Hamers, R. J.; Geiger, F. M., Alteration of Membrane Compositional Asymmetry by Licoo2 Nanosheets. *ACS Nano* **2015,** *9*, 8755-8765.

22. Soblosky, L. Molecular Interactions between Various Model Cell Membranes and Membrane Active Peptides Studied by Sum Frequency Generation Vibrational Spectroscopy. PhD Thesis, University of Michigan, 2014.

23. Soblosky, L.; Ramamoorthy, A.; Chen, Z., Membrane Interaction of Antimicrobial Peptides Using E. Coli Lipid Extract as Model Bacterial Cell Membranes and Sfg Spectroscopy. *Chem. Phys. Lipids* **2015,** *187*, 20-33.

Merve Doğangün

2145 Sheridan Road • Evanston, IL • 60208 • 847-4915043 (Work)
mervedogangun2018@u.northwestern.edu

EDUCATION

Northwestern University, Chemistry PhD 2013-2018
Advisor: Dr. Franz Geiger

Northwestern University, Kellogg School of Management for Scientists and Engineers 2017
Certificate program

Middle East Technical University (METU), Bachelor of Science in Chemistry 2013
Top Ranked Student, Department of Chemistry

ACADEMIC RESEARCH EXPERIENCE

Graduate Research Assistant, Northwestern University 2013-2018
Advisor: Prof. Dr. Franz M. Geiger
NSF Center for Sustainable Nanotechnology Director: Prof. Dr. Robert J. Hamers

–Investigated interactions of engineered nanomaterials with model cell membranes to design new nanoscale energy materials with reduced environmental impacts

Undergraduate Summer Research Trainee, Northwestern University 2012
Advisor: Prof. Dr. Franz Geiger

–Worked with a graduate student to examine the interactions of functionalized gold nanoparticles and DNA strands to aide in the development of biosensors

Undergraduate Researcher, METU 2011-2013
Advisor: Assoc. Dr. Okan Esentürk

–Awarded a collaborative undergraduate research project with a pharmaceutical company for the Industry Integrated National Research Project, Turkish Scientific & Technological Research Council, to characterize pharmaceutical active ingredients to distinguish the original drugs from the counterfeit

PUBLICATIONS

Doğangün, M.;[#] Ohno, P. E.;[#] Liang, D.;[#] McGeachy, A. C.; Be, A. G.; Dalchand, N.; Li, T.; Cui, Q.; Geiger, F. M. Hydrogen Bond Networks Near Supported Lipid Bilayers from Vibrational Sum Frequency Generation Experiments and Atomistic Simulations. *J. Phys. Chem. B* **2018**, *122*, 4870.

McGeachy, A. C.; Dalchand, N.; Caudill, E. R.; Li, T.; **Doğangün, M.;** Olenick, L. L.; Chang, H.; Pedersen, J. A.; Geiger, F. M. Interfacial electrostatics of poly (vinylamine hydrochloride), poly (diallyldimethylammonium chloride), poly-l-lysine, and poly-l-arginine interacting with lipid bilayers. *Phys. Chem. Chem. Phys.* **2018**, *20,* 10846.

Olenick, L. L.; Chase, H. M.; Fu, L.; Zhang, Y.; McGeachy, A.; **Doğangün, M.**; Walter, S. R.; Wang, H.-f.; Geiger, F. M. Single-Component Supported Lipid Bilayers Probed Using Broadband Nonlinear Optics. *Phys. Chem. Chem. Phys.* **2018**, *20*, 3063.

Doğangün, M.; Hang, M. N.; Machesky, J.; McGeachy, A. M.; Dalchand, A. M.; Hamers, R. J.; Geiger, F. M. Evidence for Considerable Metal Cation Concentrations from Li Intercalation Compounds in the Nano-Bio Interface Gap. *J. Phys. Chem. C.* **2017**, *121*, 27473.

Olenick, L. L., Troiano, J. M., Vartanian, A., Melby, E. S., Mensch, A. C., Zhang, L., Hong, J., Qiu, T., Bozich, J., Lohse, S., Zhang, X., Kuech, T. R., Millevolte, A., Gunsolus, I., McGeachy, A. C., **Doğangün, M.**, Li, T., Hu, D., Walter, S. R., Mohaimani, A., Schmoldt, A., Torelli, M. D., Hurley, K. R., Dalluge, J., Chong, G., Feng, Z. V., Haynes, C. L., Hamers, R. J., Pedersen, J. A., Cui, Q., Hernandez, R., Klaper, R., Orr, G., Murphy, C. J., and Geiger, F. Lipid Corona Formation from Nanoparticle Interactions with Bilayers and Membrane-Specific Biological Outcomes. *ChemRxiv.* **2017**.

Doğangün, M.; Hang, M. N.; Troiano, J. M.; McGeachy, A. C.; Melby, E. S.; Pedersen, J. A.; Hamers, R. J.; Geiger, F. M. Alteration of Membrane Compositional Asymmetry by $LiCoO_2$ Nanosheets. **2015**, *ACS Nano 9*, 8755.

Troiano, J. M.; Olenick, L. L.; Kuech, T. K.; Melby, E. S.; Hu, D.; Lohse, S. E.; Mensch, A. C.; **Doğangün, M.;** Vartanian, A. M.; Torelli, M. D.; Ehimiaghe, E.; Walter. S. R.; Fu, L.; Anderton, C. R.; Zhu, Z.; Wang, H.; Orr, G.; Murphy, C. J.; Hamers, R. J.; Pedersen, J. A.; Geiger, F. M. Direct Probes of 4 nm Diameter Gold Nanoparticles Interacting with Supported Lipid Bilayers. *J. Phys. Chem. B* **2015**, *119*, 534.

PRESENTATIONS

Surface-Specific Explorations at the Nano-Bio Interface Gap. **Invited Talk.**
Argonne National Laboratory, **2018**, Lemont, IL.

Alteration of Membrane Compositional Asymmetry by $LiCoO_2$ Nanosheets. **Oral**.
Argonne National Laboratory, **2017**, Lemont, IL.

Explorations at the Nano-Bio Interface Gap. **Oral** and **Poster.**
Pacific Northwest National Laboratory, CSN All Hands Meeting, **2016**, Richland, WA.

Alteration of Membrane Compositional Asymmetry by $LiCoO_2$ Nanosheets. **Oral.**
252th National ACS Conference, **2016**, Philadelphia, PA.

Redox Active Nanomaterial Interactions with Model Cell Membranes. **Poster.**
Gordon Research Seminar and Conference on Vibrational Spectroscopy, **2016**, Biddeford, ME.

Direct Views of the Nano-Bio Interface. **Oral.**
250th National ACS Meeting, **2015**, Boston, MA.

Developing a Novel Terahertz Spectroscopy Method for Pharmaceutical Active Material Analysis. **Poster.**
National Congress of Pharmaceuticals, **2013**, Antalya, Turkey.

LEADERSHIP

2017 Graduate Sidekick, Northwestern University 2017-2018
–Served as a peer mentor to new international students to promote better transition to life in the US
–Planned the Graduate International Student Orientation, September 2017
Laboratory Safety Designate, Geiger Group, Northwestern University 2016-2017
–Monitored the health and safety regulations of lab workers and managed hazardous waste
–Implemented new safety measures, attended Office for Research Safety Meetings at NU
Student Board Member, CSN Professional Development Committee 2016-2018
–Planned Professional Development Activities to CSN members, conduct surveys

HONORS and AWARDS

Cross-Cultural Leadership Certificate, the International Office, Northwestern University 2017
Wender Fellowship, Department of Chemistry, Northwestern University 2017
Young Entrepreneurs Award, International Year of Chemistry, Akkim Chemical Company 2011
High Honor Roll, METU 2010-2013

ACTIVITIES

Science Blog Peer Editor and Contributor, Sustainable Nanotechnology Blog 2014-2018
http://sustainable-nano.com
Volunteer, Science in the Classroom, Chicago, IL 2015-2018
Volunteer, 4H Library Forensic Club, Waukegan, IL 2013
Volunteer, Science is Fun Event, Ankara, Turkey 2012
Initiator, Periodic Art Project, Foundation for Children with Leukemia, Ankara, Turkey 2011
Student Organizer, Chemistry with All Dimensions Symposium, Ankara, Turkey 2011
Student Organizer, METU Science Festivals, Ankara, Turkey 2010

WORKSHOPS AND PROFESSIONAL AFFILIATIONS

2015 Seattle Super-Resolution Microscopy Workshop 2015
9th Annual Chautauqua on Nonlinear Optics, Purdue University 2014
American Chemical Society 2014-2018
Phi Lambda Upsilon Honorary Chemical Society 2014-2018